8-2013

Polysaccharide-Based Nanocarriers for Improved Drug Delivery

Nan Zhang

Abstract

The field of drug delivery has provided a solution to the limited efficacy and high toxicity of many drugs. Nano-sized drug carriers are popular because their size allows for selective accumulation in the diseased area. Polysaccharides are non-toxic and biodegradable natural polymers that can serve as the basis for these nano-sized carriers. Polysialic acid (PSA) is such a polysaccharide with strong hydrophilicity that may reduce uptake by the reticuloendothelial system and prolong drug circulation. In this study, we developed PSA-based nanocarriers, specifically micelles and nanoparticles, for improved drug delivery with improved efficacy and minimized toxicity. PSA-based micelle systems were developed via conjugation with two hydrophobic groups, decylamine (DA) and polycaprolactone (PCL). Nanoparticles were fabricated via ionic complexation of the negatively charged PSA with positively charged N, N, N-trimethyl chitosan (TMC). All three nanocarriers possessed sizes close to 100 nm with low polydispersity (PDI) and high zeta potential values. Literature suggested that these characteristics would allow the nanocarriers to be physiologically stable and would facilitate passive accumulation within diseased areas. Rheumatoid arthritis (RA) was selected as the primary disease model for evaluation of our nanocarriers. PSA-PCL micelles and PSA-TMC nanoparticles showed low cytotoxicity, as demonstrated by high IC_{50} values (PSA-PCL: 10.5 ± 1.7 mg/ml; PSA-TMC: 7.65 ± 0.07 mg/ml) to synovial cells, the so-called conductors of joint destruction in rheumatoid arthritis. The synovial cells were also used to demonstrate effective uptake of fluorescently tagged nanocarriers. Three disease modifying anti-rheumatic drugs (DMARDs) were selected for loading into the nanocarriers. Cyclosporine A (CyA) was encapsulated within the PSA-PCL micelles, while methotrexate (MTX), and dexamethasone (DM) were entrapped within the PSA-TMC nanoparticles. PSA-PCL micelles were loaded with

0.09 ± 0.02 mg CyA per mg of PSA- PCL, while PSA-TMC nanoparticles were loaded with 0.10 ± 0.03 mg MTX and 0.10 ± 0.02 mg DM per mg of PSA-TMC. Controlled release of the DMARDs from the nanocarriers was demonstrated. An *in vitro* model of rheumatoid arthritis was used to demonstrate the anti-inflammatory nature of the MTX- and DM-loaded PSA-TMC nanoparticles. To the author's knowledge, this is the first time that PSA-based nanocarriers were successfully developed and evaluated for improved drug delivery.

POLYSACCHARIDE-BASED NANOCARRIERS FOR IMPROVED DRUG DELIVERY

By

Nan Zhang
B.S. Zhengzhou University, 2009

DISSERTATION

Submitted in partial fulfillment of the requirements for the degree of Doctor of Philosophy in Bioengineering in the Graduate School of Syracuse University

August 2013

Acknowledgements

I would like to express my deepest gratitude to my advisor, Dr. Rebecca (Becky) A Bader, for providing me the opportunity and believing in my abilities as a scientist for the past four years. She gave me an excellent atmosphere to learn, think, and accomplish and also gave supportive advice countless times on my way to be a professional scientist. Because of her support, I was able to interact with other professionals in academia and industry. Under her advisement in the past four years, I have become a more confident and independent scientist. Thank you Becky.

I am grateful to have a very supportive and loving family. They provided me an atmosphere with love and peace to grow up and are always there to encourage and support me. Even they have not experienced what I was facing, they tried their best to help me make the best decisions by carefully evaluating my situation. I especially want to thank my parents for starting to teach me to be an independent and self-motivated person, and only do good things when I was a little kid. I am really grateful that my dad had spent a lot of time with me whenever I showed interests to different things, including growing plants, making clocks, boats, and water wheel, and setting up simply electric appliances. These many tiny experiences gave me strong interests and common sense to biology, chemistry, and physics.

Thanks to my laboratory mate Patricia Wardwell. There were so many times I felt I was too frustrated to continue my experiment, she was the one listened to me and helped me reach the right decision. In addition, Tricia had provided me a lot of help with my research for *in vitro* evaluation of materials.

Thanks to Pine Yang, Shiril Sivan, and Kimberly Wagoner for their help with HPLC, AFM, and cell culture. They are the ones who made my life easier. Shiril also provided me with many suggestions for my important presentations.

My gratitude goes to Wenting Ding, Dr. Bin Deng, Huan Gu, and Chen Gong for being my best friends and great companies in Syracuse. Thank you for everything you added to my life. You made my life colorful and gave me courage to keep fighting.

Thanks to the faculty members in Syracuse Biomaterials Institute (SBI) and SBI to provide such as excellent place to study and discover. Also thanks to Karen Low and Michelle Lissner for all their assistance and kindness during my study in the past three years.

Finally, thanks to all of my thesis committee members. Thank you for your time, patience, and precious suggestions and helps for my study.

I truly want to thank you all. Without you, I would not be where I am today. Thank you for your help and support.

Table of Contents

List of tables and figures

Tables and figures

Chapter 1 Introduction

Due to rapid clearance and random distribution, employment of many drugs is limited by low efficacy and non-site specific toxicity. Drug delivery provides a method to overcome the latter deficiencies. Among drug delivery systems, nanocarriers have been widely investigated because of their specific targeting to diseased tissues and potential for long circulation in human body. In this dissertation, we aimed to develop nano-sized systems based on polysaccharides with low-toxicity that could be used for the treatment of many diseases. Emphasis was given to the application of these systems to the treatment of rheumatoid arthritis (RA), a systemic autoimmune disorder. The polysaccharide polysialic acid (PSA) was used to develop nano-sized carrier systems to improve the efficacy of conventional therapeutics. PSA is a non-toxic, biocompatible, biodegradable, and non-immunogenic polysaccharide that has been found on the surface of both mammalian and bacteria cells. In prior studies reported by Gregoriadis et al, PSA had been used to extend circulation time of drugs through conjugation [1-6]. By extending the circulation time, the chance of drug accumulation at the diseased tissues was increased. Although PSA had been used for conjugation, PSA had not been used in the formation of nano-sized particulate carrier systems. We hypothesized that nanocarriers based on PSA would improve the therapeutic efficacy of conventional therapeutics used for RA and other diseases. Our goals were (1) to develop stable PSA-based nanocarriers; (2) characterize PSA-based nanocarriers in terms of size, morphology, stability, and drug loading; (3) evaluate *in vitro* potential of PSA-based nanocarriers in terms of cytotoxicity, cellular uptake, and efficacy.

To achieve the goals, this dissertation developed two PSA-based micelle systems, PSA-decylamine micelles (Chapter 3) and PSA-polycaprolactone micelles (Chapter 4), and one PSA-

based nanoparticle system, PSA-N, N, N-Trimethyl chitosan nanoparticles (Chapter 5, 6). Details about the development, characterization, and evaluation of these PSA-based nanocarriers were described in separate chapters, including synthesis, size, stability, drug loading, cytotoxicity, cellular uptake, and anti-inflammatory efficacy. At last, all studies were summarized (Chapter 7) and future research direction was discussed (Chapter 8).

Chapter 2 Background and significance

Drug delivery systems (DDSs) have been highly investigated to improve conventional treatments for diseases. Encapsulation by DDSs can endow drugs with tunable *in vivo* behavior without affecting the therapeutic efficacy. To date, DDS-based on nanocarriers have drawn much attention due to their (1) good outcome in terms of preferable accumulation in tissues with enhanced permeability and retention effect (EPR) and (2) ability to escape recognition and clearance by reticuloendothelial system (RES). Additionally, targeting moieties on these nanocarriers can further increase tissue specificity and improve efficacy. Polysaccharides, as biodegradable and biocompatible macromolecules with low immunogenicity, are ideal candidates for the development of nanocarriers. Several polysaccharides, including pullulan, dextran, chitosan, cellulose, and hyaluronic acid, have been used to prepare nanocarriers and improve treatment for diseases. Among many nanocarriers, polyethylene glycol (PEG) has been used to prolong circulation of drugs. However, usage of PEG may be limited for drug delivery by reported drawbacks, including high toxicity and frequent stimulation of immune responses. As an alternative, polysialic acid (PSA), as a polysaccharide, has functional similarity to PEG to prolong circulation and all the merits of polysaccharides. Therefore, PSA-based nanocarriers may serve as improved drug delivery systems.

2.1 Drug delivery

In the past 35 years, various drug delivery systems had been designed and commercialized based on medical needs [7]. The principle of drug delivery was to optimize *in vivo* behavior of drugs via passive targeting and active targeting. Passive targeting was a methodology to increase the ratio of drugs at desired/non-desired organs, tissues, and cells via physical and chemical interaction, such as hydrophobic and electrostatic interactions, size, and mass. As an example, tumor tissues possessed poorly organized vasculature, and macromolecules preferably extravasted at these sites due to enhanced permeability, an effect known as EPR. Therefore, many anti-tumor drug carriers were designed with EPR in mind. Active targeting was a methodology used in conjunction with passive targeting to increase drug delivery to targeted organs, tissues, and cells via biological interaction, such as antigen-antibody and ligand-receptor binding. Additionally, drug carriers could be developed with stimuli-sensitive materials. Selective delivery of drugs could be achieved only with the presence of specific stimuli, such as pH, temperature, and chemicals.

To date, the most investigated drug carriers include polymer-drug conjugates, liposomes, nanoparticles, micelles, and dendrimers. Polymer-drug conjugates were the earliest drug carriers and dated back to 1950s. Most polymer-drug conjugates could decrease drug toxicity, alter drug distribution, and increase therapeutic efficacy [8]. Liposomes were first developed in the early 1970s. Composed of a lipid bilayer, liposomes are structurally similar to cell membrane. In the past, liposomes had been extensively investigated as carrier systems of drugs and vaccines for many diseases, such as cancers and infections. Despite a prolonged retention time and improved

targeting towards tumors, liposomes had some issues, including high pre-mature leakage of drugs and undesirable activation of the immune system [9].

Micelles are self-assembled, nanosized colloidal particles with a hydrophobic core and hydrophilic shell [10]. The specialized structure makes micelles suitable carriers for poorly water-soluble drugs that account for approximately 25% of conventional, commercially available therapeutics and nearly 50% of candidates identified through screening techniques. Insoluble drugs often are characterized by poor bioavailability and rapid clearance after administration, characteristics that are associated with low therapeutic efficacy and high toxicity [11]. Micelles had been under investigation the past two decades to solve these issues [12]. Drug solubility has been greatly improved because of the hydrophilic shell of the micelle; and due to the tunable size of micelles, drugs could be directed to tissues where permeability was enhanced, particularly tumor and inflammatory tissue. Moreover, when modified by functional molecules that recognized molecular cues specific to diseased sites, micelles could achieve higher tissue specificity and cellular uptake [13, 14]. To date, numerous micelle drug delivery systems have been developed, with some achieving clinical testing. However, some concerns, including material toxicity, immunogenicity, low cellular uptake, short half-life, and tissue accumulation, have arisen [15].

Nanoparticles are colloidal particles with high stability and drug loading capacity. Nanoparticles can be used to carry water-soluble and/or less water-soluble therapeutics by varying composites of nanoparticles [16]. Similar to micelles, nanoparticles are small enough to extravasate loose blood vessels and accumulate locally. This phenomena has been demonstrated in cancer and inflamed tissues and has been used to design and develop treatments for cancer and inflammatory diseases [17].

Detailed reviews of micelle and nanoparticle systems will be provided in the following sections. Drug delivery systems can be developed based on various materials, such as metals, synthetic polymers, and natural polymers. Polysaccharides are the selected materials for drug carriers in this study because our goals are to design and develop a platform for drug delivery with low toxicity and immunogenicity.

2.2 Polysaccharides as the basis of Drug Delivery Systems

2.2.1 Merits of polysaccharides

Polysaccharides are a diverse class of polymeric materials of natural (animal, plant, algal) origin formed via glycosidic linkages of monosaccharides [18]. Dependent upon the nature of the monosaccharide unit, polysaccharides can have a linear or branched architecture. In addition to structural diversity, polysaccharides have a number of reactive groups, including hydroxyl, amino, and carboxylic acid groups, indicating the possibility for chemical modification [16]. Moreover, polysaccharide molecular weight can vary between hundreds and thousands of Daltons, further increasing diversity [19]. Herein, we will describe characteristics, including biocompatibility, solubility, potential for modification, and innate bioactivity, of several polysaccharides that lend credence to their potential for use in drug delivery systems.

2.2.1.1 Biodegradability and Biocompatibility

In contrast to many synthetic polymers, polysaccharides have very low (if any) toxicity levels [20-22]. For example, dextrans are biopolymers composed of glucose with α-1, 6 linkages, with possible branching from α-1, 2, α-1,3, and α-1,4 linkages, that exhibit low toxicity and high

biocompatibility. Consequently, dextrans have formed the basis of biocompatible hydrogels for controlled prolonged therapeutic release [23]. Likewise, dextrans have exhibited biocompatibility when they were formulated into microspheres, as suggested by a lack of an inflammatory response following subcutaneous injection into rats [24].

Also owing to their native presence within the body, most polysaccharides are subject to enzymatic degradation. Through enzyme catalysis, polysaccharides can be broken down to their monomer or oligomer building blocks and recycled for use as storage, structural support, or even cell signaling applications [25]. For example, glycosidases are common, constituting 1%–3% of the human genome [26], and can readily catalyze the hydrolysis of many different glycosidic linkages [25]. In contrast to glycosidase, other enzymes are more polysaccharide specific. Hyaluronidase, for instance, specifically degrades the polysaccharide hyaluronic acid (HA) by cleaving β-1, 4 linkages between D-glucuronic acid and D-*N*-acetylglucosamine, particularly in regions of high HA concentration [25]. Of note, some polysaccharides are particularly susceptible to degradation by lysosomal enzymes, including glycosidases, esterases, and proteases, following endocytosis [27]. For example, lysozyme, *N*-acetyl-β-D-glucosaminidase, and a range of proteases play a role in the degradation of chitosan [28, 29]. Thus, enzymatic degradation provides a mechanism of release for therapeutics associated with polysaccharide-based carrier systems [27].

2.2.1.2 Solubility

The functional groups along polysaccharide backbones, particularly hydroxyl and, to a lesser extent, amine groups, typically yield high aqueous solubility. However, this solubility can often be adjusted via monomer modification. For example, chitosan, composed of β-1, 4 linked *N*-acetyl-D-glucosamine and D-glucosamine, is prepared via deacetylation of chitin. By varying the degree of deacetylation of the parent compound, the solubility of chitosan in acidic

conditions can be tuned. Higher degrees of deacetylation correspond to an increased number of available, protonated free amino groups along the polysaccharide backbone and, consequently, enhanced solubility [30]. Likewise, *O*-acetylation of glucomannan, a polysaccharide formed via β-1, 4 linkage of D-mannose and D-glucose, can be used to modulate the formation of intermolecular hydrogen bonds with water, thereby altering aqueous solubility [31].

2.2.1.3 Ease of Modification

Polysaccharides are extremely amenable to modification. For example, glucose-based polysaccharides, such as amylose, amylopectin, glycogen, and cellulose, offer an abundance of free reactive hydroxyl groups [15]. Other polysaccharides possess both hydroxyl and carboxylic acid moieties that can be readily modified. For example, a review was recently published focusing on the derivatization of alginate, a polysaccharide composed of β-D-mannuronic acid and α-L-guluronic acid with 1,4 linkages. Alginate modification can be used to give rise to a variety of different physiological behaviors. For instance, hydroxyl group oxidation enhances biodegradability, while sulfonation generates a heparin-like polysaccharide with increased blood compatibility (see Section 2.4.1.5 for additional details on heparin) [32]. Modification of chitosan has also been extensively reviewed. Specifically, quaternization of the primary amines with various alkyl groups can be used to enhance solubility and alter bioactivity [33-35].

2.4.1.4 Bioactivity

Many polysaccharides possess innate bioactivity, particularly mucoadhesive, antimicrobial, and anti-inflammatory properties. Mucoadhesion refers to the interaction of a material with a mucosal layer, such as in the gastrointestinal (GI) tract, nasal pathway, or airway. Chitosan, the only natural, positively charged polysaccharide, is capable of binding to the

negatively charged mucosal layers through charge interactions [36-38]. Thus, numerous investigators have explored the use of chitosan for oral drug delivery. For neutral or negatively charged polysaccharides, such as HA, hydrogen bonding provides an alternative mechanism for mucoadhesion [39]. Several polysaccharides are also antimicrobial in nature. The cidal effects of chitosan, for example, are presumed to be due to a strong interaction of the protonated amines with the negatively charged bacterial cell wall [40]. Other polysaccharides are known to reduce inflammation. For instance, heparin, which is composed of repeating disaccharides of β-D-glucopyranosiduronic acid or α-L-idopyranosiduronic acid linked to *N*-acetyl or *N*-sulfo-D-glucosamine, has the strongest negative charge of any polysaccharide, which enables interaction with a variety of proteins. Thus, anti-inflammatory activity is thought to be due to binding with immune-related acute phase and complement proteins [37, 41]. In addition, heparin can bind to the lysine-rich region of anti-thrombin, thereby catalyzing the inhibition of blood clotting [42, 43].

2.2.2 Polysialic acid

Among polysaccharides, polysialic acid (PSA) is especially interesting. PSA is a linear homopolymer of α-2, 8-linked 5-N-glycolyneuraminic acid (Neu5Ac) with high water solubility and biocompatibility as well as low toxicity and immunogenicity. PSA is produced by pathogenic bacteria, as well as mammalian cells. Studies have shown that PSA was highly involved and had multifarious roles in a wide variety of biological, immunological, and pathological processes [44-47]. In pathogenic bacteria, a thick PSA coating was found on the cell surface, which allowed the bacterial easily evade host. Further studies found that the hydrophilic PSA coating was resistant to bindings of proteins and adhesion of immune cells, therefore,

endowed pathogenic bacteria with stealth properties in the physiological environment [48]. In mammals, production of PSA on cell surface can regulate the cell-cell and cell-extracellular matrix interaction and promote neutral plasticity by inhibiting cellular adhesion and migration [49, 50]. So far, no receptor for PSA has been reported in human body. The latter property has inspired Gregoridadis et al. proposed PSA as an anti-adhesive material with the potential to prolong drug circulation [1]. A series of studies were conducted. Improved stability and prolonged half-life were noticed in the polysialyated insulin [6], asparaginase [4, 5], and catalase [2, 3]. In addition, reduced immunogenicity and antigenicity of these exogenous proteins were observed with PSA conjugation. Therefore, PSA was concluded to form the "watery cloud" around proteins and to protect them from degradation and clearance [51, 52]. However, to the authors' knowledge, PSA has not been used to prepare nanocarriers, such as micelles and nanoparticles, formulations that may provide improved drug delivery. Therefore, PSA has much potential that needs to be fully explored for nanocarrier-based drug delivery.

2.2.3 Progress of Polysaccharide-Based Nanoparticle and micelle Systems for improved Drug Delivery

Early clinical results suggest that micelles and nanoparticles should be designed and developed with careful attention towards material selection. Ideally, micelles and nanoparticles developed for drug delivery should be biodegradable and should have high stability, high biocompatibility, and low immunogenicity. Natural polysaccharides meet the latter requirements and can be used to develop micelles and nanoparticles in lieu of synthetic polymers. In addition, polysaccharides can be readily modified and exist in positive, negative, or neutral charge states. Finally, some polysaccharides are bioactive and can be used to augment the therapeutic efficacy

of an associated drug or can enhance the targeting ability of a carrier system [32, 53]. Despite these advantages, polysaccharide-based micelle and nanoparticle systems are still under development and the outcomes have not met the clinical need. Here in, we will: (1) provide a more detailed depiction of the advantages offered by polysaccharides; (2) discuss the progress that has been made towards the application of polysaccharide-based micelles and nanoparticles to drug delivery; and (3) offer suggestions for future research to expedite translation of polysaccharide-based drug delivery systems from the laboratory to a clinically relevant setting.

2.2.3.1 Passive targeting delivery systems

Several polysaccharides have been used to develop micelles and nanoparticles for drug delivery. The structures of commonly used polysaccharides are given in Figure 1. The numerous functionalities along backbone of polysaccharides facilitate attachment of hydrophobic moieties and reaction with other composition that can be used to initiate self-assembly to micelles and form nanoparticles, respectively. The most prevalent hydrophobic groups used in micelle formation are provided in Table 1.

2.2.3.1.1 Pullulan-Based Systems

Pullulan is a water-soluble, neutral, non-toxic bacterial exopolysaccharides [54]. Since Akiyoshi et al. first reported cholesterol-bearing pullulan (CHP) as a self-aggregated colloidal system with high stability [55, 56], numerous studies related to or based on CHP have been carried out. In the original report, CHP was synthesized by grafting 1.6 cholesterol groups to every 100 glucose units on pullulan (M_w 55,000 g/mol, M_w/M_n = 1.54) in a random manner. The average hydrodynamic radius of CHP self-aggregates was measured by dynamic light scattering (DLS) and determined to be 13.3 nm. Morphology studies by negatively stained transmission

electron microscopy (TEM) confirmed that CHP can self-aggregate as spherical particles with relatively uniform size.

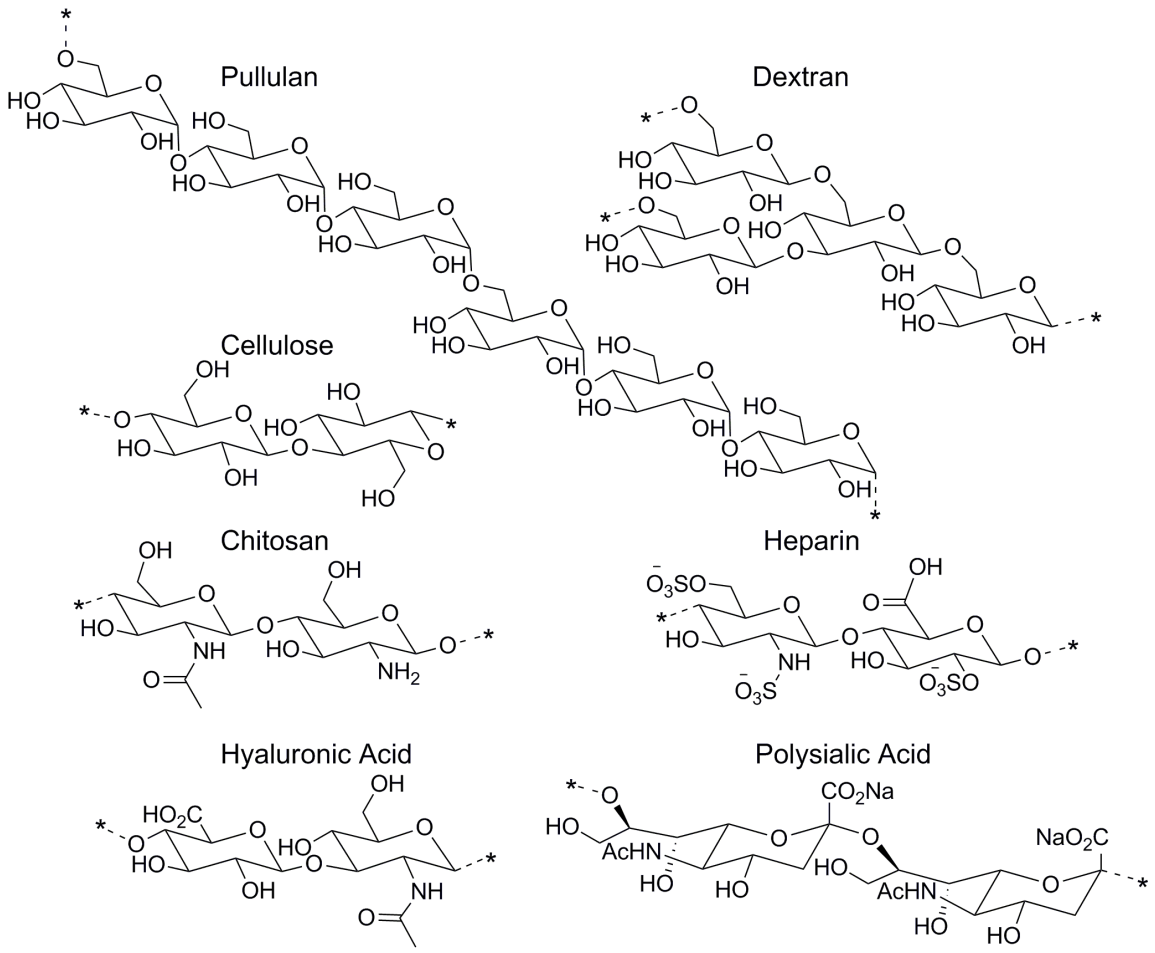

Figure 1. Structures of polysaccharides that are used in the development of micelle drug delivery.

Further studies via size exclusion chromatography (SEM) and ^{1}H-NMR provided information that one CHP self-aggregate was composed of approximately 13 CHP molecules and that these molecules formed a rigid hydrophobic cholesterol core with a relatively mobile pullulan shell. More importantly, CHP self-aggregates revealed very high colloidal stability [56] and have since been investigated as a way of protecting proteins from the physiological environment.

Studies have shown that CHP self-aggregates can be loaded with insulin with high binding constant (K=2x10^6 M), thereby protecting the entrapped protein from thermal denaturation and enzymatic degradation [57, 58].

More recently, CHP has been further modified to form more complex drug delivery systems for higher demand. For example, CHP cross-linked hydrogels with thiol-bearing PEG [59] and CHP cross-linked membranes (diameter 6mm, thickness 0.4mm) [60] have been used for critical bone defect treatment. Results showed that the crosslinked CHP membrane could stimulate and promote bone regeneration with an improved outcome relative to a control, collagen membrane [60]. Moreover, the CHP crosslinked hydrogel was successfully used to co-deliver recombinant human bone morphogenetic protein 2 and fibroblast growth factor 18 (FGF 18) to induce enhanced bone repair [59]. CHP has also be used to deliver vaccines [61], anti-tumor agents [62, 63], and wound healing agents with improved solubility and stability. Of note, blank CHP, i.e. CHP used in the absence of additional therapeutics, showed a positive effect on wound healing compared to control [64].

Other pullulan based-micelle systems include pullulan acetate [65], poly(DL-lactide-co-glycolide)-graft pullulan [66], pullulan-g-poly(L-lactide) [67], and pullulan hydrophobic drug conjugates, such as pullulan-doxorubicin (DOX) [68] and pullulan-biotin [69]. These systems were mainly investigated in regards to chemical synthesis, physicochemical characterization, and drug release. To elucidate the potential of these systems for drug delivery, additional studies should focus on the interaction of the micelles with cells, tissues, and living systems.

Table 1. Names and structures of hydrophobic moieties used in the development of polysaccharide-based micelle drug delivery systems. Functional groups used for grafting onto polysaccharides are highlighted in red.

Name	Structure	References
Cholesterol	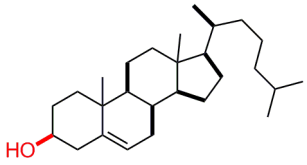	[55, 56, 70]
Cholic Acid	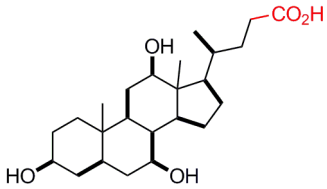	[71, 72]
Deoxycholic Acid	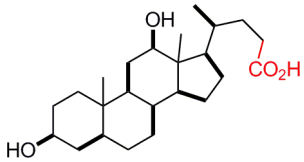	[71, 73, 74]
Poly(lactide)	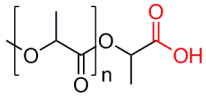	[67, 75]
Poly(lactide-co-glycolide)	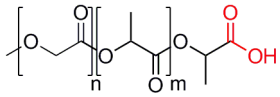	[66]
Pluronic	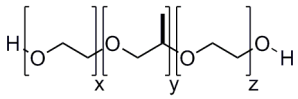	[76]
Polycaprolactone	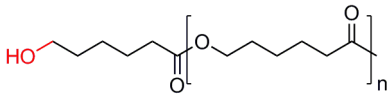	[77]
Stearic Acid	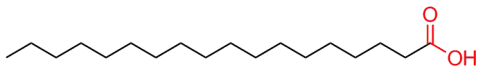	[71]

Nanoparticles have been formed by complexing sulfated and aminated derivatives of pullulan with oppositely charged chitosan and carrageenan, respectively [78]. These nanoparticles had a size of 180-270 nm and were able to associated with a model protein, bovine serum albumin (BSA), for eventual use in transmucosal delivery.

2.2.3.1.2 Cellulose-Based Systems

Cellulose is the most abundant naturally occurring polysaccharides and its derivatives have been widely used in the pharmaceutical field. For example, hydroxypropyl cellulose (HPC) was produced by modifying some of the cellulose hydroxyl groups with propylene oxide to improve the cellulose solubility and control drug release [79]. To improve the oral delivery of hydrophobic drugs, which often have poor bioavailability after administration, Winnik et al. further modified HPC with hydrophobic polyoxyethylene hexadecyl (C_{16}) or octadecyl (C_{18}) group ester $(POE)_{10 \text{ or } 20}$-$C_{16 \text{ or } 18}$. With five hydrophobic molecules per HPC chain, the critical micelle concentration (CMC) was 65-135 mg/L while with ten hydrophobic chains, the CMC dropped to 15-22 mg/L. Cyclosporin A (CyA), a poor water-soluble immunosuppressant, was used as a model drug in this study. With lower hydrophobic modification, the maximum loading was 0.025 mg CyA/mg micelle, while, as anticipated, with higher modification, the loading capacity increased to 0.067 mg CyA/mg micelle. With the same quantity of hydrophobic moieties, PEO-C_{16} provided an improved solubilizing environment for CyA relative to PEO-C_{18}. With the encapsulation of CyA, the polymeric micelles size dropped from 78-90 nm to 44-74 nm. Presumably, the encapsulation of CyA enhances the hydrophobic interactions in the core and produces more compact particles. *In vitro* studies showed HPC-PEO-C_{16} micellar system had high affinity to mucus and could enhance the permeability of entrapped therapeutics across

intestine epithelial-Caco-2 cells [80-82]. These studies demonstrated the great potential of HPC-based micelles for improved oral delivery of hydrophobic molecules.

Other work has focused on the design and synthesis of cellulose-based micelles; however, how these systems can be applied to the field of drug delivery has not yet been described. Such systems include HPC-polycaprolactone [83] and cellulose-C_{15}-pyrene micelle. Of interest, micelles prepared from cellulose-C_{15}-pyrene with longer cellulose chains (M_w = 4860 g/mol, number average degree of polymerization (D_n) = 30) were smaller in size (~40.0 nm, monolayer micelle) relative to those prepared from short chain cellulose (M_w = 2106 g/mol, Dn = 13) (~108.8 nm, multilayer micelle) [84].

Cellulose has also been used to form gel nanoparticles. Thiolated hydroxyethyl cellulose was reacted with tripolyphosphate (TPP) and covalently crosslinked via a disulfide bond formation using H_2O_2 as oxidant. These nanoparticles were 270-360 nm and were able to help drug absorption across the mucosa intestines [85].

2.2.3.1.3 Dextran-Based Systems

Dextran is another polysaccharide that has long been used in drug formulation and has shown no toxicity [86]. For this reason, Winnik et al. conducted a series of studies on dextran-based micelles for CyA oral delivery that were nearly identical to the experiments conducted for modified CHP. Similar to HPC-PEO-C_{16}, they demonstrated dextran-PEG-C_{16} had a higher loading capacity of CyA relative to dextran-PEG-C_{18} (0.048 vs. 0.03 mg CyA/ mg micelle), although the dextran-based systems yielded higher loading capacities overall compared with the HPC-based systems. The size of dextran-PEG-C_{16} was very small (9 ± 0.3 nm), and CyA loading did not significantly affect micelle size (10 ± 0.3 nm). Although not yet tested, this small size may limit future in vivo applications. Dextran-PEG-C_{16} showed no toxicity to Caco-2 cells after

4 h of exposure, although free PEG-C_{16} did inhibit cell growth [87]. Additional in vitro studies demonstrated that dextran-PEO-C_{16} could significantly improved CyA permeability across Caco-2 cells, although the improvement was lower than that achieved by CyA loaded HPC-PEO-C_{16} [82] and, unlike HPC-PEO-C_{16}, dextran-PEO-C_{16} showed no affinity to mucus [81]. To improve the relative low transport efficiency, vitamin B_{12} was conjugated to the micelle and the vitamin B_{12}-dextran-PEO-C_{16} showed increased transportation of CyA across the Caco-2 monolayer and internalization of CyA by Caco-2 cells via the vitamin B_{12} pathway [88].

Another highly investigated system is dextran-cholic acid. Cholic acid is one of the major bile acids that help to deliver and digest hydrophobic fats in the human small intestine via bile acid self-aggregates. Early dextran-cholic acid systems had low stability, as indicated by a high CMC value (0.02-0.2 g/ml) [73]. Improved systems were developed by Yuan et al. [89] and Xu et al. [90] based on periodate-oxidized dextran which possessed free aldehyde and hydroxyl group that were used to form hydrogen bonds to increase system stability. Moreover, the micelles served as good depots for the hydrophobic drug indomethacin (~0.299 mg drug/ mg micelles) and showed sustained release up to 14 days at acidic and neutral condition. More recently, dextran sulfate-cholic acid was investigated to deliver superoxide dismutase (SOD) orally. SOD-loaded dextran sulfate-cholic acid had a high stability against the acidic environment of the stomach and release in the small intestine was controlled up to 100 hrs. Moreover, dextran sulfate-cholic acid facilitated SOD cellular uptake, suggesting that cholic acid enhanced the interaction of micelles with the intestinal membrane [72]. Additional dextran-based micelles have been synthesized by grafting of polycaprolactone [91], poly (L-lactide) [75], polystyrene [92], lauryl group [93], and methyl methacrylate-ethylene glycol dimethacrylate [94] to the dextran backbone.

Dextran is a FDA-approved material and has long been used as blood plasma expander. Due to existing FDA approval, dextran is also an attractive polysaccharides for gel nanoparticles. Dextran was chosen by Morgen et al. as the core for a cationic nanoparticle system. The nanoparticles were prepared by emulsion method and were injected into the knee joint. Due to the positive charge, nanoparticles had enhanced retention after injection by attaching to the anionic hyaluronate in the knee joint. Results showed that 70% of nanoparticles was retained in the knee joint for 1 week after injection [95]. Another study reported that PEGylated dextran nanogels might be a suitable carrier for siRNA as they did not aggregate in human plasma and exhibited reduced interactions with blood cells [96]. Dextran-based nanoparticles were also developed via a phase separation method with another FDA-approved material, gelatin. These nanoparticles were able to carry and release vascular endothelial growth factor (VEGF) in a sustained manner to induce angiogenesis [97].

2.2.3.1.4 Chitosan-Based Systems

Chitosan and its derivatives have been the most widely investigated material for drug delivery due to the superior properties. To improve delivery of hydrophobic molecules, many studies have focused on chitosan-based micelle systems. Most of these core-shell systems were developed by modifying chitosan with hydrophobic moieties that include stearic acid [98-102], (deoxy)cholic acid [71, 103-105], glucyrrhetinic acid [71, 106], polycaprolactone [77, 107], etc. Self-assembly of the modified chitosan can lead to the formation of spherical micelles with a size range of 20-500 nm in aqueous solution. Higher hydrophobic moieties modification percentage usually gives rise to a smaller micelle diameter due to stronger hydrophobic interactions. Various anti-tumor therapeutics such as paclitaxel (PTX) [98, 107-109], doxorubicin [71, 104, 105, 110-112], and camptothecin [113], have been used as model drugs and encapsulated by chitosan-

based micelles. The chitosan-based micelles improved the solubility of the hydrophobic drugs significantly. Moreover, the micelles showed controlled or sustained release of the hydrophobic drugs, and the release rate was tunable by the degree of substitution (DS) of the hydrophobic moieties of the micelles. Higher DS usually indicated slower drug release despite insignificant changes in the loading efficiency. The therapeutic-loaded micelles showed significantly higher toxicity to tumor cells in vitro compared to free drugs due improved drugs internalization.

Due to the muco/bioadhesive nature of chitosan, chitosan-based micelles have been used extensively to improve the oral drug delivery. Evaluated by a Caco-2 cell monolayer, chitosan-based micelles were demonstrated to inhibit the activity of P-glycoprotein 1 (P-gp) ATPase, which, consequently, can inhibit drug efflux and enhance drug permeation [101, 108]. Moreover, the chitosan opened the tight junctions between cells and further enhanced drug absorption. The chitosan-based micelles were characterized by low CMCs, suggestive of high stability [114] and resistance to the harsh environment of the GI tract. In vivo studies showed that N-octyl-O-sulfate chitosan can improve the oral bioavailability of TPX by 6 folds compared to the current commercially improved formulation-Taxol (Bristol-Myers Squibb, New York, NY) [108]. Additionally, chitosan-based micelles were demonstrated to be a relatively safe carrier for oral formulation [115]. Chitosan-based micelle systems have also been investigated for applications in antivirus [100], anti-thrombogenicity [116], and antiplatelet aggregation [114].

Chitosan is also a popular material for nanoparticle preparation due to its positive charge. Chitosan-based nanoparticles have been fabricated via ionic gelation. For example, surfactant Lipoid S100-coated chitosan and glycol chitosan nanoparticles were prepared for systemic delivery of low molecule weight heparin (LMWH) via the pulmonary route [117] while acyclovir-loaded chitosan nanoparticles [118] and chitosan-dextran sulfate nanoparticles [119]

were designed for ocular delivery. These studies showed positive results, including efficient delivery of LMWH to the blood stream via pulmonary aerosolization as compared to free LMWH and increased residence time of nanoparticles on the ocular surface due to mucoadhesion. Another study reported that with addition of a pH-sensitive component, methotrexate-loaded chitosan nanoparticles could be developed with greater cytotoxicity in acidic tumor environment [120]. Further investigation of chitosan-based nanoparticles as an anti-tumor delivery system was conducted by W Wei et al [121]. Telomerase reverse transcriptase (mTERT) siRNA and paclitaxel (PTX) were co-encapsulated into chitosan nanoparticles via Oil/Water/Oil double emulsion method. These nanoparticles were 130-140 nm and had a narrow size distribution. siRNA-loaded chitosan nanoparticles showed improved intestinal absorption and enhanced tumor cellular uptake. Moreover, chitosan nanoparticles were able to simultaneously transport mTERT siRNA and PTX into tumor cells, and this formulation achieved synergistic effects that were much more effective than the traditional cocktail therapy.

2.2.3.1.5 Heparin-Based Micelle Systems

Heparin is a polysaccharide that has a variety of biological functions, such as anticoagulant activity, inhibition of angiogenesis and anti-tumor development [122, 123]. Therefore, several studies have focused on heparin-based micelle systems for improved cancer treatment. Pluronic block copolymer, composed of hydrophilic poly (ethylene oxide) (PEO) and hydrophobic poly (propylene oxide) (PPO) in triblock structure: PEO-PPO-PEO, can improve oral availability of hydrophobic drugs by increasing the solubility and permeability while inhibiting the activity of P-gp mediated drug efflux and cytochrome P450 metabolism [124, 125]. To develop oral anti-tumor formulation, heparin-pluronic micelles were developed to improve drug absorption. These systems showed proper diameter for tumor accumulation and

high loading efficiency for PTX and RNase A, an anti-tumor protein. The therapeutic-loaded heparin-pluronic micelles showed 5-6 folds higher permeability through rat intestines relative to the clinical PTX formulation, Taxol [76, 126]. Oral availability was also improved by grafting deoxycholic acic to low molecular weight heparin. Deoxycholic acid-heparin micelles possessed a diameter of 100-200 nm and were absorbed in the small intestine via a bile acid transporter, as shown with a nude mouse model [74, 127]. Other micelle systems included heparin-PTX [128, 129] and heparin-photosensitizer [130].

2.2.3.1.6 Other polysaccharide-Based Micelle Systems

One important advantage of polysaccharides is their large diversity of biological functions. Advances of polysaccharide research have provided more candidates as potentially functional biomaterials. In addition to the most investigated polysaccharides described above, several other polysaccharides have also been used to develop micelle systems. Polysialic acid (PSA), in particular, is a non-toxic polysaccharide that can be used to protect and increase body circulation of therapeutics and has been developed into micelle systems for the delivery to inflamed tissue. Using CyA as a model drug, a high loading capacity was achieved and CyA-loaded micelles showed high uptake by inflamed synovial fibroblasts (unpublished data) [131]. Alginic acid-PEG showed very significant enhancement of hypocalcemia efficacy in rats after intraduodenal administration and can improve the oral absorption of salmon calcitionin via alginic acid-PEG facilitated transcytosis across Caco-2 cells [132]. Mannan based-micelle systems with high stability were developed by grafting cholesterol [133] or hexadecanethiol (C_{16}) [134, 135] to mannan. In addition, Modolon et al. have led an investigation of maltoheptaosyl-based micelles composed of hydrophilic maltoheptaosyl and hydrophobic peracetylated maltoheptaosyl [136]. The all polysaccharide micelles are expected to exhibit better properties and functions.

2.2.3.2 Active targeting delivery systems

2.2.3.2.1 Hyaluronan-Based Systems

HA is bioactive in that it can bind to the CD44 receptor that is overexpressed in tumor and inflammatory tissues. Thus, HA has been investigated as an active targeting agent in drug delivery for enhanced efficacy. Most recent HA-based micelle systems have focused on cancer treatment with DOX [137-140], PTX [141-143], siRNA [144], and curcumin [145]. These systems possessed high physiological stability and a diameter range of 100-200 nm, which is expected to facilitate passive accumulation of the micelles in the tumor. HA-based micelles showed significantly higher cellular uptake by a CD44 overexpressed cancer cell line compared to that of CD44 negative cell line, NIH3T3 [138]. Moreover, by blocking the CD44 receptor with free HA molecules, cellular uptake of HA-based micelles was significantly decreased [137, 139]. Therefore, HA-based micelle systems were demonstrated as potential systems for improved drug efficacy via CD44-mediated endocytosis. To further improve targeting, folic acid, another active targeting agent was conjugated to HA and higher cellular uptake was observed with folic acid-HA-octadecyl group compare to that of HA-octadecyl group [142]. However, due to the high affinity of HA to liver sinusodidal endothelial cells that have another HA receptors (HARE), HA-based micelles have a high propensity for accumulation in the liver after systemic administration. To improve this, PEG was conjugated to HA-5 beta-cholanic acid and liver accumulation of micelles was significantly suppressed, while the tumor accumulation was increased to 1.6 folds. Intravital tumor imaging also confirmed PEG-HA-5 beta-cholanic acid had rapid extravasation into tumor tissue [146].

In addition to sufaced-modified micelles, HA-based nanoparticles have been widely investigated for anti-tumor delivery [147], ocular delivery [148, 149], and transmucosal delivery

[150]. HA-based nanoparticles could be formed by reaction with chitosan or its derivatives. The size of HA-chitosan nanoparticles was tunable between 300-600 nm by varying HA: chitosan ratio. These nanoparticles showed an efficient loading of both bovine serum albumin (hydrophilic molecule) and cyclosporine A (hydrophobic molecule) [150]. Additionally, significantly better tolerance of cisplatin-loaded HA-chitosan nanoparticles was reported compared to cisplatin alone during tumor treatment for mice [147]. Moreover, plasmid DNA-loaded HA-chitosan nanoparticles provided high transfection levels (up to 15% of cells were transfected) to cornea and conjunctiva cells via hyaluronan receptor CD44-mediated fluid endocytosis [148, 149].

2.2.3.2.2 Active Targeting Agents

Micelles and nanoparticles with proper size, charge, and shape facilitate improved delivery. However, this may not be enough because of the defenses of human body. To enhance target site accumulation and uptake, additional targeting agents are often incorporated into the micelle systems. Active targeting agents used in polysaccharide-based micelles and nanoparticles can be divided into three categories: peptides, small molecules, and polysaccharides. Peptides include octreotide targeting for the somatostatin receptors on tumor cells [104, 151], the A54 hepatocarcinoma binding peptide [102], and Arg-Gly-Asp (RGD) containing peptide for $\alpha_v\beta_3$ and $\alpha_v\beta_5$ integrins [152, 153]. Small molecules include glycyrrhetinic acid, a liver targeting ligand [71, 106], vitamin E succinate-specific toxicity to tumor cells [109], and folic acid with a high affinity to the folate receptor overexpressed on tumor cells [98, 103, 130, 142, 154-156]. Through peptide and small molecule conjugation, micelle systems have shown higher tumor accumulation and cellular uptake relative to blank micelles. Moreover, polysaccharides themselves can act as active targeting agents due to their bioactivity. As described above, HA

has a high affinity to the HA receptor on the liver sinusoidal endothelial cells and the CD44 receptor that is overexpressed on the tumor cells and inflamed synovial fibroblast. Therefore, HA has been highly investigated as an active targeting agent to tumor tissue or liver with many micelle systems. In addition, heparin-based micelles have demonstrated enhanced inhibition of tumor growth and angiogenesis, while cellulose, chitosan, and pullulan-based systems promoted drug absorption across the small intestine due to enhanced mucoadhesion.

2.2.3.3 Multifunctional delivery systems

2.2.3.3.1 Stealth Coating

To achieve high therapeutic efficacy, therapeutics must have a long circulation time in the body to ensure that an effective concentration at the target site is achieved. However, free drugs and many carrier systems bind to plasma proteins and are rapidly cleared. To minimize clearance and prolong the circulation, PEG has been conjugated or coated to many micelle systems. For example, studies have shown that PEG protected octyl-succinyl-chitosan from plasma protein absorption [151] and that PEG modification could prolong HA-ceramide circulation [138]. Moreover, PEG could inhibit liver uptake of HA-conjugated micelles, thereby increasing the systemic circulation [146].

Despite the demonstrable improvements relative to unmodified systems, there are potential drawbacks of PEG usage, such as the non-biodegradable PEG backbone, continuous accumulation in the body, and possible induction of an immune response [48, 157, 158]. In addition, the PEG coating may interfere with cellular uptake of drugs because PEG has been reported to reduce drug-cell interaction and to hinder the drug release from carrier systems [159-161]. As an alternative, other molecules that are hydrophilic, biodegradable, non-toxic, and non-

immunogenic have been sought. For example, polysialic acid (PSA) meets all of the latter criteria and, of equal importance, PSA has no known receptors in the human body, suggesting the possibility for further improvement in circulatory stability. Gregoriadis et al. have investigated a series of PSA-protein conjugate and shown prolonged circulation of insulin [6], asparaginase [4, 5], and catalase [2, 3]. Recently, Bader et al. synthesized PSA-based micelle systems for future applications in drug delivery[131].

In another study, a cationic polysaccharide nanoparticles showed stealth behavior after loading of an anionic molecule-dipalmitoyl phosphatidyl glycerol (DG) and a polyanionic molecule-BSA. The authors reported DG and BSA-loaded nanoparticles had comparable anti-adhesive property with long chain PEG because of neutralization of surface charge by DG and BSA [162].

2.2.3.3.2 Stimuli-Sensitive Systems

Stimuli-sensitive systems can provide more controllable drug delivery with better efficacy. Based on the solution to gel phase transition properties of polymer, thermo-sensitive systems have been developed. For example, Kim et al. reported an injectable, low molecular weight methylcellulose-pluronic gel/micelle system that was a solution at 25°C and gel at physiological temperature. The solution phase is expected to facilitate injection, while the gel phase was demonstrated to sustain drug release for approximately 3 weeks [163]. Likewise, a pullulan-based micelle system contained thermo-sensitive poly (L-lactide) that gelled at 42°C. Gelation induced additional anti-cancer drug release and, consequently, better inhibition of tumor cell growth [67].

pH-sensitive system have also been developed. Several intracellular structures, particularly endosomes and lysosomes, are characterized by a low pH. In addition, tumor and

inflamed tissue often possess a pH that is slightly lower than normal (6.5-7.2). Thus, by developing pH-sensitive systems, premature leakage of drugs from the micelles can be reduced and maximum drug release can be achieved at the target site. To date, almost all such systems have been developed for tumor treatment. Selective release at the tumor site is accomplished by incorporating various moieties with hydrophobic and electronic interactions that change with pH [105, 139, 151, 164, 165].

Additional, chitosan-heparin nanoparticle system was stable in gastric acid of the gastric lumen and was able to adhere and infiltrate into the mucus layer of the gastric tract while unstable in neutral pH [166]. This system could be used to protect drugs from digestion of gastric tract and to release drug in target sites.

Chemical signals can also provide a method for site-specific drug release from micelles. For instance, glutathione (GSH) concentration in tumor cells is 4 folds higher than in mammalian cells and 3 orders higher than in plasma. The high concentration of GSH in tumor cells can attack the unsaturated and disulfide bonds that exist within macromolecules and facilitate degradation or other structural changes. Therefore, polysaccharide-based micelle systems that contain these sensitive bonds (so called “redox (reduction-oxidation)-sensitive systems”) have been investigated for tumor targeting and intracellular efficacy enhancement. As an example, a negligible amount of pro-drug was released from carboxymethyl chitosan-based micelles without GSH and at low concentrations of GSH; however, 75% of the conjugated drug was released with the presence of GSH at 20 mM [167, 168]. Likewise, Li et al. led a study of redox-sensitive micelles, specifically HA-deoxycholic acid conjugates that were loaded with PTX for tumor targeting. At GSH 20 mM, the micelles underwent fast disassemble and released the PTX into the cancer cells. The redox-sensitive, PTX-loaded HA-based micelles showed higher tumor

targeting capacity and more potent efficacy towards cancer cells compared to an insensitive control [141]. Heparin-pluronic-based micelles that are responsive to high GSH concentrations have also been developed [152].

Although not well explored, evidence suggests that photosensitive polysaccharide-based micelles may serve as functional, smart materials in drug delivery. Modification of pullulan with spiropyrane yielded hydrophobized polysaccharide that self-assembled into micelles. The amphiphilicity of the spiropyrane core was modulated through irradiation with visible light, which consequently impacted the interaction and release of associated proteins [105, 107]. Similarly, release of model compounds from micelles formed from azobenzene-dextran was controlled through exposure to UV-Vis light [169].

2.3 Drug delivery systems for the treatment of rheumatoid arthritis (RA)

2.3.1 RA

RA is a chronic autoimmune disease with a general prevalence around 1% [170]. RA patients experience chronic joint pain and swollenness in the initial stage and cartilage destruction and bone absorption in the late stage. In severe RA cases, irreversible impair occurs to multiple organs and the life span is shortened [171, 172]. Despite much research, causes of RA are unclear. Current understandings are that RA may be initiated by an interplay of genetic factors, sex hormones, infectious agents, and/or immune activating agents [173]. RA joints are characterized by inflammation, synovial hyperplasia, and abundant immature blood vessel

formation. Common treatments are disease-modified anti-rheumatic drugs (DMARDs), non-steroidal anti-inflammatory drugs (NSAIDs), glucocorticoids (GCs), and biological agents. These treatments are all associated with severe side effects, including infection, osteoporosis, hypertension, lung fibrosis, liver damage, and kidney failure. These adverse consequences of the drugs are caused by poor affinity to the inflamed joint, metabolism in the liver, and quick excretion from the kidney. In clinical practice, rheumatologists usually prescribe combinations of these treatments, which may increase the risk of side effects.

2.3.2 Drug Delivery for RA

The leaky vasculature can be exploited for delivery of drug-loaded nanocarriers. Encapsulation endows the drugs with an increased size from 1-10 nm to 50-150 nm. The larger size increases the chance of accumulation in the diseased tissue and reduces the likelihood of clearance by RES. Moreover, the RA synovium undergoes a series of abnormal metabolic changes, including over-expression of certain cell surface proteins and receptors that can be used as targets for delivery. Drug delivery techniques will not change the structure of drugs, however, *in vivo* behavior will be modified in hopes of improving efficacy of treatment and minimizing side effects.

To treat RA, several macromolecular conjugate formulations have been developed. For example, human bovine serum-MTX conjugates showed increased accumulation in the inflamed paw of arthritic mice and could suppress secretion of pro-inflammatory proteins [174, 175]. Another conjugate was based on pH-sensitive N-(2-hydroxypropyl) methacrylamide (HPMA) copolymer and dexamethasone (DM) [176]. When HPMA-DM was administrated systemically in an adjuvant-induce arthritis rat model, HPMA-DM showed long lasting anti-inflammatory

effect relative to free DM. Better bone and cartilage preservation of rats were also observed. In addition, maximum release of DM was achieved in the acidic arthritic joints.

Liposomes are the most frequently used drug carriers and some liposomal formulations have been approved for marketing [177, 178]. MTX-loaded liposomes showed a prolonged retention time in the joint [179, 180] and liposomal corticosteroids were effective as a 10-fold higher dose of free drug in rat adjuvant-induced arthritis (AIA) and murine collagen-induced arthritis (CIA) [181]. In addition, PEGylated liposomes have also shown prolonged body circulation and tissue retention [182-184]. However, further studies have shown that liposomes possessed low physicochemical stability, a high likelihood for drug leakage, and a propensity in liver and spleen [181, 185]. More stable carriers are needed to achieve the goal of safe and targeted delivery.

Nanoparticles have good stability and a high drug loading. To date, investigators have used nanoparticles to deliver anti-rheumatic drugs, and positive results were reported, including reduced inflammation, improved efficacy, and higher specificity. Examples of nanoparticle systems included betamethasone sodium phosphate loaded PLGA nanoparticles,[186] IL-1 receptor antagonist (IL-1Ra) loaded chitosan-folate nanoparticles [187], anionic photosensitizers loaded chitosan-hyaluronate nanoparticles [188], and sterically stabilized micelles decorated with vasoactive intestinal peptide[189].

The future of drug delivery for RA will be passively targeted drug carriers with active targeting agents based on stealth and stimuli-sensitive materials to achieve optimal drug delivery based on the needs of diseases.

2.5 Summary

Drug delivery has provided a method to optimize drug administration and disease treatment. However, the demand for new, innovative drug delivery and technology remains. Ideal drug carriers act to protect drugs from degradation and clearance, while allowing drugs to arrive and release at target sites. Polysaccharides are good candidates for drug carriers because of their good solubility, high biocompatibility, low immunogenicity, stealth properties, muco-adhesion, ease of modification, etc. Although much research of polysaccharide-based drug delivery systems has initiated, advanced multifunctional systems are needed due to the complexity of diseases and the many barriers in human body. RA was selected as the primary disease model for our studies based on the paucity of research on RA drug delivery. This chapter has highlighted the advantages of polysaccharide as the basis for drug delivery systems and has provided an overview of the polysaccharide-based micelles and nanoparticles that have been developed to date. In subsequent chapters, we will describe the work we have done in the field of polysaccharide-based nanoparticles and micelles for RA treatment.

Chapter 3 Polysialic Acid-Based Micelles for Encapsulation of Hydrophobic Drugs

Despite improvements relative to unmodified counterparts, poly (ethylene glycol) (PEG) conjugation may not be the ideal solution for improving circulatory stability of current nanoparticle carriers or free drugs. Polysialic acid (PSA), a natural polymer for which the body possesses no receptors, has been conjugated directly to biologically active molecules to prevent premature clearance; however, this concept has not yet been applied to nanoparticle drug carrier systems. In the current study, PSA was modified with a long-chain hydrocarbon through reaction of the carboxylic acid side groups with *N*-decylamine (DA). The resultant PSA-DA conjugates self-assembled into micelles for encapsulation of hydrophobic drug molecules, as demonstrated with Cyclosporine A. Cytotoxicty was dependent on the degree of substitution with DA. On the basis of size and zeta potential, the micelles are capable of passively targeting diseased regions, such as cancer and inflammatory tissue. Further investigations are necessary to explore whether the PSA-based micelles possess stealth properties similar to those of PEG and to establish *in vitro* and *in vivo* efficacy.

3.1 Introduction

Poly (ethylene glycol) (PEG) conjugation has customarily been used to improve the circulatory stability of free drugs, as well as nanosized drug delivery systems [190-194]. However, despite improvements relative to unmodified counterparts, PEG may not be the ideal solution for improving circulatory stability. There is evidence of continued uptake by the reticuloendothelial system (RES), and concerns remain about the non-degradable nature of the synthetic polymer as well as potential immunogenicity, as indicated by observation of complement activation and the formation of anti-PEG antibodies following administration [157, 158].

Polysialic acid (PSA), a natural, biodegradable carbohydrate polymer primarily composed of R-2, 8-linked 5-*N*-glycoly-neuraminic acid (Neu5Ac) is a relatively unexplored material for the prevention of premature clearance. PSA has been found on the surface of both mammalian and bacterial cells. In mammalian tissue, PSA is a post-translational modification of neural cell adhesion molecule (NCAM), and the large, negatively charged chains are thought to act via a steric mechanism to promote neural plasticity by reducing cell-cell interactions, thereby permitting cell migration. PSA is highly expressed by embryonic neural tissue and is associated with axon path finding and targeting as well as cell migration and muscle development. Most tissues in adults are not associated with PSA; however, patterns of expression are still observed in brain tissue with known plasticity and in damaged neural tissue [195]. Cancer cells also express PSA, and the polysaccharide is thought to play a role in tumor growth and metastasis [196]. Bacteria express PSA with chemical and immunological properties identical to those of mammalian-produced PSA; therefore, PSA is used to mask the antigenicity of invading

organisms from the immune system of the host [195, 197]. Furthermore, PSA-specific receptors have not been identified in the body [1, 48, 198, 199]. Given the lack of immunogenicity, in conjunction with the absence of receptors and high hydrophilicity, PSA should confer stealth properties to associated molecules.

The potential for PSA to improve the circulatory stability of existing therapeutics was initially recognized by Gregoriadis, et al. in a series of studies [1, 5, 48, 198, 199]. Gregoriadis proposed that the hydrophilic polymer chains would lead to the formation of a "watery cloud" that would thereby prevent interaction with proteins and cells of the immune system. As a result, a protective envelope would effectively be formed around drug molecules covalently linked to PSA, thus masking the therapeutic molecule and preserving structure and function. Furthermore, the large size (~30 kDa) and anionic charge of PSA would permit the drug molecule to reside in the body for longer periods of time by reducing urinary excretion and hepatic uptake [1, 48, 198, 199]. Studies on pharmacokinetics have revealed that a high molecular weight and a weakly anionic charge are typically indicative of macromolecules that will form the basis of good polymer-based drug carrier systems [200].

Initial studies on polysilylation demonstrated that asparaginase half-lives can be significantly extended. Furthermore, native asparagines elicited an immune response, whereas PSA conjugated to asparaginase did not, suggesting that PSA can suppress antigenicity [5]. Conjugation to reduce clearance has been extended to other biologically active compounds [201-203], and polysialylated derivatives of insulin [6], granulocyte colony stimulating factor (GCSF), and interferon R-2b (IFN-α2β) are currently in the preclinical stages of drug development for the treatment of type II diabetes, neutropenia, and hepatitis C, respectively.

Although in-depth studies on how PSA acts to prevent uptake by the RES have not yet

been conducted, the "watery cloud" that Gregoriadis refers to presumably functions in a manner similar to the fixed aqueous layer of PEGylated liposomes. In addition to providing a physical barrier, mechanistic investigations have revealed that PEG chains interact with surrounding water molecules to form an aqueous layer that prevents attraction and binding of serum proteins [204]. An increase in the fixed aqueous layer thickness of PEGylated liposomes has been associated with a reduction in uptake by macrophages [205] and an increase in the efficacy of the associated therapeutic [204].

Despite success with conjugation, the concept of using PSA in drug delivery for targeted drug delivery has yet to be extended to nanoparticle carrier systems. In this study, we modified PSA with long-chain alkyl amines, and the resultant compounds self- assembled to form polymeric micelles. Cytotoxicity was assessed using the MH7A rheumatoid arthritis synovial fibroblast cell line via a WST-8 assay. The ability of the micelles to encapsulate hydrophobic therapeutics was demonstrated with Cyclosporine A. The choices in cell line and therapeutic were based on future intended applications of this work toward targeted drug delivery for treatment of rheumatoid arthritis.

3.2 Materials and Methods

3.2.1 Material

Colominic acid sodium salt (PSA, isolated from *E. coli*) was obtained from Nacalai USA (San Diego, CA). The marketed molecular weight of 30 kDa was confirmed via HPLC. *N*-(3-Dimethyl- aminopropyl)-*N*′-ethylcarbodiimide (EDC), *N*-hydroxysuccinimide (NHS), decylamine (DA), and acetonitrile were purchased from Sigma-Aldrich. (St. Louis, MO) and

used as received. The MH7A synovial fibroblast cell line was provided by the Riken BRC through the National Bio-Resource Project of the MEXT, Japan. RPMI-1640, D-PBS, HEPES, L-glutamine, fetal bovine serum (FBS), and penicillin-streptomycin were obtained from Lonza (Allendale, NJ).

3.2.2 Preparation of Decylamine-Modified Polysialic Acid (PSA-DA) Micelle

The synthesis of DA-modified polysialic acid (PSA-DA) is depicted in figure 2. To obtain a 50-60% degree of substitution (DS) of Neu5Ac monomers, EDC (23.0 mg, 0.12 mmol) and NHS (13.8 mg, 0.12 mmol) were added to PSA (60 mg, 0.19 mmol repeating units) dissolved in 10 mL of DI water. After stirring at room temperature for 30 min, DA (18.8 mg, 0.12 mmol) was added, and the reaction was allowed to proceed overnight. The solution was dialyzed against DI water for 24 h (MWCO ≈ 5 kDa) and lyophilized to yield the desired PSA-DA product. Proton (^{1}H) NMR (Bruker 300) showed formation of the desired amide bond between DA and PSA as well as an *N*-acylurea side-product resultant from rearrangement of the *O*- acylisourea intermediate. PSA-DA was also prepared with degrees of substitution of 15-25, 30-40, and 90-100% following the same protocol with appropriate amounts of EDC, NHS, and DA relative to Neu5Ac monomers. To generate a control for PSA-DA in cytotoxicity studies, we modified PSA with EDC using the above procedure, omitting the addition of DA.

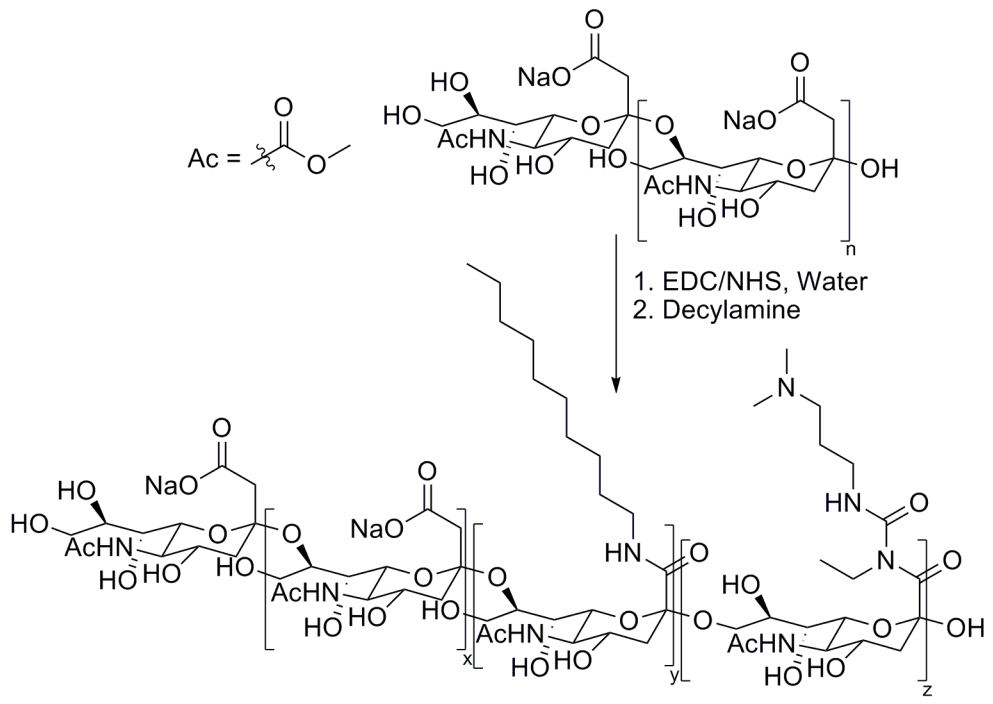

Figure 2. Synthesis of Decylamine modified Polysialic acid (PSA)

3.2.3 Characterization of PSA-DA Micelle

3.2.3.1 Size and Zeta Potential

Particle size, size distribution, and zeta potential of the PSA-DA micelles, both with and without encapsulated CyA, were obtained with a Zetasizer Nano ZS (Malvern Instruments). Aqueous samples were prepared at a concentration of 10 mg/mL in ultrapure water and used without filtration. For dynamic light scattering measurements, the temperature was set to 25 °C and the scattered light was detected at an angle of 173°. Particle sizes for each DS are reported as the mean of the sizes derived from the number distributions plus/ minus the standard deviation, whereas size distributions are reported as the mean plus/minus the standard deviation of the polydispersity indices (PDIs) (N = 6-9 for each DS). To ensure that sizes and zeta potentials

remained the same at an elevated temperature, we also characterized PSA-DA with a DS of 50-60% at 37 °C, both with and without encapsulated CyA. To observe the impact of dilution, we also made size measurements on CyA-loaded PSA-DA micelles (DS 50-60%) at concentrations of 1 and 0.1 mg/mL.

3.2.3.2 Critical Micelle Concentration

The critical micelle concentrations (CMCs) for PSA-DA prepared with various degrees of substitution were determined with steady-state fluorescence measurements using pyrene as a probe. We added 8.1 μL of 1.24×10^{-4} M pyrene stock solution in acetone to nine individual vials, and the acetone was allowed to evaporate. To each vial was added 5 mL of aqueous solutions of PSA-DA with concentrations ranging from 0.01 μg/mL to 1.0 mg/ mL. The solutions were sonicated for 30 min at room temperature and heated with shaking at 65 °C for 4 h to permit equilibration. After cooling in the dark overnight, excitation spectra were recorded at an emission wavelength of 390 nm with a QuantaMaster-4/2005 sensitivity- enhanced (QM-4/2005 SE, Photon Technology International) fluores- cence spectrophotometer. The CMCs were determined from plots of I_{339}/I_{337} versus log concentration via the intersection of the tangent of the inflection point with the horizontal tangent through low concentration points [206].

3.2.3.3 Atomic Force Microscopy

The morphology of the PSA-DA micelles prepared with a DS of 50-60%, with and without encapsulated CyA, was observed using atomic force microscopy (AFM). A drop of aqueous sample was placed on a glass coverslip and allowed to dry in a vacuum desiccator for several hours. Images were obtained with a Nanoscope III AFM (Veeco Instruments) in contact mode.

3.2.4 Hydrophobic Drug Encapsulation

Hydrophobic cyclosporine A (CyA) was encapsulated within the PSA-DA micelles using a cosolvent evaporation method [207]. A stock solution of CyA in acetone was prepared at a concentration of 6 mg/mL. We added 167, 334, 501, and 668 μL of CyA stock solution to vials containing 10 mg of PSA-DA dissolved in 1 mL of DI water to yield CyA weight percentages of 10, 20, 30, and 40 relative to PSA-DA. The solutions were stirred gently at room temperature for 4 h to permit encapsulation of CyA within PSA-DA micelles. We removed acetone by heating at 65 °C for 15 min such that the solution volume was returned to the original volume (1 mL), and insoluble non-encapsulated CyA was separated by centrifugation at 11 000*g* for 5 min.

High-performance liquid chromatography (HPLC) was used to assess the loading capacity and encapsulation efficiency of the PSA-DA micelles. Following an established protocol, we added 600 μL of acetonitrile to a 200 μL aliquot of CyA-loaded micelles in water, prepared as described above, to release encapsulated drug [208]. The resultant solutions were assayed for CyA with a Prominence UFLC (Shimadzu Corporation) equipped with a Shim-pack XR-ODS reversed-phase column (3 mm i.d. × 50 mm) and a dual-wavelength UV-vis detector. A mobile phase of 3:1 acetonitrile/water was used with a flow rate of 0.5 mL/min. The column temperature and detection wavelength were set to 40 °C and 210 nm, respectively. 100 μL was injected for each sample, and CyA was observed as a broad peak centered at an elution time of 4.2 min. The area under the peak was determined following Loess smoothing using PeakFit 4.2 software. A calibration curve was generated from a five- parameter logistic model using standard solutions prepared in 3:1 acetonitrile/water with CyA concentrations that ranged from to 6.25 to 100 μg/mL. Following IUPAC guidelines, the limit of detection (LOD) was calculated from six blank samples as the mean plus three times the standard deviation, whereas the limit of

quantification (LOQ) was taken as the mean plus ten times the standard deviation [209]. Loading capacity and encapsulation efficiency of CyA-loaded PSA-DA micelles were calculated as

$$\text{LC} = \frac{W_{CyA-loaded}}{W_{PSA-DA}} \qquad (3.1)$$

$$\text{LE} = \frac{W_{CyA-loaded}}{W_{CyA-added}} \times 100 \qquad (3.2)$$

where $W_{\text{CyA-loaded}}$ is the amount of CyA incorporated into the micelles, as determined using the calibration curve, $W_{\text{PSA-DA}}$ is the amount of PSA-DA used, and $W_{\text{CyA-added}}$ is the amount of CyA added to the PSA-DA solution.

3.2.5 PSA-DA Micelle Stability

3.2.5.1 Freeze-Drying/Resuspension

CyA-loaded PSA-DA micelles (DS 50-60%), prepared as described above with 10 wt % CyA relative to PSA-DA, were frozen in a -80 °C freezer without the addition of a cryopreservative and lyophilized with a freeze-dryer. Samples were reconstituted by simple shaking after the addition of DI water. The reconstituted micelle solutions were immediately characterized by AFM and dynamic light scattering.

3.2.5.2 Mechanical and Thermal Stability

CyA-loaded PSA-DA micelles (DS 50-60%), prepared as described above with 10 wt % CyA relative to PSA-DA, were tested for mechanical and thermal stability. Samples for mechanical stability testing were immediately subjected to 5 additional minutes of centrifugation at 11 000g for 5 min, whereas samples for thermal stability testing were incubated at 37 °C with

shaking for 1 week. Upon completion of the thermal stability test, non-encapsulated CyA was removed by centrifugation. CyA content was assessed immediately following both tests via HPLC, as described above.

3.2.6 Cytotoxicity of PSA-DA

Cytotoxicity of the PSA-DA micelles was evaluated via WST-8 assay (Cayman Chemical Company) using the MH7A synovial fibroblast cell line. Reduction of the WST-8 tetrazolium salt by NADH produced within the mitochondria yields formazan dye, which can be quantified by measuring the absorbance at 450 nm. Cells were seeded into a 96-well cell culture plate at a density of ~5000 cells per well and cultured for 24 h. PSA-DA of various DS values was added at concentrations ranging from 15.6 to 500 μg/mL, and the cultures were maintained at 37 °C, 5% CO_2. After 24 h, 10 μL of WST-8 solution was added to each well, and incubation was continued for 90 min. The absorbance at 450 nm was measured with a Synergy 2 multimode microplate reader (BioTek Instruments). The cytotoxicity of CyA alone, PSA reacted only with EDC/NHS, and CyA-loaded PSA-DA (DS 50-60%) was also evaluated over an identical range of concentrations following the above procedure. CyA-loaded PSA-DA was used after freeze-drying. As a control, MH7A synovial fibroblasts were grown in media without any additives. For each DS, the absorbance relative to the control was plotted versus the concentration, and the data were fit to a five-parameter logistic to determine the IC_{50}.

3.3 Results and Discussions

3.3.1 Synthesis of PSA-DA Micelle

PSA is a natural, biodegradable polymer that may be used in lieu of poly (ethylene glycol) to improve the circulatory stability of free drugs and nanoparticle drug carriers. Polymeric micelles for hydrophobic drug encapsulation were prepared from DA-modified polysialic acid (PSA-DA), as depicted in figure 2. NHS was necessary to obtain the expected degrees of substitution (DS) of Neu5Ac monomers, as determined by ^{1}H NMR. DS was calculated from the relative intensity of the terminal methyl ($-CH_3$) peak in DA to the acetyl ($-NHCOCH_3$) peak in PSA. The reaction also yielded the N-acylurea side product resultant from the rearrangement of the O-acylisourea intermediate. As assessed by the N-dimethyl ($-N(CH_3)_2$) peak, 20-25% of the Neu5Ac monomers were modified with the N-acylurea side product when the DS for DA was between 10 and 60% (Figure 32, Figure 33). A survey of the literature demonstrated that the N-acylurea side product is typically obtained when EDC/NHS is used in the synthesis of polysaccharide-based bioconjugates and hydrogels [210-214]. Furthermore, the N-acylurea group has been shown to be nontoxic toward cells [210, 214, 215], and, when released from hyaluronan- based hydrogels, the urea has been shown to exhibit anti-inflammatory properties [216, 217]. Therefore, the presence of N-acylurea does not preclude the use of PSA-DA in drug delivery, and characterization was continued.

3.3.2 Characterization of PSA-DA Micelle

Pyrene was used as a fluorescent probe to evaluate the CMC for PSA-DA. As pyrene partitions between the hydrophobic environment of the micelle core and the hydrophilic aqueous environment, there is a shift in the excitation spectrum, as well as a corresponding change in the relative intensities of the vibrational bands. Only the shift in the excitation spectrum yields an unambiguous assignment of the CMC; therefore, plots of I_{339}/I_{337} versus concentration were constructed [206]. CMCs for each DS range were determined using the intersection of the tangent of the inflection point with the horizontal tangent of the low concentration points. Representative plots for PSA-DA with a DS of 50-60% As expected, on the basis of the results obtained via HPLC and particle size analysis that suggest an increase in micelle stability with higher DS, the CMC was found to decrease with increasing DS (Table 2). A clear CMC could not be identified for PSA-DA with a DS of 15-25%. Although the CMCs were higher than those observed for the well-known PEG-PCL system, the values were again consistent with dextran modified with PEG and hydrophobic alkyl chains (Figure 2) [82, 87, 88].

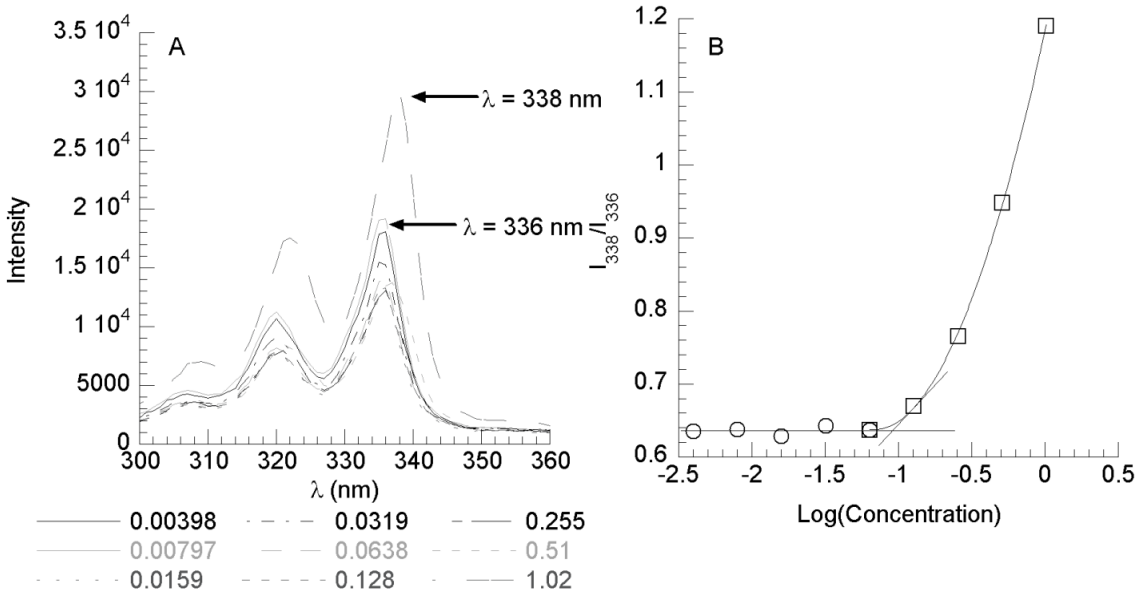

Figure 3. Excitation spectra for pyrene in a range of concentration (mg.ml) of PSA-DA (A) and a plot showing the change in I_{338}/I_{336} as the concentration of PSA-DA (mg/ml) is increased (B)

Table 2. Characteristics of PSA-DA micelle with various DS values

DS	CMC (μg/ml)	Size without CyA (nm)	PDI without CyA	Size with CyA (nm)	PDI with CyA
15-25%	-	25.5 ± 7.4	0.40 ± 0.07	41.9 ± 14.1*	0.49 ± 0.12
30-40%	99.6	54.7 ± 25.4	0.31 ± 0.01	90.1 ± 46.2	0.26 ± 0.06
50-60%	73.0	91.2 ± 5.4	0.24 ± 0.05	107.6 ± 16.2*	0.21 ± 0.02
90-100%	53.9	138.9 ± 4.0	0.15 ± 0.02	151.2 ± 18.8	0.18 ± 0.03

*Significantly different than the size without CyA ($p < 0.05$) as determined by Student's t test.

3.3.3 Hydrophobic Drug Encapsulation

Cyclosporine A (CyA) is currently used as an immunosuppressant to prevent organ rejection following transplantation and is regularly used as a disease-modifying anti-rheumatic drug (DMARD) in the treatment of rheumatoid arthritis [218]. The immunosuppressive effect of CyA appears to be largely a result of inhibition of T-cell activation [218]; however, CyA has also been linked to a reduction in the secretion of pro-inflammatory mediators by inflammatory cells

[219, 220]. Our long-term goal is to use polysaccharide-based micelles for targeted drug delivery of DMARDs to inflamed joint tissue; therefore, CyA was used to demonstrate the propensity of PSA-DA to encapsulate hydrophobic drugs. The bioavailability of CyA is highly variable because of poor solubility and side effects, particularly nephrotoxicity, result from nonspecific delivery, in combination with unfavorable pharmacokinetics [221]. Encapsulation within PSA-DA-based micelles should increase the efficacy of the drug by increasing the solubility, and therefore the bioavailability, while simultaneously providing a new mode of delivery that minimizes organ toxicity by facilitating targeting of diseased regions.

HPLC was used to assess the amount of CyA loaded into the PSA-DA-based micelles. Following release from the PSA-DA micelles by dissolution with acetonitrile, the amount of encapsulated CyA was quantified based on a calibration curve generated from CyA standards (6.25-100 μg/mL). Following IUPAC guidelines [209], the LOD was found to be 3.78 μg/mL, whereas the LOQ was found to be 5.75 μg/mL. A high initial concentration of PSA-DA (10 mg/mL) was used to ensure that the amount of CyA encapsulated fell within the limits of the calibration curve for all loading conditions.

PSA-DA with DS values of 50-60 and 90-100% were found to encapsulate CyA successfully with loading capacities of 0.0241 and 0.0268 and encapsulation efficiencies of 23.6 and 26.8%, respectively, when CyA was added at 10 wt % relative to PSA-DA. In contrast, DS values of 15-25 and 30-40% yielded low loading capacities (≤0.013). PSA-DA with a DS of 50-60% was used to explore further the effect of the wt % of CyA added on the loading capacity and encapsulation efficiency (Table 3). A maximum loading capacity of 0.0350 with a corresponding loading efficiency of 11.7% was achieved, with the addition of 30 wt % CyA. Unexpectedly, the loading capacity decreased at 40 wt % CyA. The latter occurrence has been observed for

hydrophobic drug encapsulation within chitosan-based micelles and can be attributed to precipitation of the drug from the aqueous phase concurrent with drug encapsulation [222]. The values for loading capacity and encapsulation efficiency determined for CyA in PSA-DA with DS values of 50-60 and 90-100% were less than those established for the common PEG-PCL micelle system [223] but nearly identical to those found for dextran modified with PEG and long-chain hydrocarbons (C_{18} and C_{19}) [82, 87, 88].

Table 3. Loading capacity and encapsulation efficiency of CyA-loaded PSA-DA micelles with a DS of 50-60%

*Wt. % of CyA**	*Loading Capacity (mg CyA/mg PSA-DA)*	*Encapsulation Efficiency (%)*
10	0.0241 ± 0.0017	23.6 ± 2.2
20	0.0301 ± 0.0007	15.0 ± 0.3
30	0.0350 ± 0.0004	11.7 ± 0.1
40	0.0294 ± 0.0003	7.3 ± 0.1

*Wt.% of CyA refers to the weight percent of CyA added relative to the weight of PSA-DA.

3.3.4 PSA-DA Micelle Stability

To assess micelle stability, we re-evaluated the amount of encapsulated CyA within PSA-DA micelles (DS 50-60%) following mechanical and thermal testing. Additional centrifugation at high speed did not significantly affect the loading capacity or encapsulation efficiency. However, after the drug-loaded PSA-DA micelle solutions were gently shaken at 37°C for 1 week, the loading capacity and encapsulation efficiency were reduced to 0.012 and 12.0%, respectively. Additional studies to determine if the drug is released in a controlled fashion or if the CyA is thermally degraded are currently under way. In correlation with the results obtained via HPLC, PSA-DA prepared with DS values of 15-25 and 30-40% yielded small micelles with

broad size distributions, whereas PSA-DA prepared with DS values of 50-60 and 90-100% gave rise to larger micelles with narrow size distributions (Table 2). PSA-DA therefore forms micelles of higher stability that are more suitable for encapsulation of hydrophobic drugs at higher degrees of substitution. Both with and without CyA, the micelles increased in size with higher degrees of substitution. The result is in contrast with a number of literature reports that suggest polysaccharide-based micelle size should decrease with increased hydrophobic DS [224-227]. On the basis of studies on the evolution of micelle size with diblock copolymers [228], the increase in size is likely a result of an increased aggregation number as the merger of smaller, less stable micelles is facilitated by the increased number of hydrophobic alkyl chains. Evidence of micellar aggregation is further provided by a reduction in the size of CyA-loaded PSA-DA micelles, with a corresponding increase in size distribution, with 10 and 100 fold dilutions (Figure 4). According to previous studies, the reduction in size, and consequently aggregation number, are necessary upon micelle dilution to prevent instabilities in the system [228], The choice in using drug-loaded micelles to study dilution was made on the basis of the assumption that the drug-loaded micelles will be diluted upon clinical administration. As anticipated based on other micelle systems [224, 227, 229], drug encapsulation increased micelle size when PSA-DA of the same DS with and without CyA were compared, although this difference was only statistically significant for a DS values of 15-25 and 50-60%. An increase in the amount of CyA initially added to the PSA-DA solution (DS 50-60%) from 10 to 30 wt % during micelle preparation yielded significantly larger micelles (180.6 ± 12.2).

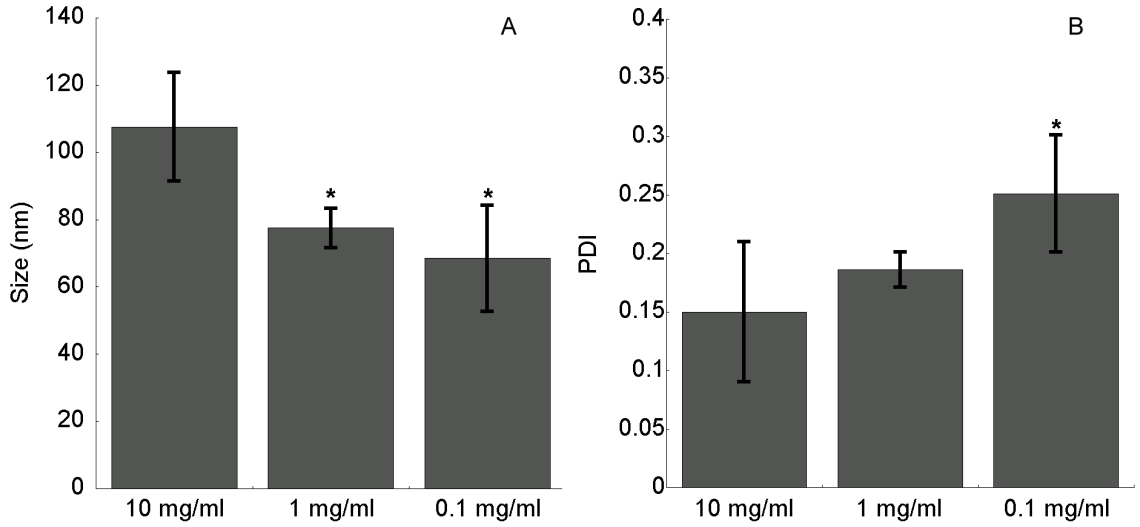

Figure 4. The effect of dilution on the size (A) and polydispersity (B) of CyA loaded PSA-DA micelles with a DS of 50-60%. Asterisks indicate a significant different ($p < 0.05$) relative to PSA-DA micelles at a concentration of 10 mg/ml as determined using ANOVA followed by post hoc Fisher's LSD.

To better assess the stability of the micelles in a physiological setting, the impacts of temperature change upon the micelle size were probed using PSA-DA micelles with a DS of 50-60%. A rise in temperature from 25 to 37 °C did not significantly affect the micelle size. Regardless of dilution or DS, the particle sizes obtained for the stable PSA-DA micelles are large enough to permit passive targeting. In cancer and inflammatory diseases, particularly rheumatoid arthritis, therapeutic carriers with large hydrodynamic radii to prevent renal filtration and increase circulation time can passively accumulate in the diseased tissue as a result of leaky vasculature, an effect referred to as "enhanced permeation and retention" [230-232]. AFM was used to confirm that the PSA-DA micelles, with and without CyA, possessed a spherical morphology (Figure 5).

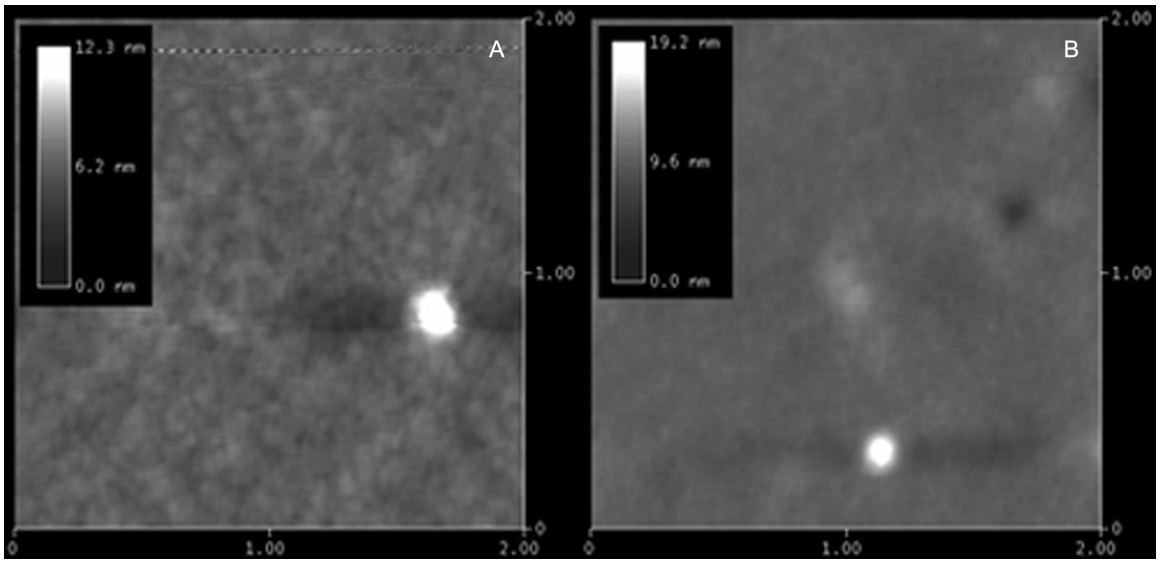

Figure 5. AFM height images of unloaded (A) and CyA loaded (B) PSA-DA micelles. The samples were diluted such that only one spherical micelle, as illustrated by the white spots, could be observed in each image. The image scale is in microns.

Micelles were further characterized by zeta potential. Although there was significant day-to-day variability, likely resultant from slight changes in the ionic strength of the water, for all DS values, the zeta potential varied between -30 and -40 mV. The zeta potential provides a gauge of the surface charge resultant from interaction with counter ions in a specified medium. Previous research has demonstrated that zeta potentials with absolute values >30 mV will permit electrostatic stabilization [233]. Therefore, the values obtained are indicative of micelle stability.

For long-term storage, CyA-loaded PSA-DA micelle solutions with a DS of 50-60% were slowly frozen in a -80 °C freezer and lyophilized. Often, without the use of a cryoprotectant, aggregates will be observed following slow freezing and freeze-drying as a result of phase separation with an increase in concentration in one phase [234, 235]. Likewise, larger micelles can be formed following reconstitution if the micelles are broken as a result of physical stress during the freezing process [236]. Neither of these phenomena was observed for the PSA-DA

micelles, and dynamic light scattering yielded a size nearly identical to that obtained prior to lyophilization (106.6 ± 4.2). AFM further confirmed that the micelles were maintained through the freeze-drying process (Figure 6).

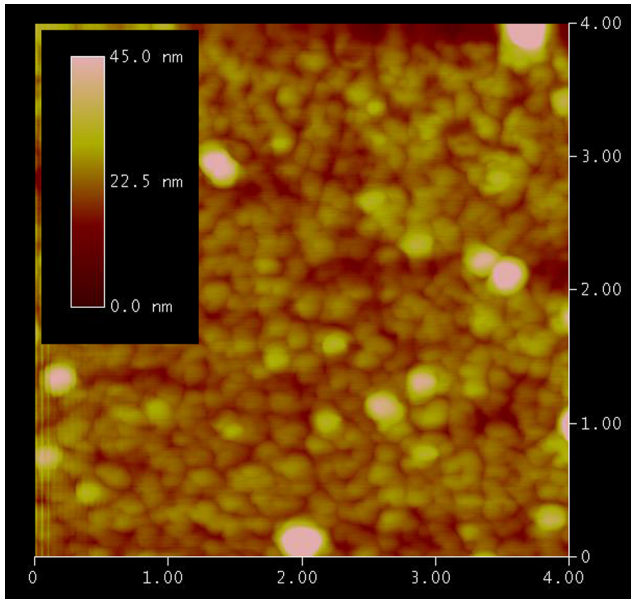

Figure 6. AFM height imaged of CyA loaded micelles following lyophilization. The samples were reconstituted at high concentration and immediately prepared for imaging. The image scale is in microns.

To the authors' knowledge, only poly(lactic-co-glycolicacid)-poly(carboxybetaine) (PLGA-PCB)-based micelles have been reported to maintain their properties through the freeze-drying process without the addition of a cryoprotectant. Similar to the PLGA-PCB system, the observed behavior likely results from strong hydration of the PSA, in combination with the formation of a protective shell of hydrophilic PSA around the distinctly hydrophobic DA core [237]. Of note, PEG-based micelle systems typically require the use of a cryoprotectant because PEG will crystallize and aggregate upon freeze-drying [238-241].

3.3.5 Cytotoxicity of PSA-DA Micelle

Cytotoxicity of PSA-DA was assessed using MH7A rheumatoid arthritis synovial fibroblasts using the WST-8 assay. The cell line was chosen based on future intended applications of the CyA-loaded PSA-DA micelles in targeted drug delivery for the treatment of rheumatoid arthritis. As shown in Figure 7, the IC_{50} was strongly dependent upon the DS, suggesting a role for DA in cytotoxicity. Presumably, the N-alkyl group interacts with the membrane and induces cell fragmentation, as has previously been reported for N-alkylated imino sugars [242]. PSA reacted only with EDC and NHS was shown to be nontoxic toward the cells, verifying that the side product did not contribute to cytotoxicity. As expected, CyA alone was also nontoxic toward the cells and encapsulation did not affect the IC_{50} of PSA-DA with a DS of 50-60%. As suggested by studies on N-aklyated imino sugars, a small change in the length of the alkyl chain may have a large impact on cytotoxicity, with minimal influence on the CMC [242], and this will be a topic of further investigations.

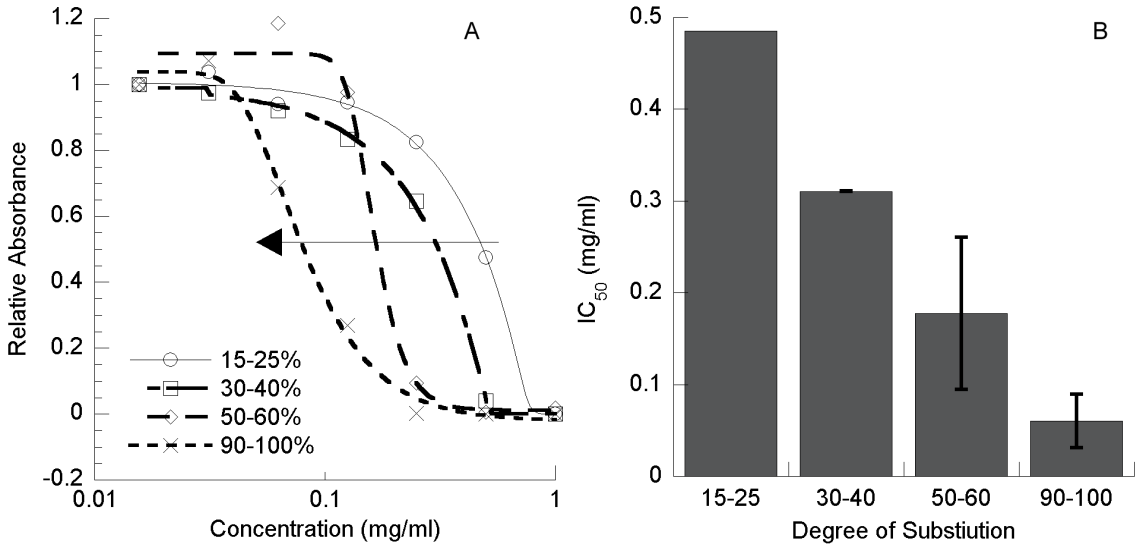

Figure 7. WST-8 assay of MH7A synovial fibroblasts following incubation with PSA-DA of varying DS values for 24 hours at 37°C at concentrations from 0.015 – 0.5 mg/ml. The data was fit with a five parameter logistic, and the IC_{50} curves showed a shift to the left, as indicated by the arrow, with increasing DS (A). Therefore, as DS increased, the calculated IC_{50} decreased (B).

3.4 Conclusion

PSA is a relatively unexplored material for the prevention of premature clearance. In this study, preliminary investigations were conducted to demonstrate that PSA could be readily modified with a long-chain alkylamine to develop a material that naturally self-assembles in aqueous solution to form spherical micelles that can be used to encapsulate hydrophobic molecules, particularly cyclosporine A (CyA). Sizes and zeta potentials of the loaded and unloaded micelles indicate that the drug carriers possess acceptable properties for passive targeting of diseased regions; however, control of cytotoxicity warrants additional study. Future investigations will be aimed at assessing whether the PSA does prevent binding of serum

proteins and macrophage uptake, as claimed by previous researchers, and on in vitro and in vivo efficacy.

Chapter 4 Development, characterization, and *in vitro* efficacy of polysialic acid-polycaprolactone micelles

Polysialic acid (PSA) has been identified as a natural, hydrophilic polymer that can be used to extend circulation time and improve therapeutic efficacy when used as the basis of drug carrier systems. Here, to further investigate the potential of PSA to alter the pharmacokinetic and pharmacodynamics profiles of associated therapeutics, PSA-based micelles were formed via self-assembly of PSA grafted with polycaprolactone (PCL) at a critical micelle concentration of 84.7 ± 13.2 μg/ml. Cyclosporine A (CyA), a therapeutic used in the treatment of rheumatoid arthritis, was loaded into the PSA-PCL micelles with a loading capacity and loading efficiency of 0.09 ± 0.02 mg CyA/mg PSA- PCL and 29.3 ± 6.4 %, respectively. CyA loading resulted in a size increase from 66.8 ± 6.2 nm to 107.5 ± 9.3 nm, a favorable size range for drug delivery to inflamed tissue characterized by leaky vasculature, as occurs during rheumatoid arthritis pathogenesis. As an indicator of the stealth nature the micelles are expected to exhibit in vivo, the fixed aqueous layer thickness of the PSA-PCL micelles was determined to be 0.63 ± 0.02 nm, comparable to that obtained for traditionally utilized poly(ethylene glycol) coated liposomes. The PSA-PCL micelles had a negligible effect on the viability of the SW982 synovial fibroblast cell line. Fluorescent microscopy was utilized to demonstrate uptake by the synovial fibroblasts through a non-receptor mediated form of endocytosis and intracellular separation of CyA from the micelle.

4.1 Introduction

Due to the high cost and lengthy implementation timeline involved with drug discovery, drug delivery may serve as an alternative method to advance pharmaceutical sciences and human health. In addition, a numbers of therapeutics are characterized poor bioavailability, unfavorable biodistribution, and high cytotoxicity, particularly when administered systemically. Drug carrier systems are needed to improve drug efficacy and reduce cytotoxicity in the human body. To date, many studies have been conducted based on the theory proposed by Paul Ehrlich [243] to develop therapeutics which can be site-specifically delivered to the target tissue, with reduced accumulation in the healthy tissue. Most of these delivery systems are designed with the advantages of increased solubility, prolonged circulation stability, and high tissue specificity [13].

Among various nanoparticle systems, polymeric micelles have drawn much attention for the encapsulation of hydrophobic drugs since first reported in 1984 [12]. These micelles are formed from macromolecules composed of hydrophobic and hydrophilic segments. In an aqueous environment, the amphiphilic polymers self-assemble into a core-shell structure due to the aggregation of the hydrophobic moieties. Thus, hydrophobic drugs can be physically encapsulated into the core via hydrophobic interactions. In general, micelles provide therapeutics with improved solubility, enhanced stability, and an extended circulation time [14].

When administered systemically, the majority of drugs are eliminated rapidly by the reticuloendothelial system (RES). Short drug circulation times have been a major challenge and have been liked to poor drug efficacy. Increased surface hydrophilicity can reduce the recognition and binding of plasma proteins to drug carriers and, thus, decrease the elimination of

drugs and prolong the circulation time. Consequently, the likelihood that the drugs will reach the target disease tissues is improved. To date, poly(ethylene glycol) (PEG)-based modification ha been the most common method to improve hydrophilicity and provide the drugs with so-called "stealth" properties to evade detection by the RES [244-246]. However, PEG may not be the ideal solution due to a non-biodegradable backbone, evidence of continuous accumulation inside the body, and problems with immunogenicity [48, 157, 158]. Moreover, the PEG coating is known to interfere with some of the steps involved in drug delivery. After localization to the diseased tissue, PEG coatings have been reported to hinder drug release from the carrier systems and reduce requisite drug-cell interactions [159-161].

As an alternative, polysialic acid (PSA) is a relatively unexplored natural, non-toxic, and biodegradable polysaccharide that has the potential to prolong the circulation time of associated rugs and provide additional benefits. PSA is a linear homopolymer of α-2, 8-linked 5-N-glycolyneuraminic acid (Neu5Ac) and is widely produced by pathogenic bacteria, as well as the cells of vertebrates and higher invertebrates. Thus, PSA is highly involved and has multifarious roles in a wide variety of biological, immunological, and pathological processes [44-47]. Some pathogenic bacteria can escape the host immune system and evade the host tissues by producing a thick PSA coating on the cell wall [48]. In mammals, the major function of PSA is believed to be anti-adhesive properties that can change the cell-cell and cell-extracellular matrix interaction and promote neutral plasticity. PSA acts as a post-translational modification of neural cell adhesion molecules (NCAM), and the fifth Ig domain of NCAM is able to carry PSA at a high loading capacity. The significant negative charge and large hydrated volume of PSA can reduce NCAM-mediated adhesion and enable neuron cell migration. Typically, PSA expression is down-regulated in most tissues of the adults. However, during the neural injuries [49, 50] and

tumorigenesis [247, 248], PSA is expressed on the cell surfaces, which serves to alter cellular to abrogate cell adhesion and facilitate cell migration. The anti-adhesive properties are further supported by immune studies that demonstrate that the removal of PSA generates an “eat me” signal to macrophages to recognize and clear the uncoated bacteria, excess proteins, or dead cells [249].

Due to the natural anti-adhesive properties highlighted above, PSA has drawn attention in the field of drug delivery. Based on a series of studies on sialyated or polysialyated proteins, Gregoriadis et al. proposed that PSA was a potential material to increase the stability and circulation time of therapeutics inside the bodies [1]. PSA-drug conjugation has been used to increase the half-life of insulin [6], asparaginase [4, 5], and catalase [2, 3]. As a result, immunogenicity and antigenicity were reduced, and the efficacy of the proteins was improved. To date, several PSA-protein conjugates and Neu5Ac derivatives have been developed as vaccines and therapeutic agents [250, 251].

Compared to other drug delivery systems, nanoparticle-based targeted drug delivery systems have been shown to accumulate passively within tumor tissue and inflamed tissue due to the enhanced permeability of the leaky vasculature [252]. Previously, our lab developed micelles from PSA modified with a long chain hydrocarbon, decylamine [253]. Despite possessing the necessary physical properties in regards to size and surface charge, the micelles were cytotoxic towards a synovial fibroblast cell line. Here in, we develop and characterize non-cytotoxic, PSA-based micelles via grafting of the PSA with amine-terminated polycaprolactone (PCL), a hydrophobic, non-toxic polymer that can be degraded in the human body by ester hydrolysis (Figure 8) [254]. The protective role the PSA is thought to play *in vivo* was preliminarily evaluated by measurement of the fixed aqueous layer thickness (FALT). FALT has previously

been correlated with the ability of carrier systems to prevent opsonization and, consequently, uptake by the RES [205, 255-258]. Cyclosporine A (CyA), a therapeutic used in the treatment of rheumatoid arthritis was used as a model compound to demonstrate the capacity of the micelles to encapsulate hydrophobic molecules. Fluorescence microscopy experiments were used to demonstrate cellular uptake of the drug-loaded micelles and release of the CyA from the micelles.

4.2 Materials and Method

4.2.1 Material

Colominic acid sodium salt (PSA, isolated from E. coli, Mw 30 kDa) was obtained from Nacalai USA (San Diego, CA). N-(3-Dimethylaminopropyl)-N′-ethylcarbodiimide (EDC), N,N'-dicyclohexylcarbodiimide (DCC), N-hydroxysuccinimide (NHS), ethylenediamine, m-chloroperoxybenzonic acid, benzyl alcohol, 1,5,7-triazabicyclo[4.4.0]dec-5-ene (TBD), ε-caprolactone (ε-CL), and Boc-gly-OH were purchased from Sigma-Aldrich (St. Louis, MO) and used as received. Trifluoroacetic acid (TFA) (peptide synthesis grade), HPLC grade acetonitrile, dichloromethane, and anhydrous DMSO were also obtained from Sigma-Aldrich. (St. Louis, MO). Dichloromethane was distilled before use. Dowex 50WX 2 ion-exchange resin and pyrene were purchased from Acros organics (Pittsburgh, PA) and tetrabutylammonium bromide was obtained from Fluka (St. Louis, MO). The SW982 synovial fibroblast cell line was acquired from ATCC (Manassas, VA). Fetal bovine serum (FBS) was obtained from Lonza (Allendale, NJ) and cyclosporine A (CyA) was puchased from Enzo Life Sciences (Farmingdale, NY.). Dulbecco's Modification of Eagle's Medium (DMEM) supplemented with 4.5 g/L glucose, L-glutamine &

sodium pyruvate was procured from Mediatech, Inc. (Manassas, VA). Purified soluble collagen was purchased from Devro Pty Ltd. (Bathurst, NSW, Australia). Alexa Fluor® 488 succinimdyl ester and sulforhodamine 101 cadaverine were acquired from Invitrogen (Grand Island, NY) and AnaSpec (Fremont, CA), respectively. 1, 2-dipalmitoyl-sn-glycero-3-phosphocholine (DPPC), cholesterol and 1,2-distearoyl-sn-glycero-3-phosphoethanolamine-N-[methoxy(polyethylene glycol)-2000] (DSPE PEG 2000) were obtained from Avanti Polar Lipids (Alabaster, AL) and used without further purification. (Dimethylamino)pyridine-p-toluensulfonic acid (DPTS) was formed from hydrated p-toluenesulfonic acid and 4-(dimethylamino)pyridinium following a known protocol [259].

4.2.2. Preparation of polysialic acid-polycaprolactone (PSA-PCL) micelles

4.2.2.1. Synthesis of polycaprolactone (PCL)

PCL-OH was synthesized according to a published procedure [260]. To a previously incubated solution of benzyl alcohol (5.5 μL, 5.31×10^{-2} mmol) and TBD (0.04 M in toluene, 3.7 mL, 0.148 mmol), ε-CL (0.82 mL, 7.4 mmol) was added and the mixture was stirred at room temperature, under nitrogen, for 2.5 hr. The polymerization was then quenched by precipitation into cold methanol and PCL-OH was isolated as colorless oil. Residual catalyst and unreacted monomer were removed from the isolated polymer by repeated precipitation into cold methanol. Polymer formation was confirmed by ^{1}H NMR and gel permeation chromatography in chloroform with polystyrene standards was used to estimate molecular weight (Mw =8216 g/mol).

4.2.2.2. Synthesis of Amine-Terminated PCL (PCL-gly-NH_2)

A two-step process was used to generate PCL-gly-NH2 [261]. 200 mg of hydroxylterminated PCL (0.026 mmol), 5.5 mg DCC (0.026 mmol), and 14.6 mg DPTS (0.026 mmol) were dissolved in 6 ml anhydrous dichloromethane under nitrogen, and 4.6 mg BOC-glycine (0.026 mmol) were added. The reaction solution was stirred for 48 h at room temperature. After filtration, the solution was added drop-wise into 30 ml of cold methanol. The white precipitate was collected and dried under vacuum oven overnight. The resultant 141.1 mg of PCL-gly-Boc (Mw =8374 g/mol, ~ 0.017 mmol) was dissolved in 7 ml anhydrous dichloromethane and 7 ml of TFA was added via syringe. The mixture was stirred at room temperature for 2 h under nitrogen. The product was obtained by rotary evaporation followed by drying at 70°C in a vacuum oven. Formation of PCL-gly-Boc and deprotection to yield PCL-gly-NH_2 were confirmed by ^{1}H NMR (300 MHz, CD_3Cl).

4.2.2.3. Synthesis of PSA-PCL

To improve the solubility of PSA in DMSO, the sodium ion was exchanged for tetrabutylammonium using a procedure adapted from the literature [262]. 600 mg Dowex 50 WXZ and 750 mg tetrabutylammonium bromide (2.26 mmol) were mixed in 15ml of DI water, and the mixture was stirred gently for 1 hour. The Dowex 50 WXZ was washed several times with DI water to remove unbound tetrabutylammonium bromide. The washed Dowex was transferred into 10 ml of 2% aqueous (w/w) PSA (200 mg, 0.65 mmol sialic acid monomer), and the solution stirred for 2 hours at room temperature. The resin was separated from the liquid by centrifugation at 1000 rpm for 5 min. Ion exchanged PSA was isolated via lyophilization.

To conjugate PCL-gly-NH_2 to PSA, 100 mg of ion exchanged PSA (0.32 mmol sialic acid monomer), 10.1 mg DCC (0.048 mmol, 0.15 equiv relative to sialic acid monomer), and 26.8 mg DPTS (0.048 mmol, 0.15 equiv) were combined in 6 ml of anhydrous DMSO, and the solution was stirred for 1 h at room temperature under nitrogen. Simultaneously, 133 mg PCL-gly-NH_2 (0.016 mmol, 0.05 equiv) were dissolved in 6 ml anhydrous dichloromethane in a separate round bottom flask. After 1h, the dichloromethane solution was transferred to the DMSO solution via cannula. The mixture was allowed to stir overnight at room temperature. After filtration, the solution was dialyzed against 150mM NaCl solution overnight to remove solvent and exchange tetrabutylammonium for sodium. Residual dichloromethane was removed by rotary evaporation, and the product was isolated by lyophilization. The product was washed with DI water and lyophilized again to ensure removal of unreacted PCL-gly-NH_2. The formation of PSA-PCL was confirmed by ^{1}H NMR. The degree of substitution (DS) of PCL to sialic acid monomer found by

$$DS = \left(\frac{3}{2}\right)\left(\frac{A_{1.35}}{A_{2.1}}\right)\left(\frac{M_w PCL}{M_w \varepsilon - CL}\right) \qquad (4.1)$$

where A1.35 and A2.1 are the peak areas at δ 1.35 and 2.1 ppm, respectively.

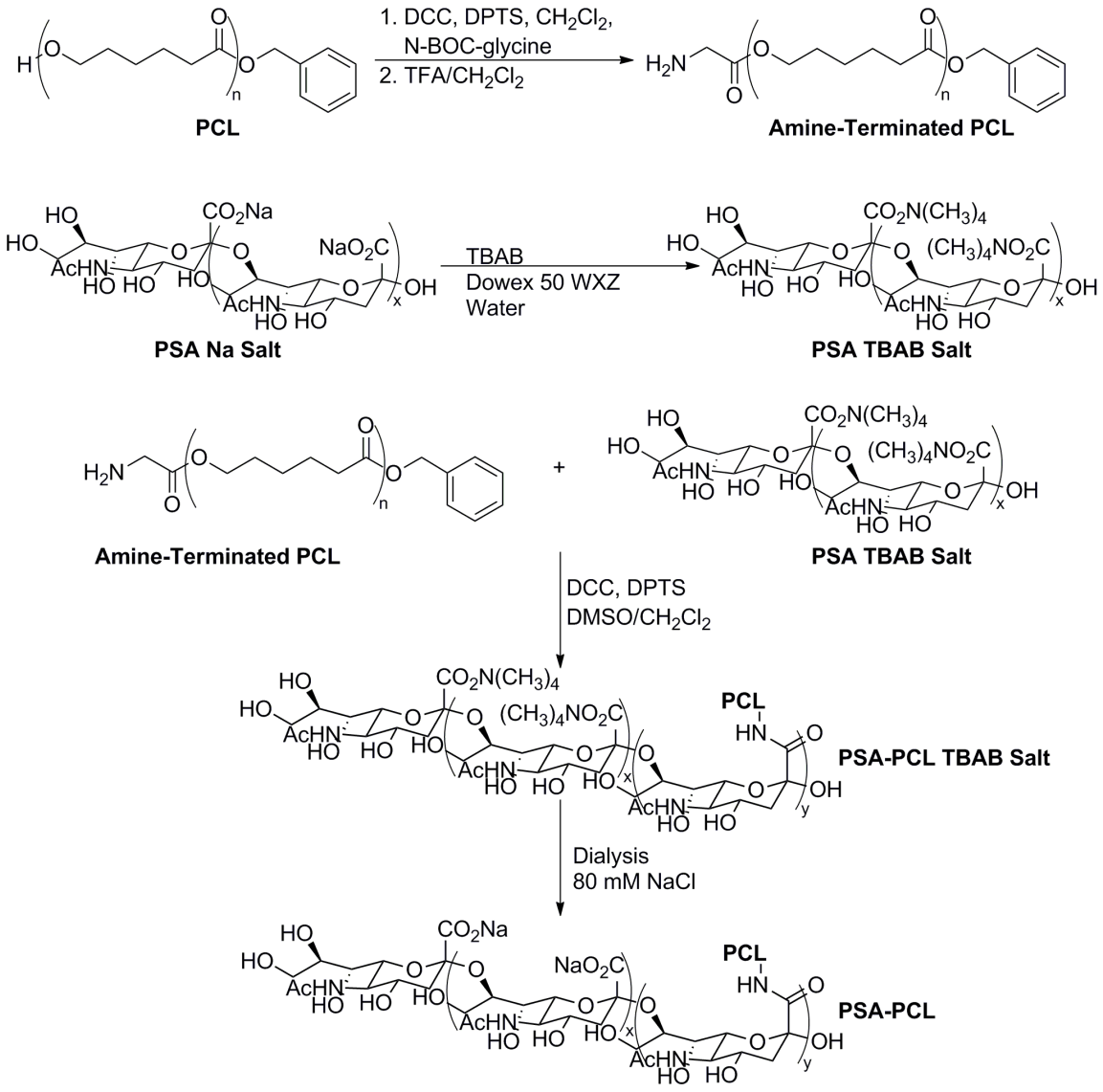

Figure 8. Synthesis of polysialic acid-polycaprolactone (PSA-PCL) for micelle formation.

4.2.3 Characterization of PSA-PCL micelles

4.2.3.1. Critical micelle concentration (CMC)

CMC was evaluated via steady-state fluorescence using pyrene as a probe [206, 263]. 8.1 μL of a 1.24×10^{-4} M pyrene stock solution in acetone was added to nine individual vials, and

the acetone was allowed to evaporate by placing on a 65°C hot plate for 15 min. Simultaneously, a dilution series of aqueous PSA-PCL solutions with concentrations ranging from 1 mg/ml to 3.9 μg/ml was prepared. 1 ml of the aqueous micelle solutions was added to the nine vials with pyrene. The solutions were sonicated for 30 min at room temperature and heated with shaking at 65 °C for 4 h to achieve equilibration. After cooling in the dark overnight, excitation spectra were recorded at an emission wavelength of 390 nm with a QuantaMaster-4/2005 sensitivity enhanced (QM-4/2005 SE, Photon Technology International) fluorescence spectrophotometer.

4.2.3.2. Size and zeta potential

Size, polydispersity, and zeta potential of PSA-PCL micelles, with and without encapsulated CyA, were obtained with a Zetasizer Nano ZS (Malvern Instruments). Aqueous samples were prepared by dissolving 2 mg PSA-PCL in 1 ml DI water. For dynamic light scattering, the temperature for measurement was 25°C, and the angle of scattered light was 173°. Micelle sizes are reported as the mean of the sizes derived from the number distributions plus/minus the standard deviation, while size distributions are reported as the mean of the polydispersity indices plus/minus the standard deviation.

4.2.3.3. Transmission electron microscopy (TEM)

Lyophilized PSA-PCL was dissolved in DI water at a concentration of 0.1 mg/ml to facilitate self-assembly of micelles. 20 μl of the PSA-PCL micelle solution was pipetted onto a formvar/carbon coated copper grid (Electron Microscopy Sciences, Inc.). The excess micelle solution was removed, and the sample was stained with methylamine vanadate prior to imaging with a JEOL 2000EX TEM at 100 kV at the N.C. Brown Center for Ultrastructure Studies at the SUNY College of Environmental Science and Forestry.

4.2.3.4. Cytotoxicity

Cytotoxicity of PSA-PCL was evaluated via WST-8 assay (Cayman Chemical Company, Ann Arbor, MI) using the SW892 synovial fibroblast cell line. Cells were seeded into a 96-well plate at a density of 10,000 per well and cultured for 24 h with DMEM plus 10% FBS at 37°C, 5% CO_2. Following sterile filtration, PSA-PCL micelles were added at concentrations ranging from 0.156-20 mg/ml. After incubating for 24 h, the media was removed and 10 µl of WST-8 reagent and 100 µl of fresh media were added to each well. After a 90 min incubation period, the absorbance was measured at 450 nm by a Synergy 2 multimode microplate reader (Biotek Instruments). SW982 cells cultured without PSA-PCL were used as controls. The experiment was repeated independently three times. IC_{50} concentrations were determined from a four parameter logistic generated using Kaleidagraph software.

4.2.4. Encapsulation of cyclosporine A (CyA)

CyA was encapsulated using a previously established approach [264]. 3 mg of CyA was dissolved in 4 ml of a 1:1 mixture of methanol and DMSO. 10 mg of PSA-PCL were added. To initiate micelle formation, 1 ml of DI water was added. The solution was transferred to a dialysis membrane (6-8 kDa) and dialyzed against DI water for 2 days to remove organic solvent and facilitate self-assembly with entrapped CyA. Drug-loaded micelle was isolated by lyophilization. Dynamic light scattering measurements confirmed that the micelles were stable to the freeze-drying procedure without the addition of a cryoprotectant.

Loading capacity (LC) and loading efficiency (LE) of the CyA-loaded PSA-PCL micelles were assessed with a Prominence Ultrafast Liquid Chromatography System (UFLC, Shimadzu Scientific Instruments, Japan) equipped with an SPD-20AV UV detector, a SIL-20A

autosampler, a DGU-20A3 degasser, and a Shim-pack XRODS/ C8/Phenyl column (3mm i.d. ×50mm). 10 mg of lyophilized, CyA-loaded PSA-PCL was dissolved in 4 ml of mobile phase, a 65:35 mixture (v/v) of pure HPLC grade acetonitrile and DI water, and mixed well. All samples were filtered through 0.25 μm filter prior to injection. An injection volume of 100 μL was used, and the flow rate and detection wavelength were set to 210 nm and 0.5 ml/min, respectively. At a column temperature of 40°C, CyA was observed as a broad peak centered at an elution time of 8.3 min. A calibration curve was constructed by determining the area under the peak using PeakFit 4.2 software for eight CyA solutions with known concentrations ranging from 50 to 400 μg/ml. Samples of CyA-loaded micelles were diluted with acetonitrile to release encapsulated drug (65 acetonitrile: 35 water). LC and LE were determined as:

$$\text{LC}= \frac{W_{CyA-loaded}}{W_{PSA-PCL}} \quad (4.2)$$

$$\text{LE}= \frac{W_{CyA-loaded}}{W_{CyA-added}} \quad (4.3)$$

where $W_{\text{CyA-loaded}}$ is the amount of CyA incorporated into the micelles, as determined using the calibration curve, and $W_{\text{PSA-PCL}}$ and $W_{\text{CyA-added}}$ are the amounts of PSA-PCL and CyA used, respectively .

4.2.5 Comparison of PSA-PCL micelles to PEG-coated liposomes

4.2.5.1. Preparation of PEG-coated liposomes

Small unilamellar vesicles of average diameter of 100 nm composed of 62 mol% DPPC, 33 mol% cholesterol and 5 mol% DSPE-PEG 2000 were prepared by the vesicle extrusion methods. In brief, the lipids were suspended in chloroform and mixed in a round bottom glass

vial. The solvent was evaporated, and the dried lipid film was resuspended with double deionized water and hydrated overnight at 4 °C. The total lipid concentration was 2 mg/ml. The liposomes were homogenized by passing them with 1800 kPa 11 times through polycarbonate filters of 100 nm pore diameter (Whatman Inc., Clifton, NJ) using a high-pressure extruder (Northern Lipids Inc., Vancouver, Canada).

4.2.5.2. Determination of the fixed aqueous layer thickness (FALT)

The FALTs of PSA-PCL micelles and PEG-coated liposomes were determined following a previously described method based on the Gouy-Chapman theory. Zeta potentials for micelles and PEG-coated liposomes were obtained in the following concentrations of aqueous NaCl: 10, 50, 100, 150, and 200 mM. Using eq. 4, FALT was estimated from a plot of zeta potential ψ) versus the Debye-Huckel parameter ($\kappa = \sqrt{(C/0.3)}$, where C is the molality of NaCl).

4.2.6 Cellular uptake of CyA-loaded PSA-PCL micelles

4.2.6.1. Synthesis of cyclosporine amine (CyA-NH_2)

To facilitate attachment of a fluorescent tag, a CyA analog with a reactive functional group was prepared. The procedure outlined herein for the preparation of CyA-NH_2 was adapted from a previous study on the synthesis of cyclosporine A derivatives [265] (Figure 9). Briefly, 200 mg CyA (166 μmol), 32 mg m-chloro-peroxybenzonic acid (186 μmol), and 40 mg anhydrous sodium carbonate (380 μmol) were combined in 20 ml of anhydrous methylene chloride, and the reaction solution was stirred overnight under N_2 at room temperature. The solution was washed with 20% sodium bisulfite and 10% sodium carbonate. The organic layer was dried over anhydrous magnesium sulfate, filtered, and concentrated to yield 190 mg of

crystalline product. This was immediately dissolved in 20 ml of anhydrous THF and refluxed under N_2 with excess ethylenediamine (400 µl, 359.6 mg, 5.98 mmol) for 24 h at 80°C. The solution was concentrated, and flash chromatography on silica gel (SiliaFlash® F60) was used to isolate the product. The colorless byproduct was eluted first with hexane/acetone (1:2), and then methanol/dichloromethane (4:1) was used to obtain the product as a yellow residue. Product formation was confirmed by high resolution electrospray ionization mass spectrometry on a Bruker 12 Tesla APEX –Qe FTICR-MS with an Apollo II ion source at the COSMIC laboratory of Old Dominion University. HRMS calculated for CyA-NH_2 [M+Na]+ 1300.8942; Found 1300.8904 (Figure 34).

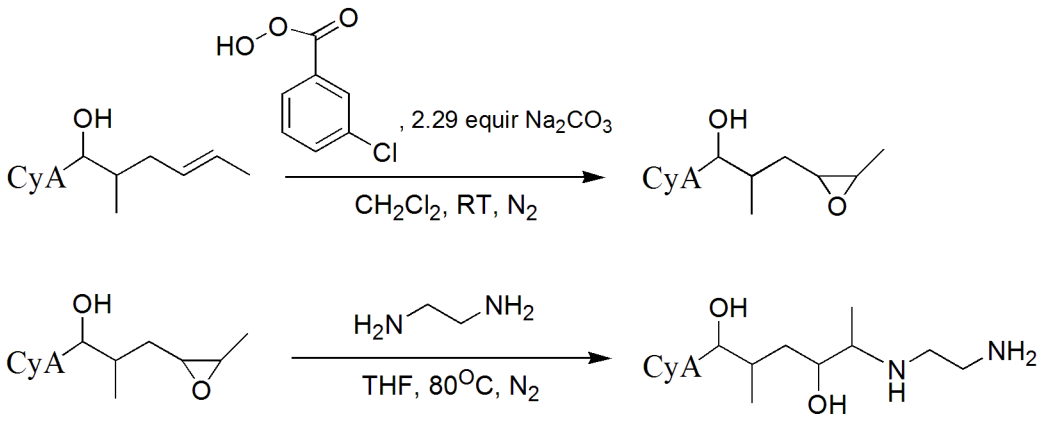

Figure 9. Synthesis of amine-terminated CyA

4.2.6.2. Preparation of fluorescently tagged CyA and PSA-PCL

Fluorescently labeled PSA-PCL was prepared by dissolving 40 mg of PSA-PCL in 4 ml of DI water, followed by the addition of 15.5 mg EDCI (99.9 µmol), 11.5 mg NHS (99.9 µmol) and 400 µl sulforhodamine 101 cadaverine (1 mg, 1.45 µmol). The pH was adjusted to 4.75, and the solution was stirred overnight with protection from light at room temperature. Fluorescently

labeled PSA-PCL was isolated by lyophilization. Fluorescently labeled CyA was encapsulated within fluorescently labeled PSA-PCL as described above for unlabeled material.

Fluorescently labeled CyA was synthesized by dissolving 12 mg of CyA-NH_2 in 1 ml DMSO, followed by the addition of 250 µl (0.25 mg, 0.39 µmol) Alexa Fluor® 488 carboxylic acid, succinimidyl ester, mixed isomers in DMSO. The solution was stirred for 2 h with protection from light at room temperature and then dialyzed overnight to remove unreacted fluorescence tag. Fluorescently labeled CyA was isolated by lyophilization.

4.2.6.3. Microscopy

35 mm Glass-bottom dishes (MatTek, Ashland, MA) were coated with collagen prior to use to improve cell viability and morphology. Collagen was dissolved in 0.02 M acetic acid at a concentration of 50 µg/ml, and 1 ml of the resultant solution was sterile filtered and added to each microscopy plate. After 1 h at room temperature, excess collagen solution was removed by gentle aspiration, and the plates were rinsed 3 times with 1xPBS. The plates were air dried overnight inside a biosafety cabinet. SW982 cells were seeded into the collagen-coated plates at a density 1 million cells/plate. After 24 h of incubation at 37°C, the media was removed and sterile filtered fluorescently labeled CyA-loaded PSA-PSA micelle solution was added, The plates were washed 3 times with 1xPBS before imaging, and images were obtained with a Nikon Eclipse Ti inverted microscope at 15 and 60 min post-administration. Experiments were conducted at both room temperature and 4 degrees in order to garner a better understanding of the uptake mechanism.

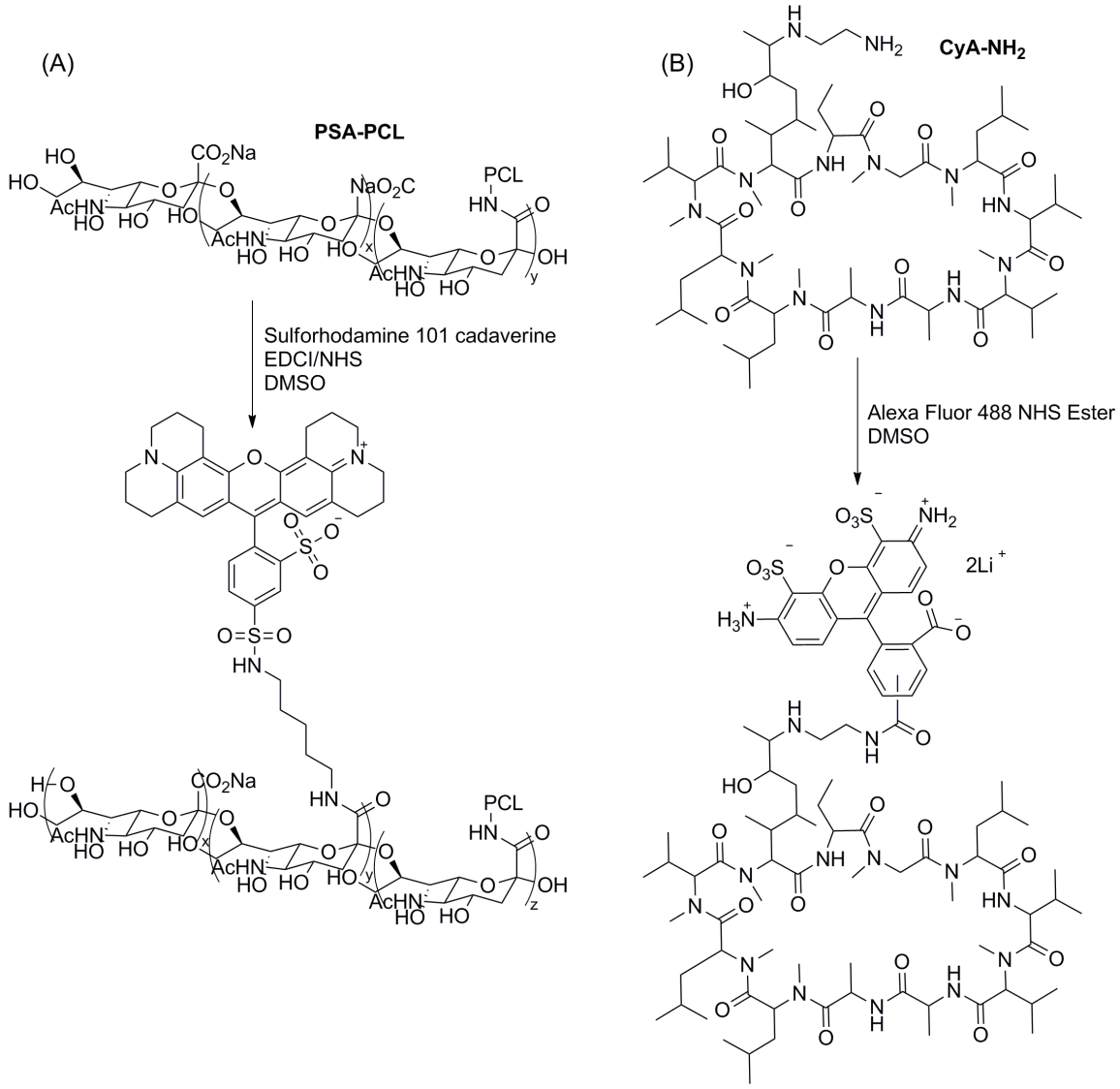

Figure 10. To observe cellular uptake and intracellular separation of PSA-PCL and CyA, (A) PSA-PCL was conjugated to sulforhodamine 101 cadaverine, while (B) CyA modified to include a free amine moiety was linked to Alexa Fluor® 488.

4.3 Results and discussion

4.3.1. Synthesis and characterization of PSA-PCL micelles

PSA-PCL was successfully synthesized via amide bond formation between PSA and amine-terminated PCL (Figure 8). Low molecular weight PCL (Mw ~ 8000) was synthesized via dual activation of the benzyl alcohol initiator and ε-caprolactone monomer with 1, 5, 7-triazabicyclo[4.4.0]dec-5-ene (TBD) catalyst [260] (Figure 35). The terminal hydroxyl group of the PCL polymer was subsequently conjugated to Boc-protected glycine (Figure 36). Acid-catalyzed deprotection yielded the desired amine-terminated PCL [261] (Figure 37). To facilitate the reaction between organic soluble PCL and water soluble PSA, the counterion of PSA was exchanged from sodium to tetrabutylammonium [262]. Following PSA-PCL conjugation in a mixture of methylene chloride and DMSO, the ion was changed back to sodium by dialyzing the product against 150 mM aqueous NaCl for 2 days. The latter step was necessary to prevent potential toxicity from the tetrabutylammonium salt. From ^{1}H NMR, the degree of substitution, defined as the percentage of monomers on the PSA backbone grafted with PCL, was determined to be approximately 1%, or a weight ratio of 4 PSA: 1 PCL (Figure 38).

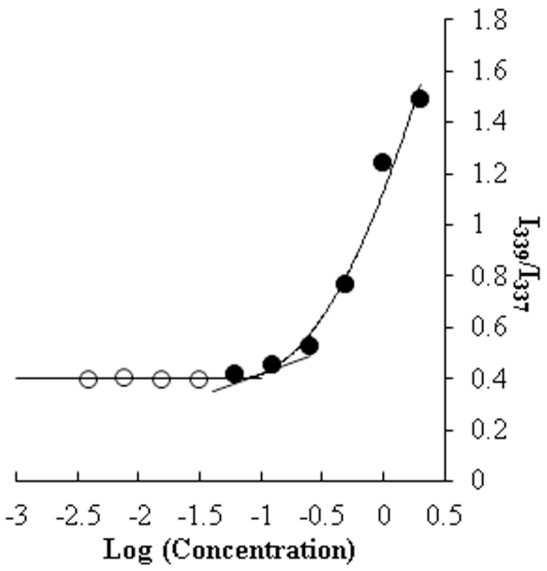

Figure 11. A representative plot showing the change in I339/I337 for pyrene as the concentration of PSA-PCL (mg/mL) is increased.

The capacity for PSA-PCL to self-assemble into micelles was assessed using pyrene as a fluorescent probe based upon established methodology [206, 263]. As the PSA-PCL concentration was increased past that required for micelle formation, i.e. the critical micelle concentration (CMC), the pyrene achieved a new equilibrium between the hydrophobic core of the micelle and the hydrophilic aqueous solution. These changes in the distribution between the hydrophilic and the hydrophobic phases resulted in a measureable shift in the pyrene excitation spectrum. By plotting the ratio of intensities at 339 and 337 nm (emission wavelength = 390 nm), as a function of the log of PSA-PCL concentration, the CMC was determined to be 84.7 ± 13.2 μg/ml from the intersection of the tangent of the inflection point with the horizontal tangent of the low concentration points (Figure 11). The low value obtained for PSA-PCL is consistent with the CMC of decylamine-modified PSA [253] and other polysaccharides based micelle systems [206, 263, 266]

The size of the PSA-PCL micelles without encapsulated therapeutics was 66.8 ± 6.2 nm, as determined by dynamic light scattering and confirmed by transmission electron microscopy (Figure 12 and figure 13).

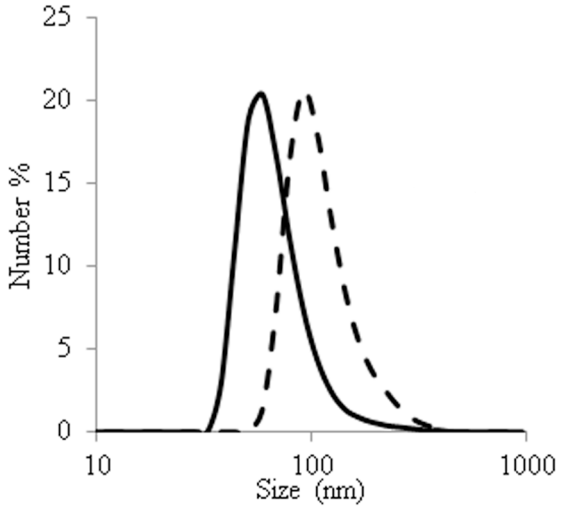

Figure 12. Dynamic light scattering was used to determine the size and polydispersity of PSA-PCL micelles without (solid line) and with (dashed line) encapsulated Cyclosporine A. Drug loading resulted in a significant size increase; however, both sizes were within the preferred size range for drug delivery.

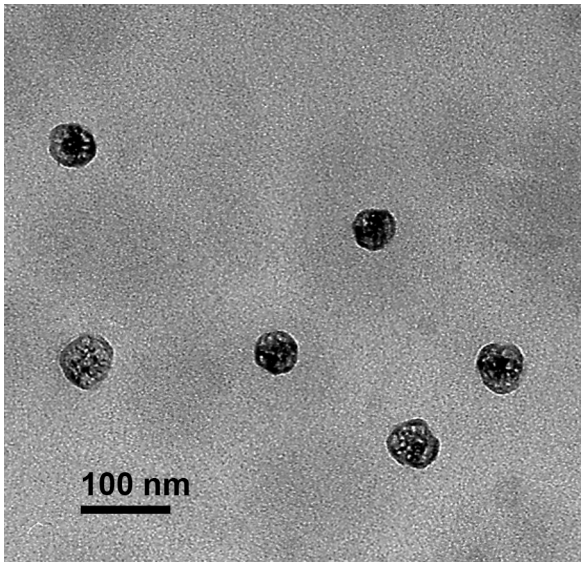

Figure 13. Transmission electron microscopy was used to confirm spherical micelles with a size of approximately 70 nm were obtained via self-assembly of PSA-PCL.

Based on size alone, PSA-PCL micelles are suitable for use as part of a treatment strategy. In drug delivery, particle size has a known significant impact on drug distribution, excretion, and efficacy [267]. Microparticles primarily accumulate in the lungs, while nanoparticles with a size range larger than 200 nm are usually trapped and eliminated quickly by reticuloendothelial system (RES). In contrast, if the size is under 10 nm, the particles are often rapidly excreted by the kidneys. Therefore, the particles intended for long circulation should ideally possess a size between 10 and 200 nm, as was obtained here [256]. Moreover, inflamed tissue, such as that found in rheumatoid arthritis, has poorly organized vascular structure due to angiogenesis, immune cell accumulation, and an imbalance in the secretion of signaling molecules [268, 269]. Nanoparticles with sufficient size to evade kidney filtration, but small enough to avoid RES uptake, will passively accumulate within inflamed tissues [182].

To provide an initial assessment of the surface properties, the zeta potential of the PSA-PCL micelles was determined to be -29.7 ± 8.0 mV. As empirically established, an absolute value between 30-40 mV indicates a stable colloidal particle system with low affinity to blood proteins [270]. Thus, initial size and surface charge measurements suggest that PSA-PCL micelle may serve as effective carrier system. As discussed below, to obtain a better sense of surface properties, zeta potential measurements were also used in conjunction with Guoy-Chapman theory to assess the fixed aqueous layer thickness (FALT).

Cytotoxicity was assessed using the SW982 human synovial sarcoma cell line via WST-8 assay. The cell line was chosen based upon future in vitro tests that will be used to assess the efficacy of CyA-loaded PSA-PCL micelles in the treatment of rheumatoid arthritis. As represented in Figure 14, the IC_{50} for PSA-PCL was determined to be 10.5 ± 1.7 mg/ml, a value greater than or comparable to other polymeric micelle systems that are considered to be non-cytotoxic [271, 272]. In addition, the IC_{50} value obtained here was significantly greater than that obtained previously for micelles prepared from polysialic acid modified with short chain hydrocarbons [253]. The lack of observed cytotoxicity provides an indicator of biocompatibility for subsequent in vivo experiments. Notably, CyA has previously been shown to be non-cytotoxic towards human synovial fibroblasts [253].

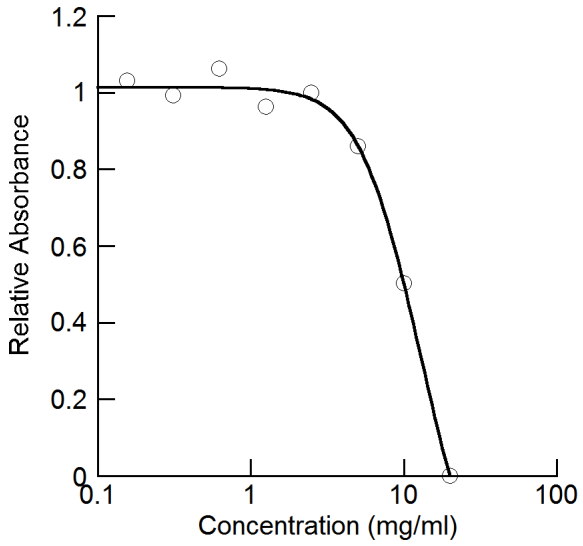

Figure 14. A representative plot illustrating the use of the WST-8 assay to assess cytotoxicity upon administration of a range of PSA-PCL concentrations (0.08 – 20 mg/ml) to the SW982 synovial cell line for 24 h at 37°C. A four parameter logistic curve fit was used to determine an IC_{50} of 10.5 ± 1.7 mg/ml (N = 3).

4.3.2 Encapsulation of cyclosporine A (CyA)

CyA was chosen as a representative drug to evaluate the potential of PSA-PCL as a carrier system for use in the treatment of rheumatoid arthritis. CyA is a regularly used disease modifying anti-rheumatic drug with strong immunosuppressive properties. Despite a demonstrated ability to alter the progression of rheumatoid arthritis in many patients, CyA is nephrotoxic; therefore, frequent monitoring for signs of possible renal dysfunction and kidney damage is necessary [219, 273]. In part, the observed toxicity is likely a consequence of the large, between-patient variability in pharmacokinetic parameters [274]. Thus, CyA is an ideal candidate for incorporation into a drug delivery system that will serve to improve the pharmacokinetic profile.

The therapeutic efficacy of CyA is primarily attributed to inhibition of T cell activation [275, 276]; however, CyA has also been shown to reduce the expression/secretion of pro-inflammatory cytokines, adhesion molecules, metalloproteinases, and angiogenic growth factors by several other cell types associated with rheumatoid arthritis, particularly synovial fibroblasts [277-279]. The mechanism by which CyA acts in rheumatoid arthritis and other pathologies has not been fully elucidated. Although numerous studies have demonstrated the interference of CyA with calcium-dependent signaling pathways [275, 276], initial activity has been postulated to be due to partitioning of the hydrophobic drug into the phospholipid membrane and subsequent alteration of phospholipid metabolism [280, 281]. As will be discussed further below, a fluorescently tagged CyA derivative was used in this study to allow for visualization of CyA partitioning to the membrane following administration of the drug-loaded micelles.

An established dialysis method was used to facilitate loading of CyA into the PSA-PCL micelles [264]. A solution of CyA and PSA-PCL in a mixture of methanol, DMSO, and water was extensively dialyzed against water until drug-loaded micelles were formed and most of the residual organic solvent within the dialysis tubing was removed. After dialysis, non-encapsulated CyA was removed by centrifugation, and the drug-loaded micelles were isolated for storage as a white powder via lyophilization. Size measurements before and following re-dispersion in water verified that the CyA-loaded PSA-PCL micelles were stable to freeze drying without the addition of a cryoprotectant, as is typically required for PEG-modified systems [234, 282]. The size of the micelles increased to 107.5 ± 9.3 nm upon CyA loading; however, the polydispersity index was significantly lowered from 0.32 ± 0.05 to 0.16 ± 0.01, suggesting that the interaction of the PCL with the CyA enhances the stability of the micelles.

CyA encapsulation was quantified by high performance liquid chromatography. The loading capacity and loading efficiency were determined to be of 0.09 ± 0.02 mg CyA/mg PSA-PCL and 29.3 ± 6.4 %, respectively. Of note, these values were significantly higher than those obtained for a previously developed polysialic-acid based micelle system that utilized short chain hydrocarbons to initiate self-assembly [253]. Presumably, the large, hydrophobic CyA molecules have more favorable interactions with the long hydrophobic chains of PCL relative to the short chain hydrocarbons. The latter result correlates with the observed reduction in the polydispersity index. Moreover, these values were comparable to those obtained by other researchers for drug loaded polymeric micelle systems [283, 284].

4.3.3. Comparison of PSA-PCL micelles to PEG-coated micelles

PEG modification has long been used as a method to reduce undesirable interactions with the RES and extend the circulation time of drug delivery systems. One of the proposed mechanisms by which PEG modification gives this so-called stealth nature to drug delivery systems, particularly liposomes, is via an increased affinity to water molecule. Thus, several researchers have begun using the fixed aqueous layer thickness (FALT) as a quantitative measure of the ability of colloidal carriers to resist opsonization and subsequent uptake by the RES [205, 255-258].

To measure the FALT, the PSA-PCL micelles were suspended in aqueous solution with increasing NaCl concentrations, and the zeta potentials were measured. Assuming a spherical particle and a homogeneous charge distribution, Guoy Chapman theory can be applied to give the zeta potential ψ (L) as a function of the Debye Huckel parameter, $\kappa = C1/2/0.3$ [205, 257, 258, 285]:

$$Ln\psi\ L = LnA - \kappa L \quad (4.4)$$

where C is the molarity of the NaCl and A is a constant. Plotting Ln ψ (L) versus κ yields a straight line with a slope L, equal to the thickness of the FALT in nm. From eq. 4.4, the FALT for the PSA-based micelles was calculated to be 0.63 ± 0.03nm. For comparison, traditional, PEGcoated liposomes were also prepared, and the FALT was determined to be 0.77 ± 0.11nm. The comparable values ($p > 0.05$) obtained for the PSA-PCl micelles and PEG-coated liposomes suggest that PSA can provide a similar aqueous layer compared to that afforded by PEG. Furthermore, the FALT of the PSA-PCL micelles was greater than and near those reported in the literature for unmodified liposomes and liposomes coated with low molecular weight PEG, respectively [205, 255-258].

4.3.4. Cellular uptake and intracellular therapeutic release

To facilitate visualization of micelle uptake and therapeutic release in vitro, the PSA-PCL micelles and CyA were labeled with red (sulforhodamine) and green (Alexa Fluor 488) fluorescent tags, respectively (Figure 15). Dynamic light scattering was used to verify that the size and zeta potential of the drug-loaded micelles were unaffected by the presence of the labeling moieties.

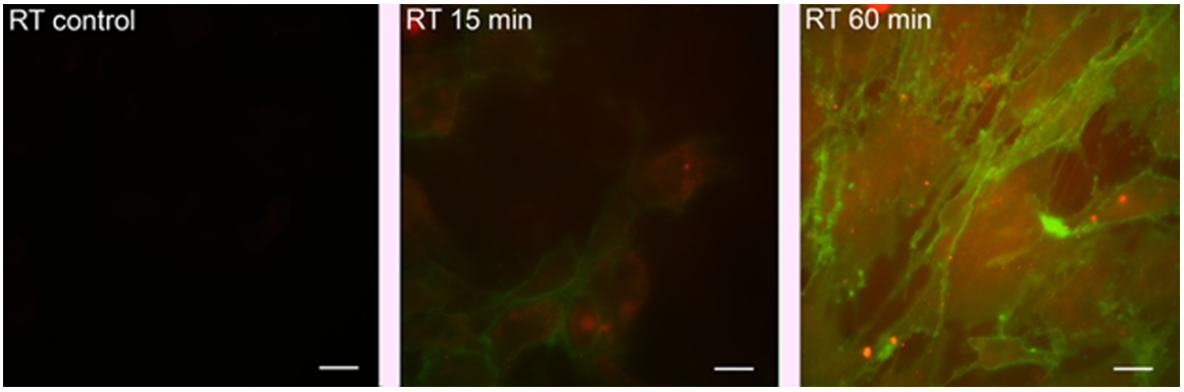

Figure 15. Color composite of fluorescence microscopy images demonstrating nanoparticle uptake and intracellular drug release at room temperature. Use of identical imaging settings permits direct comparison of fluorescence intensities. Left image: cells not incubated with nanoparticles result in negligible signal. Middle image: cells after 15 minutes incubation with the nanoparticles. Clearly visible is the separation of the PSA-PCL drug carrier (red) and CyA (green) that appear strongly localized at the plasma membrane. Right Image: Cells after 60 minutes incubation. Fluorescence signals from PSA-PCL (red) and CyA (green) are much higher indicating much increased nanoparticle uptake. Scale bars are 5 μm.

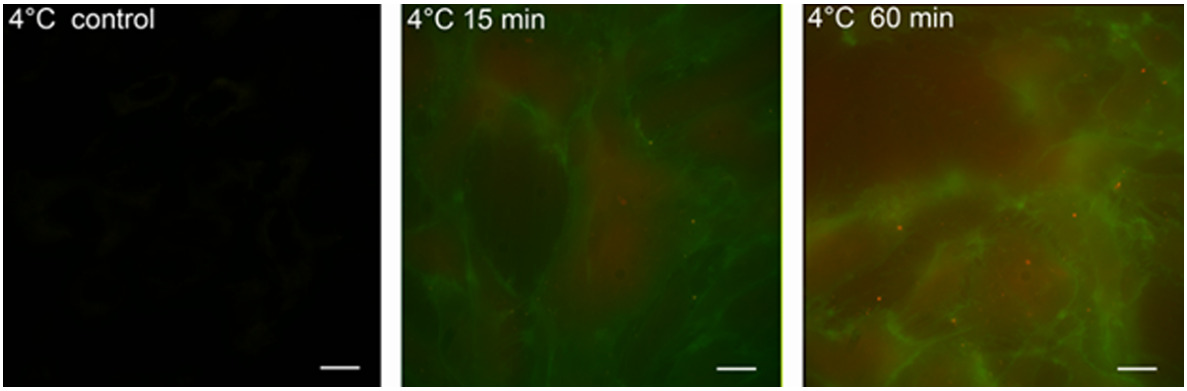

Figure 16. Color composite of fluorescence images demonstrating nanoparticle uptake and drug release at 4°C. Acquisition parameters are the same as in Figure 15, but because of significantly lower intensities different brightness settings had to be chosen. For a direct comparison see Figure B1 and B2 in APPENIX B. Left image: cells not incubated with nanoparticles result in negligible signals. Middle image: cells after 15 minutes incubation with the nanoparticles. Some uptake and separation of the PSA-PCL drug carrier (red) and CyA (green) is apparent. Right Image: Cells after 60 minutes incubation. Fluorescence signals from both PSA-PCL (red) and CyA (green) have increased indicating additional drug-carrier uptake over time. Scale bars are 5 μm.

As shown in Figure 15, the SW982 cells showed time-dependent uptake of the CyA-loaded micelles, as well as rapid intracellular release of the drug from the carrier system. The observed migration of CyA from the intracellular space to the membrane lends support to the notion that the immunosuppressive activity of CyA is, in part, a result of phospholipid bilayer disruption. Purportedly, changes in membrane organization and fluidity following interactions with CyA yield a reduction in phosopholipid metabolism that inhibits cellular activation [280, 281, 286-288]. An identical set of experiments was conducted at 4°C, rather than room temperature, to preliminarily assess the mechanism of cellular uptake (Figure 16). The significant reduction in fluorescence intensity suggests that internalization of the micelles is primarily through energy-dependent endocytic pathways [289-291]. Of note, rheumatoid arthritis synovial fibroblasts exhibit enhanced endocytic activity compared to healthy synovial fibroblasts [292]. This characteristic is expected to further enhance the targeting ability of carrier systems that enter cells via energy dependent pathways, including the PSA-PCL micelles.

4.4 Conclusion

In this study, PSA-PCL micelles were developed as carrier systems for CyA, a disease modifying anti-rheumatic drug that is associated with significant, adverse side effects. Physical characterization, including size and zeta potential, demonstrated that the micelles possess favorable properties for drug delivery. The PSA gave rise to an aqueous layer, similar to that found with PEGylated liposomes, that is expected to confer "stealth" like properties *in vivo*. *In vitro* studies verified that rheumatoid arthritis synovial fibroblasts are able to internalize the CyA-loaded micelles. Furthermore, CyA was released from the PSA-PCL micelle upon uptake

and, subsequently, partitioned into the phospholipid membrane, suggesting a mechanism of action that begins with membrane disruption.

Chapter 5 Development and characterization of polysialic acid-N, N, N-trimethyl chitosan nanoparticles

In drug delivery, the nanoparticles must be of proper size and charge to achieve high efficacy and low toxicity of associated therapeutics. In this study, nanoparticles were developed via ionic gelation of two polysaccharide-based molecules, negatively charged polysialic acid (PSA) and positively charged N, N, N-trimethylchitosan (TMC). PSA is unique in that the highly hydrated backbone may be used in a manner similar to that of poly (ethylene glycol) to extend circulation times. Although not necessary for nanoparticle formation, sodium tripolyphosphate (TPP) was added to enhance stability, as indicated by a reduced polydispersity. We investigated three different ratios by weight of PSA: TMC (0.5:1, 1:1, 1:2 and five different TPP concentrations ranging from 0.1 mg/ml to 0.8 mg/ml. As controls, nanoparticles were also formed without PSA from chitosan and TMC with TPP. Optimal size and surface charge were achieved with a PSA: TMC weight ratio of 0.5:1 and a TPP concentration 0.2 mg/ml. For the nanoparticles prepared in the latter fashion, a more in depth characterization was conducted. The nanoparticles were distinct solid, spherical nanogels with a size of 106 ± 25 nm, an ideal size to reduce uptake by the reticuloendothelial system while facilitating passive targeting of diseased tissue. The zeta potential of the nanoparticles was +33.9 ± 1.2 mV, suggesting that the nanoparticles will be stable under physiological conditions. Encapsulation and controlled release by the nanoparticles was demonstrated using methotrexate, a therapeutic indicated in both cancer and rheumatoid arthritis. The results obtained thus far strongly indicate that PSA-TMC

nanoparticles are suitable drug carrier systems for systemic administration.

5.1 Introduction

One century ago, Paul Ehrlich proposed that drugs should be developed selectively to treat diseased cells without damaging healthy tissues [243]. Directed by this concept, many studies have been done to investigate various materials as potential drug delivery systems for a number of diseases with broad goals of facilitating controlled release, improving efficacy and reducing side effects. Among the different types of drug delivery systems, nanoparticles have drawn the most attention due to numerous benefits, such as reduced toxicity, as well as improved efficacy, bioavailability, and solubility [254, 293]. Furthermore, nanoparticles have been demonstrated to accumulate passively within tumor tissue due to the EPR (enhanced permeability and retention) effect [252].

For systemic drug delivery, one of the most sought after properties is a long circulation time that can increase the chance of drugs' accumulation in diseased tissues, which can thereby improve drug efficacy. Polyethylene glycol (PEG) conjugates, micelles, and nanoparticles are commonly used to shield drugs from rapid clearance. Despite demonstrated efficacy, particularly in the treatment of cancer, PEG-carrier systems have several draw- backs when considered for the treatment of chronic conditions, such as rheumatoid arthritis and other inflammatory diseases. Of note, higher molecular weight PEG chains, with a large associated hydrodynamic radius, cannot be renally excreted. Although this effect is desirable for EPR, no long term studies have been done to date to elucidate if the PEG is cleared once the payload of the carrier sys- tem is released and/or where the PEG accumulates and the impact of this accumulation [158, 294,

295]. Furthermore, upon intravenous administration, PEGylated therapeutics may elicit an adverse immunological response through complement activation [158, 295]. Although in the short term the benefits of PEG overshadow the potential drawbacks, an alternative to PEG should be sought for diseases that require extended medical care.

The polysaccharide polysialic acid (PSA) is a rarely investigated material that has the potential to prolong the circulation time of therapeutics in vivo. Unlike PEG, PSA is biodegradable and will not accumulate in the human body, causing toxicity [48, 157, 158]. In addition, PSA is nontoxic, biocompatible, and non-immunogenic. Studies have shown that some pathogenic bacteria were surrounded by the thick PSA coating, which made them “unnoticeable" in human body. The thick PSA coating formed a large and highly hydrated structure that could help these bacteria evade the host immune system [48, 195, 296, 297]. Based on this, Gregoriadis et al. [1, 197] proposed PSA as a potential material for increasing the half-life of therapeutics, with the hydrophilic coating preventing interaction between therapeutics and enzymes and immune cells. In addition, the PSA coating might decrease the excretion of therapeutics through the kidney by increasing the size. A series of studies by Gregoriadis et al. followed this initial proposal. Several proteins such as, insulin [6], asparaginase [4, 5] and catalase [2, 3], had been either sialylated or polysialylated. PSA was shown to be advantageous with regards to the preservation of stability and function, prolongation of circulation time and pharmaceutical effect, and reduced immunogenicity and antigenicity [48, 298].

Chitosan is a very popular natural polymer for drug delivery because it is nontoxic, biodegradable, biocompatible and bioadhesive [32, 299-301]. A quaternized derivative of chitosan, N, N, N-trimethyl chitosan (TMC) is soluble and positively charged regardless of pH, as opposed to chitosan that possesses a pH-dependent charge. Therefore, TMC has also been

widely used [33]. To date, chitosan and its derivatives have been investigated as the basis of nanoparticles by many researchers for the delivery of low molecular weight drugs [302], DNA [303], proteins and antigens [304]. With the presence of chitosan and/or its derivatives, a number of the latter therapeutics have shown higher uptake by diseased tissue, less toxicity and greater specificity.

Despite the advantages given above, the application of chitosan-based nanoparticles is limited by poor stability under physiological conditions, poor efficacy in vivo, and a large size that is unfavorable for systemic drug delivery [305-309]. Researchers have previously demonstrated that 80-120 nm is the ideal size for nanoparticles intended for systemic drug delivery [310]. In this size range, nanoparticles can (1) passively accumulate in diseased tissue such as inflamed tissue or cancer tissue [252], (2) avoid excretion by the kidneys [13], and (3) reduce clearance from the circulation [311]. However, most chitosan-based nanoparticles have a size larger than 200 nm, a zeta potential lower than 30 mV, indicative of aggregation under physiological conditions, and a large size range, or polydispersity index (PDI) [305-309]. Furthermore, due to their cationic nature, chitosan-based nanoparticles are prone to react with negatively charged components in the blood circulation, which can increase the rate of clearance by the reticuloendothelial system (RES) and phagocytes [312]. Incorporation of highly hydrophilic material, such as the polysialic acid used in the current study, can decrease this type of interaction and increase the plasma circulation time of the associated drugs [313]. To date, few nanoparticles based upon chitosan or its derivatives are ideal for systemic drug delivery due to an overly cationic nature, a typically large size and a propensity to aggregate.

In this study, we developed a PSA-TMC nanoparticle system by complexing positively charged TMC with negatively charged PSA. At a weight ratio of 0.5 PSA: 1 TMC, the resultant

nanoparticles possessed a favorable size and zeta potential, indicative of a promising drug delivery system. To further demonstrate the nanoparticles capacity in drug delivery, methotrexate (MTX) a therapeutic used in the treatment of both rheumatoid arthritis and cancer, was used as a model compound for encapsulation and controlled release. Cytotoxicity and uptake of the nanoparticles was evaluated using a rheumatoid arthritis synovial fibroblast cell line (MH7A). In further study, we will investigate the anti-rheumatic effect and bio-distribution of this nanoparticle system relative to free MTX.

5.2 Materials and Methods

5.2.1 Materials

Polysialic acid was purchased from Nacalai USA, Inc. (San Diego, CA, USA). Chitosan (Mw 100k-300kDa) was purchased from Acros Organics (Fair Lawn, NJ, USA). Sodium hydroxide (extra pure, pellets), tripolyphosphate (pure) (TPP), acetonitrile (HPLC grade) were also from Acros Organics (New Jersey, USA). Sodium iodide (puriss), methyl iodide (reagent plus), 1-methyl-2-pyrrolidinone (anhydrous), ethanol (reagent alcohol), ammonium acetate, deuterium oxide, and acetic acid (ACS reagent grade) were obtained from Sigma (St. Louis, MO, USA). Hydrochloric acid (ACS plus grade) was supplied by Fisher Scientific (Hanover Park, IL, USA). Methotrexate was purchased from Enzo Life Science (Farmingdale, NY, USA). All chemical reagents were used without further purification. MH7A synovial fibroblast cell line was provided by the Riken BRC through the National Bio-Resource Project of the MEXT, Japan. RPMI-1640, D-PBS, HEPES, L-glutamine, fetal bovine serum (FBS) and penicillin-streptomycin were purchased from Lonza, Inc. (Allendale, NJ).

5.2.2 Preparation of Polysialic Acid-N,N,N-Trimethyl Chitosan (PSA-TMC) Nanoparticles

5.2.2.1 Synthesis of N,N,N-Trimethyl Chitosan (TMC)

The general procedure for TMC synthesis, as well as ionic complexation with TPP to form nanoparticles is illustrated in Figure 17. TMC was synthesized according to a one-step method, previously described by Sieval et al. [314] Briefly, in a sample procedure, 0.5 g (0.0031 mol) chitosan and 1.2 g (0.008 mol) sodium iodide were added into 20 ml anhydrous N-methyl pyrrolidinone in a nitrogen purged 3-neck flask. The solution was reacted at 60 ˚C for 1.5 h with a stirring speed of 190 rpm. Then, 4.13 ml 1M NaOH (0.0041 mol NaOH), 2.88 ml (0.046 mol) methyl iodide were added and stirring was continued for another 1 h at 60 ˚C. The reaction solution was then added dropwise to cold ethanol. The yellow precipitate was collected by vacuum filtration. For further purification, the product was dissolved in 15ml DI water and precipitated again in 62 ml 1M HCL in ethanol. 0.626 g of white, solid product was obtained after vacuum filtration and evaporation overnight in a vacuum oven. The degree of quaternization (DQ) of TMC was determined by ^{1}H-NMR (Bruker DPX-300) in D_2O. The DQ was calculated by the following equation, $DQ\ (\%) = [(\int TM/\int H) \times 1/9] \times 100$ [315]. $\int TM$ is the integral of ^{1}H trimethyl amino group peak at 3.0-3.2 ppm and $\int H$ is the integral of ^{1}H peak from C_1 of the glycoside ring from 4.9 ppm to 5.5 ppm (Figure 39).

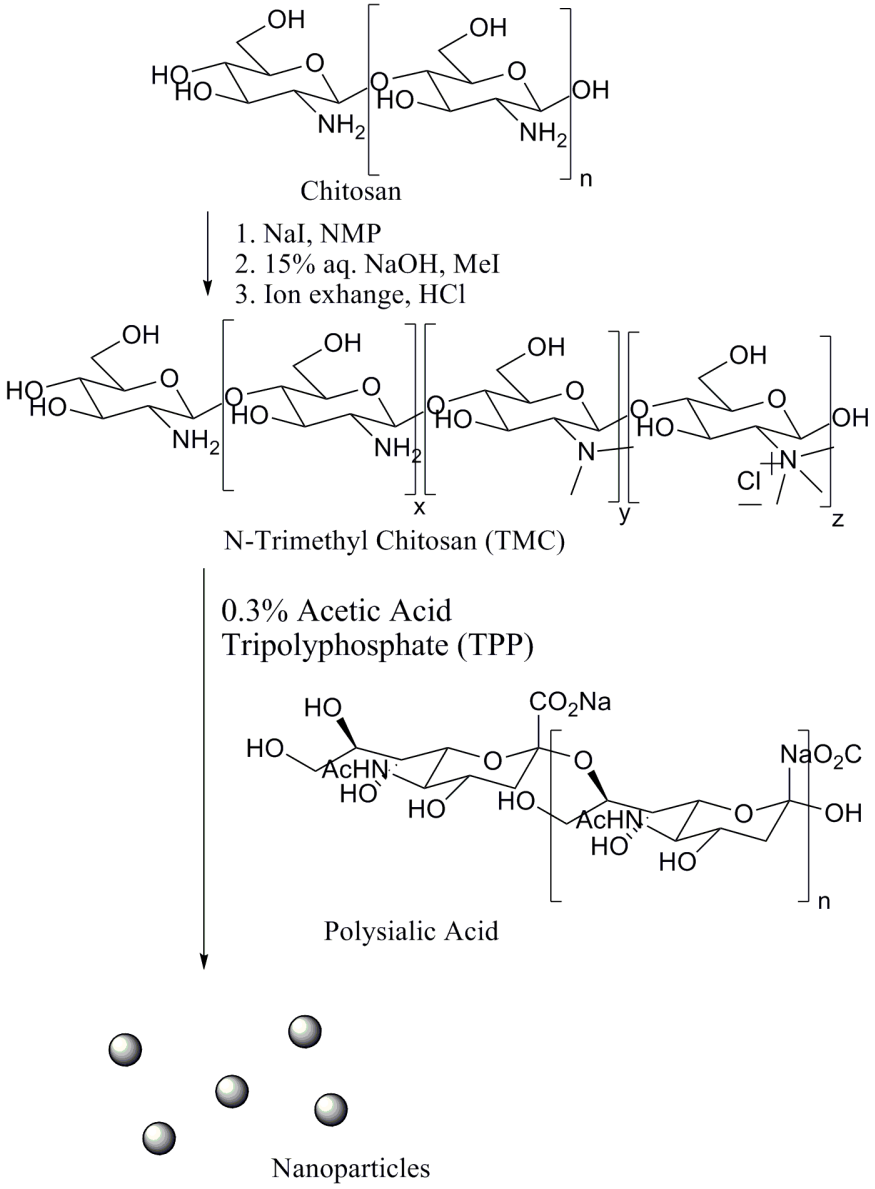

Figure 17. Synthesis of TMC and complexation with PSA in the presence of TPP to yield nanoparticles.

5.2.2.2 Preparation of PSA-TMC Nanoparticle

Ten sets of PSA-TMC nanoparticles were prepared by varying the ratio of PSA: TMC or the TPP concentration (Table 4). The method was similar to those previously established for ionic gelation of chitosan/TMC with TPP [316, 317]. As an example procedure, to prepare PSA:

TMC (0.5:1) with a TPP concentration of 0.2mg/ml (Group 3, Table 4), 6.4 mg of TMC was dissolved in 3 ml of 0.3% acetic acid in a glass vial. In a separate glass vial, 3.2 mg PSA and 1mg TPP were mixed well with 2ml deionized (DI) water. The PSA solution was added drop by drop to the TMC solution while stirring. The solution was stirred for 30 min to stabilize the nanoparticles system. A pellet of nanoparticles was obtained after centrifugation at 300 rpm for 15 min. Excess supernatant was removed.

Table 4. Different weight ratios of PSA: TMC and TPP concentrations used in the preparation of nanoparticles.

Group	PSA (mg)	TMC (mg)	0.3% Acetic Acid (ml)	DI Water (ml)	TPP (mg)
1	0	6.4 (Chitosan)	3	2	1
2	0	6.4	3	2	1
3	3.2	6.4	3	2	1
4	6.4	6.4	3	2	1
5	12.8	6.4	3	2	1
6	3.2	6.4	3	2	0
7	3.2	6.4	3	2	0.5
8	3.2	6.4	3	2	1.5
9	3.2	6.4	3	2	2
10	3.2	6.4	3	2	4

5.2.3 Characterization of PSA-TMC Nanoparticles

The size and zeta potential of the PSA-TMC nanoparticles were measured using a Malvern Zetasize NanoZS90 (Malvern Instruments Ltd., Malvern, UK). The particle size distribution of the nanoparticles was reported as a PDI. The nanoparticles were dissolved in DI water at 2 mg/ml and used without filtration. Then, the nanoparticle solutions were transferred to disposable micro-cuvettes (Malvern Instruments Ltd., Malvern, UK) for size measurements and disposable capillary cells (Malvern Instruments Ltd., Malvern, UK) for zeta potential

measurements. For dynamic light scattering measurements, the temperature was set 25 °C, and the scattered light was detected at an angle of 173°. All measurements were performed in triplicate.

Morphological examination of the nanoparticles was performed by atomic force microscopy (AFM). A drop of aqueous nanoparticle solution (2 mg/ml) was placed on a thin round glass cover slip that was dried in a desiccator overnight. Images were obtained with a Nanoscope III atomic force micro- scope (Veeco Instruments Inc., Plainview, NY) in contact mode.

WST-8 assay (Cayman Chemical Company, Ann Arbor, MI) was conducted on the MH7A rheumatoid arthritis synovial fibroblast cell line, following the manufacturer's instructions, to assess the cytotoxicity of the PSA-TMC nanoparticles. NADH produced within the mitochondria reduces WST-8 tetrazolium salt to formazan dye, which can be quantified by absorbance measurements at 450 nm. Cells were seeded into 96-well cell culture plate (2×10^4 cells per well) and cultured for 24 h at 37 °C, 5% CO_2. PSA-TMC (0.5:1) was added to yield a series of concentrations from 0.3125 mg/mL to ~20 mg/mL, and the cultures were incubated for an additional 24 h. 10 μL of WST-8 solution were added to each well. After a 90 min incubation period, absorbance was measured with a Synergy 2 multimode micro-plate reader (BioTek Instruments, Winooski, VT) at 450nm. The cytotoxicities of TMC and TPP alone, i.e., not contained within a nanoparticle, were also evaluated following the above procedure. Untreated MH7A synovial fibroblast cultures were used as controls. Relative absorbance versus concentration was plotted for each set of additives, and a four parameter logistic, constructed with Kaleidagraph software, was used to fit the data to determine the IC_{50} values. Each experiment was repeated independently at least two times.

5.2.4 Encapsulation and Release of Methotrexate (MTX)

5.2.4.1 Encapsulation of MTX

MTX was encapsulated within PSA-TMC nanoparticles (0.5 PSA: 1 TMC, 0.2mg/ml TPP) at a 25% by weight loading percentage. 2.4 mg of MTX was added to the PSA solution, as described above. The PSA solution with MTX was added drop by drop to the stirring TMC solution to yield MTX loaded nanoparticles. Again, the final solution was stirred for 30 min to stabilize the nanoparticle system. MTX loaded nanoparticles were isolated by centrifuging at 3000 rpm for 15 min. 1 ml supernatant was kept following centrifugation to assess loading capacity, while the remaining supernatant was discarded.

5.2.4.2 Release of MTX from PSA-TMC Nanoparticles

Release studies were performed on the MTX loaded PSA-TMC nanoparticles. Immediately after preparation, nanoparticle solutions were transferred to 15 ml centrifuge tubes and centrifuged at 3000 rpm for 15 min. 1 ml of supernatant was saved for the loading capacity and efficiency analysis. To begin the release experiments, the nanoparticles were re-suspended in 5 ml of DI water, and the nanoparticle solutions were transferred to Spectra/Por (Spectrum Laboratories, Rancho Dominguez, CA, USA) dialysis tubes (MWCO 12,000-14,000). Dialysis was performed against 45 ml DI water pH 7.4, at 37 ˚C under static conditions. 1 ml of external medium was withdrawn and immediately replaced with fresh DI water at the following time points: 10min, 20min, 40min, 1, 2, 4, 6, 12, 24 and 48h. The release samples were analyzed with a Prominence Ultrafast Liquid Chromatography System (UFLC, Shimadzu Scientific Instruments, Japan) equipped with an SPD-20AV UV detector, an SIL- 20A autosampler, a

DGU-20A_3 degasser, and a Shim-pack XR-ODS/C8/Phenyl column. The mobile phase was a 93:7 mixture (v/v) of 50 mM aqueous ammonium acetate and acetonitrile that was pumped at a slow rate of 0.5 ml/min. An injection volume of 100 µL was used, and the detection wavelength was set to 210 nm. A calibration curve was constructed by determining the area under the peak of eight MTX solutions with known concentrations ranging from 0.39 µg/ml to 50 µg/ml using PeakFit 4.2 software. Loading capacity (LC) and loading efficiency (LE) were determined using the following equations:

$$\text{LE} = \frac{m_{MTX,loaded}}{m_{MTX,added}} \times 100 \quad (5.1)$$

$$\text{LC} = \frac{m_{MTX,loaded}}{m_{Nanoparticles}} \quad (5.2)$$

where $m_{MTX;added}$ is the mass of MTX added to the PSA solution, $m_{MTX;loaded}$ is the mass of MTX loaded into the nanoparticles, and $m_{Nanoparticle}$ is the mass of the nanoparticles used for the release study.

5.2.5 Cellular Uptake of PSA-TMC Nanoparticles

Uptake of the PSA-TMC nanoparticles by the MH7A cells was verified with inverted fluorescence microscopy. The MH7A cells were added to lysine coated Lab-Tek® Chamber Slides, and fluorescently tagged nanoparticles (Alexa Fluor® 610, Invitrogen) were added 24 h after seeding. After a short incubation period (~45 min), the nanoparticle solution was removed, the cells were washed with PBS, and uptake was observed with a Nikon Eclipse Ti inverted microscope. The incubation period was selected based on prior optimization experiments and is consistent with other researchers with regards to the short time necessary to observe uptake of

chitosan-based nanoparticles [318-320].

5.3 Results and Discussions

5.3.1 Nanoparticle Synthesis and Characterization

From the ^{1}H NMR spectra, a DQ of ~50% was reproducibly obtained (Figure 39). Jintapattanakit et al [321] reported that, at this DQ range, TMC has higher water-solubility and mucoadhesiveness. The DQ determined the amount of positive charge in chitosan chains. This consequently had a significant impact on the surface charge of the nanoparticles, which indirectly related to the size distribution of the nanoparticles due to aggregation. Therefore, to produce TMC with a reproducible DQ of 50% was critical in obtaining reproducible nanoparticles with consistent size distribution [33].

In this study, three different weight ratios of PSA: TMC were investigated, all prepared with a TPP concentration of 0.2 mg/ml. Chitosan and 50% modified TMC, with no PSA, were used as controls. The results were summarized in Figure 18. As indicated by zeta potential values much less than an absolute value of 30, PSA: TMC nanoparticles with weight ratios of 1:1 and 1:2 were not stable. Low zeta potential values were associated with a deficiency of electronic force necessary to keep the nanoparticles separated from each other [233]. Chitosan itself did form particles, consistent with other researchers [322]; however, the size was not favorable for drug delivery. Furthermore, the size variation and size distribution were high, suggestive of a lack of stability and a propensity to aggregate [24]. Presumably, the variability in size with a high PDI was a result of the pH-dependent positive charge. In contrast, pH-independent TMC formed nanoparticles with the desired size; however, the size distribution remained high. In

addition, the lack of a hydrophilic component, such as PSA, might result in undesirable uptake by the RES during circulation [37]. A PSA: TMC ratio of 0.5:1 was identified as the only ratio that gave rise to nanoparticles with favorable size, a size distribution that was significantly

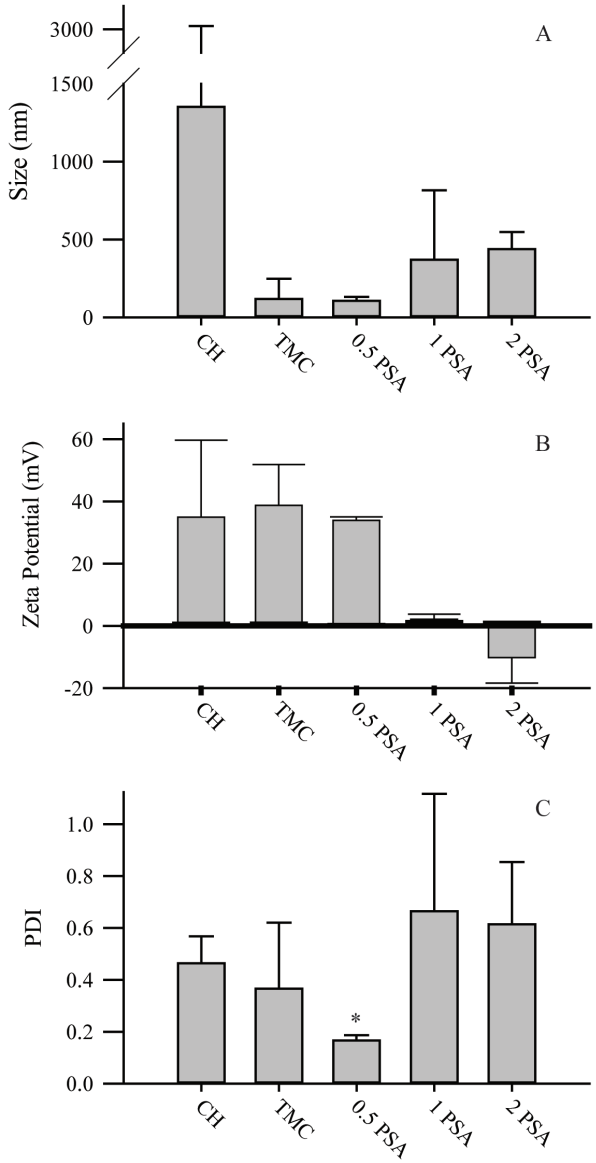

Figure 18. (A) Size, (B) zeta potential, and (C) PDI as a function of the weight ratio of PSA: TMC. *$p < 0.05$ relative to CH, 1 PSA:1 TMC, and 2 PSA:1 TMC.

lower than other formulations, and an appropriate surface charge for systemic drug delivery.

To investigate the effect of TPP concentration size distribution, five different TPP concentrations were investigated for nanoparticles prepared with a 0.5:1 PSA: TMC ratio (Figure 19). Nanoparticles prepared with no TPP were used as controls. At 0.1 mg/ml and 0.2 mg/ml TPP, the resultant nanoparticles were of an appropriate size with a narrow size distribution. As TPP concentration increased, the size of the resultant nanoparticles and size distribution became larger; however, the differences between nanoparticles prepared with 0.1 mg/ml, 0.2 mg/ml, 0.3 mg/ml and 0.4 mg/ml were not significant. As shown by the zeta potential values, an increasing amount of TPP increased the negative charge of the nanoparticles, thereby neutralizing the positive charge of the TMC. This reduction in nanoparticle surface charge could in turn be linked to an increase in the interaction between the nanoparticles, resulting in particles with larger sizes and size distributions. PSA complexed with TMC in the absence of TPP yielded nanoparticles of the appropriate size; however, the PDI was significantly larger than those prepared with 0.1 mg/ml and 0.2 mg/ml TPP. A literature survey indicated that nanoparticles prepared with higher TPP concentrations possess a greater crosslink density [49-51]; therefore, a 0.2 mg/ml TPP concentration would presumably yield nanoparticles with enhanced stability, slower release kinetics and increased loading efficiency relative to a 0.1mg/ml TPP concentration. Based upon this premise and results described herein, a 0.5:1 ratio of PSA: TMC with a TPP concentration of 0.2 mg/ml was identified as the ideal formulation for the formation of stable nanoparticles. A small size, with narrow distribution, and a spherical morphology were confirmed by AFM (Figure 20). AFM has been proven to be an ideal method for nanoparticle characterization, allowing for visualization in three dimensions [52, 53]. Although a strong surface-tip interaction might cause image distortion, this did not appear to occur with the PSA-TMC nanoparticles.

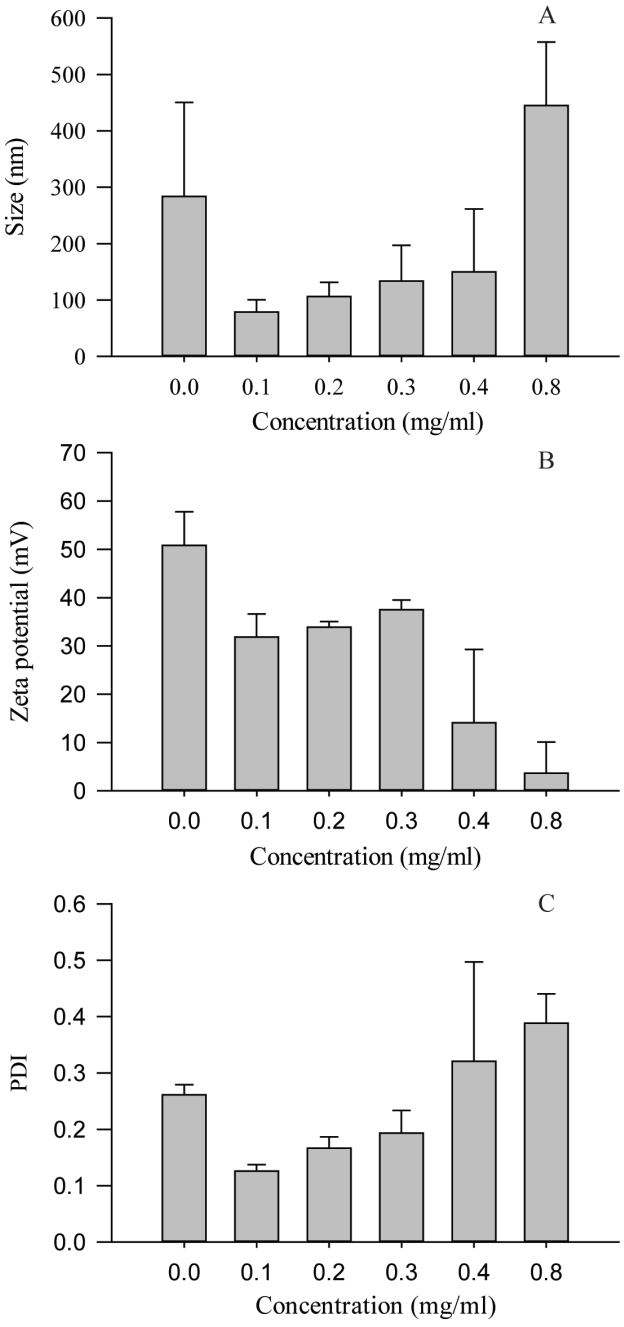

Figure 19. (A) Size, (B) zeta potential, and (C) PDI as a function of TPP concentration

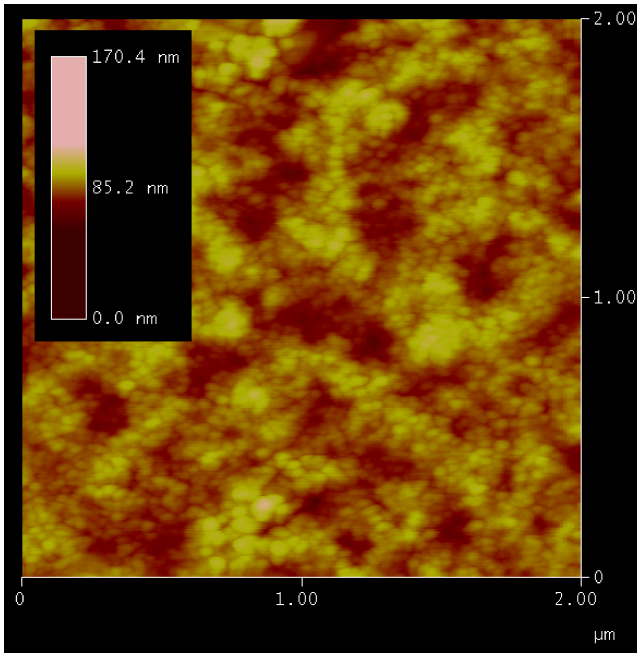

Figure 20. AFM image of PSA-TMC nanoparticles (0.5 PSA:1 TMC, 2 mg/ml TPP).

5.3.2 Encapsulation and Controlled Release of MTX

MTX was successfully encapsulated into the PSA-TMC nanoparticles with a loading efficiency and loading capacity of 46.3 ± 13.0% and 0.10 ± 0.03 mg MTX/mg nanoparticle, respectively. Dynamic light scattering was used as an additional indicator to verify MTX encapsulation. Although the difference was not significant, the MTX loaded nanoparticles were slightly larger than the unloaded nanoparticles (128.7 ± 5.3 versus 106.3 ± 25.4) (Figure 21).

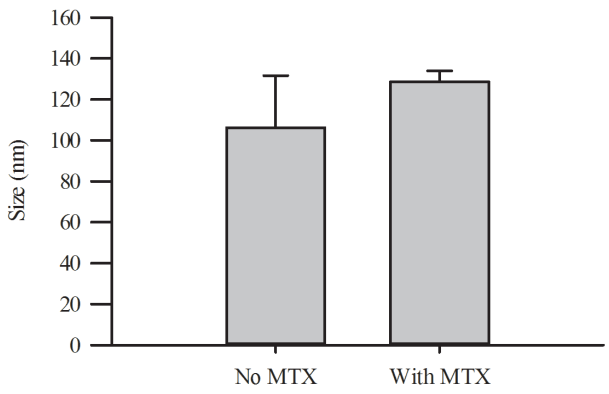

Figure 21. Size of MTX loaded nanoparticles.

Fractional release of MTX as a function of time from the PSA-TMC nanoparticles is shown in Figure 22. Although controlled release was observed, the data could not be fit to a simple diffusion controlled model, where the fractional release was proportional to the square root of time. Consistent with other hydrophobic drugs encapsulated into nanoparticles at high loading capacity (≥ 0.30), the release was presumably dissolution controlled [323]. An in depth analysis on the mechanism and kinetics of release, as well as the in vitro efficacy of encapsulated therapeutics, will be the topic of future studies.

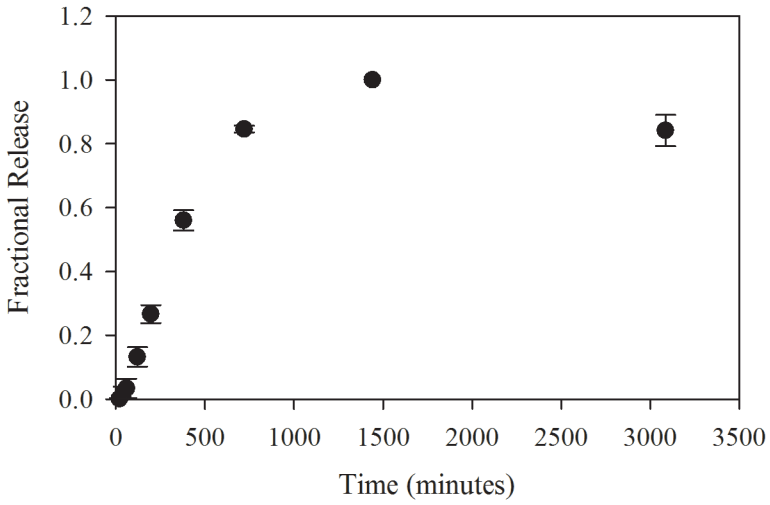

Figure 22. Fractional release of methotrexate from PSA-TMC nanoparticles (0.5 PSA: 1 TMC, 2 mg/ml TPP) as a function of time

5.3.3 Cytotoxicity

For future applications in diseases such as rheumatoid arthritis where the primary goal is not cell death, the cytotoxicity of the nanoparticles must be minimal. As shown in Table 5, TMC had some cytotoxicity as anticipated based on reports by others on the impact of chitosan quaternization on biocompatibility [321]. Previous research from our lab had demonstrated that PSA was not cytotoxic [253], and incorporation of TMC into nanoparticles with PSA resulted in significantly higher IC_{50} values than TMC alone. The TMC should be released from the nanoparticle at a slow rate that would yield only negligible levels of this potentially harmful polymer when administered *in vivo*. Somewhat surprising was the extremely low IC_{50} value observed for TPP given the prevalent use of TPP in forming chitosan TMC nanoparticles. Most recent studies have not tested (1) the cytotoxicity of TPP alone or (2) the cytotoxicity of the chitosan-TPP system as a whole based on the assumption that chitosan is nontoxic [301, 324,

325]. Despite this oversight, a manuscript was recently published on the use of TPP as an excipient that clearly demonstrated the concentration-dependent cytotoxicity of TPP [326]. Exclusion of TPP did reduce the cytotoxicity further (data not shown); however, the TPP was presumably necessary to maintain particle stability (Figure 19).

Table 5. IC_{50} values for TMC, TPP, and PSA-TMC nanoparticles

	IC_{50} (mg/ml)
TMC	2.30 ± 0.84
TPP	0.22 ± 0.04
Nanoparticles (0.5 PSA: 1 TMC)	7.65 ± 0.07

5.3.4 Internalization of Nanoparticles by MH7A Cells

To confirm that the PSA-TMC nanoparticles could be internalized by cells in the absence of an active targeting moiety that would facilitate receptor-mediated endocytotic uptake, the nanoparticles were surface modified with a near infrared fluorescent tag and incubated with the MH7A rheumatoid arthritis synovial fibroblast cell line. As illustrated in Figure 23, even after only a short incubation period, the nanoparticles were able to successfully associate with and enter the cells. The results coincided with the known interactions that occurred between chitosan/chitosan-based materials and cellular membranes [324, 327-329].

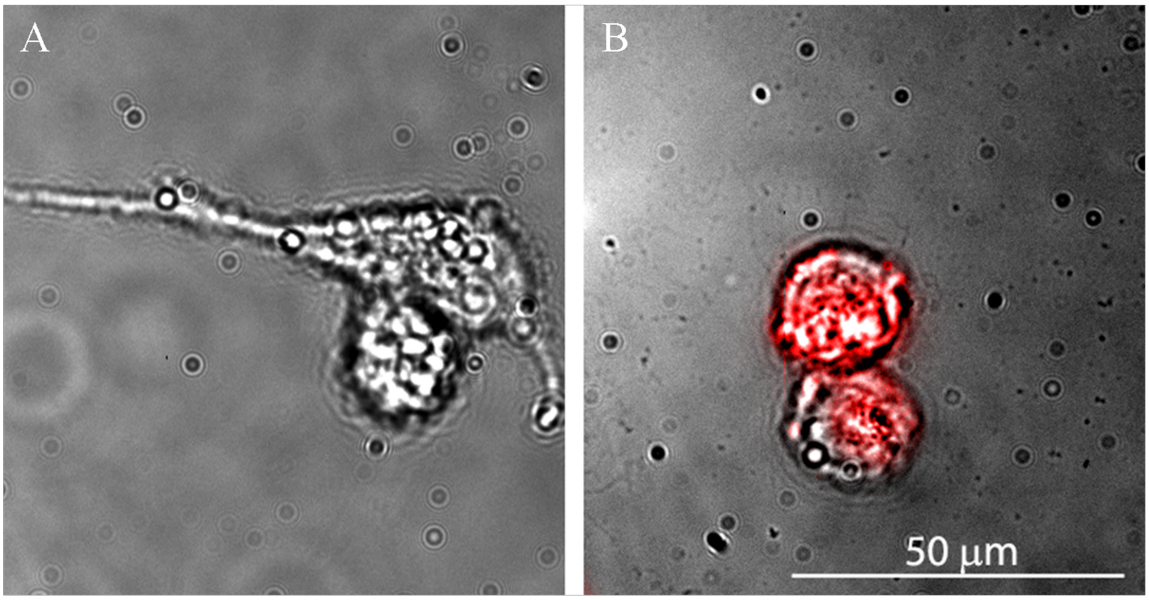

Figure 23. Relative to (A) control cells, (B) fluorescently tagged nanoparticles were readily internalized by MH7A cells

5.3.5 Comparison to Other MTX-Loaded Nanoparticles

Although numerous studies have been conducted with regards to the encapsulation/release of MTX in/from nanoparticles [327-334], most have been designed for the treatment of cancer, where the goal is to maintain or optimize the cytotoxicity that can be achieved with high doses of methotrexate. In contrast, effective carrier systems for the delivery of low, anti-inflammatory doses of methotrexate for the treatment of diseases that require long term care, such as rheumatoid arthritis, must be non-immunogenic and non-cytotoxic. Thus far, only a few systems have been designed with the latter goal in mind.

Two investigators have provided *in vivo* evidence with arthritis rat models that the efficacy of MTX in the treatment of rheumatoid arthritis could be improved by association with or conjugation to a carrier system. Encapsulation of MTX into phospholipid nanoparticles yielded a greater reduction in inflammation than free MTX [334]; however, the utility of this

carrier system for systemic administration, as is requisite for rheumatoid arthritis, has not yet been determined. Alternatively, MTX conjugated to poly(amidoamine) (PAMAM) dendrimer nanoparticles proved to be highly effective for targeted delivery to inflamed joints when administered intravenously [332]. PAMAM dendrimers were significantly smaller than the PSA-TMC nanoparticles, thus the two carrier systems would likely exhibit different pharmacokinetic profiles. In addition to the latter *in vivo* studies, Jingou et al. prepared and characterized chitosan/cyclodextrin nanoparticles with the goal of simultaneously delivering hydrophilic/hydrophobic drugs for the treatment of rheumatoid arthritis. MTX was used as the model hydrophobic compound [333]. Relative to the work described herein, Jingou's nanoparticles were less effective at entrapping MTX, and the MTX release rate from the Jingou's nanoparticles was faster. In addition, the large size of Jingou's nanoparticles was not appropriate for effective systemic delivery. The limited examples of existing carrier systems have highlighted the need for continued expansion of the field of drug delivery into the treatment of chronic diseases such as rheumatoid arthritis.

5.4 Conclusion

The nanoparticle is a type of drug delivery system that can facilitate selective accumulation of drugs in diseased areas. For systemic drug delivery, these nanoparticles systems must possess a long circulation time to have merit. In this study, we reported a gel nanoparticle system with a size of 106 ± 25 nm formed by ionic gelation between PSA and TMC in a ratio 0.5:1 (w/w) in the presence of TPP (0.2 mg/ ml). We believe that the highly hydrophilic PSA chains would significantly prolong circulation time compared to other chitosan-based systems.

MTX was chosen as the model drug in this study because of our interest in improving treatment strategies for rheumatoid arthritis sufferers. Future studies will be used to specifically address the potential for the MTX loaded nanoparticles to treat rheumatoid arthritis.

Chapter 6 *In Vitro* Efficacy of Polysaccharide-Based Nanoparticles Containing Disease-Modifying Anti-rheumatic Drugs

Purpose: To evaluate the therapeutic efficacy of dexamethasone (DM) and methotrexate (MTX) entrapped within polysialic acid (PSA)-N, N, N-trimethyl chitosan (TMC) nanoparticles using an *in vitro* model of rheumatoid arthritis (RA).

Methods: The loading capacity of the PSA-TMC nanoparticles was determined. A RA *in vitro* model was developed by stimulating a synovial cell line with a pro-inflammatory mediator. Multiplex immunoassay was used to determine changes in the secretion of interleukin-6 (IL-6), interleukin-8 (IL-8), and granulocyte-macrophage colony-stimulating factor (GM-CSF) by the *in vitro* model following administration of the DM- and MTX-loaded nanoparticles.

Results: The loading capacity of the PSA-TMC nanoparticles was approximately 0.1 mg of drug/mg of nanoparticle. When applied to our *in vitro* model of RA, there were no significant differences in the concentrations of any of the pro-inflammatory mediators when comparing the free drugs and drug-loaded nanoparticles, administered at concentration of 0.1 mg/ml and 1.0 mg/ml, respectively.

Conclusions: The present study verified that MTX- and DM-loaded nanoparticles possess therapeutic efficacies that are nearly equivalent to those of the free drugs. The demonstrated *in vitro* efficacy is expected to translate to *in vivo* success when the PSA-TMC nanoparticles are used to enhance targeting of the inflamed tissue.

ABBREVIATIONS

DM	Dexamethasone
DMARD	Disease-Modifying Anti-rheumatic Drug
GM-CSF	Granulocyte-Macrophage Colony-Stimulating Factor
IL-1β	Interleukin-1β
IL-6	Interleukin-6
IL-8	Interleukin-8
MTX	Methotrexate
PSA	Polysialic Acid
RA	Rheumatoid Arthritis
TMC	N, N,N-Trimethyl chitosan
TPP	Tripolyphosphate

6.1 Introduction

Conventional therapeutics for rheumatoid arthritis (RA) are plagued by unpredictable pharmacokinetic profiles and non-specific organ toxicity [274, 335]. To overcome these problems, nanocarriers have been proposed to increase a drug's circulatory stability and thereby raise the probability of passive accumulation within regions of enhanced permeability, particularly inflamed tissue.

A lack immunogenicity, as well as non-cytotoxicity, are requisite properties for materials used in RA drug delivery. Polysaccharides are a logical, versatile choice for the formation of biodegradable, non-immunogenic nanoparticles. Due to variations in chemical composition,

polysaccharides exhibit overall neutral, negative, or positive charge states. In addition, the macromolecular chains possess a number of functionalities, particularly amines, hydroxyl groups, and carboxylic acids that are easily amenable to modification [336]. Although a number of polysaccharides have been explored, chitosan is the most used polysaccharide to generate nanoparticles for drug delivery [337]. Often, the cationic nature of the polymer resultant from free or quaternized primary amines is used for ionic crosslinking through a polyanion crosslinker, such as tripolyphosphate (TPP) [338-341]. Chitosan can also be ionically complexed with negatively charged natural polymers, such as hyaluronic acid, alginate, heparin, peptides, and nucleic acids.[336]

As previously reported, our lab has developed nanoparticles via ionic complexation of N, N, N-trimethyl chitosan (TMC) and polysialic acid (PSA), a polysaccharide never before used in nanoparticle formation protocol [342] . By incorporating PSA, nanoparticles are obtained with a smaller size relative to chitosan and TMC nanocarrier systems developed previously. Similar to poly (ethylene glycol), PSA functions to prevent undesirable uptake by the reticuloendothelial system, thereby extending circulatory stability and facilitating passive accumulation of associated therapeutics within areas of leaky vasculature, such as tissue affected by RA [48, 198, 199].

This study aims to verify that two disease-modifying anti-rheumatic drugs (DMARDs), methotrexate (MTX) and dexamethasone (DM), are therapeutically effective when entrapped within the previously developed PSA-TMC nanoparticles. The chosen therapeutics have highly variable pharmacokinetic profiles in RA patients and are associated with adverse side effects [274, 343, 344]. MTX- and DM-loaded nanoparticles were administered to an *in vitro* model of RA generated from interleukin-1β (IL-1β) activated SW-982 synovial cells. Following treatment

of the *in vitro* model for 24 hours, the concentrations of the following pro-inflammatory proteins within the supernatant were evaluated using multiplex immunoassay on the Luminex® Platform: interleukin-6 (IL-6), interleukin-8 (IL-8), and granulocyte-macrophage colony-stimulating factor (GM-CSF). The three proteins chosen are representative of the pro-inflammatory cytokines, chemokines, and growth factors that are upregulated in those that suffer from RA [345, 346].

6.2 Materials and methods

6.2.1 Materials

Polysialic acid (PSA) was purchased from Nacalai USA, Inc. (San Diego, CA, USA). Sodium hydroxide (extra pure, pellets), sodium tripolyphosphate (pure, TPP), acetonitrile (HPLC grade), and chitosan (Mw 100 Da - 300 kDa) were obtained from Acros Organics (New Jersey, USA). Sodium iodide (puriss), methyl iodide (reagent plus), 1-methyl-2-pyrrolidinone (anhydrous), ethanol (re- agent alcohol), ammonium acetate, deuterium oxide, and acetic acid (ACS reagent grade) were procured from Sigma (St. Louis, MO, USA). Hydrochloric acid (ACS plus grade) was acquired from Fisher Scientific (Hanover Park, IL, USA). Methotrexate (MTX) and dexamethasone (DM) were purchased from Enzo Life Science (Farmingdale, NY, USA). All chemical reagents were used without further purification.

6.2.2 Cell Culture

The SW-982 human synovial sarcoma cell line was acquired from ATCC (Manassas, VA). Dulbecco's Modified of Eagle's Medium (DMEM) supplemented with 4.5 g/L glucose, L-glutamine & sodium pyruvate was procured from Mediatech, Inc. (Manassas, VA). Fetal bovine

serum (FBS) and penicillin-streptomycin were purchased from Lonza, Inc. (Allendale, NJ). Sulforhodamine 101 cadaverine was obtained from Anaspec (Fremont, CA).

6.2.3 Preparation and Characterization of DMARD-Loaded PSA-TMC Nanoparticles

Drug-loaded PSA-TMC nanoparticles were prepared from PSA and TMC (55% degree of substitution) following a previously published protocol [347]. Briefly, 6.4 mg of TMC were dissolved in 3 ml of 0.3% acetic acid in a glass vial. In a separate glass vial, 3.2 mg PSA, 1mg TPP, and 2.4 mg MTX or DM were mixed well in 2 ml of DI water. The PSA solution was sonicated for 10 min and then added drop-wise to the TMC solution with stirring. Stirring was continued for 30 min to ensure nanoparticle formation. The solution was centrifuged at 1000 rpm for 5 min to remove non-encapsulated drugs. The supernatant was collected and centrifuged for an additional 15 min at 3000 rpm to obtain MTX- or DM-loaded nanoparticles as a white pellet. Identical to the procedure previously described for MTX [347], an Ultrafast Liquid Chromatography System (UFLC, Shimadzu Scientific Instruments, Japan) equipped with an SPD-20AV UV detector, an SIL- 20A autosampler, a DGU-20A_3 degasser, and a Shim-pack XR-ODS/C8/Phenyl column was used to quantify the amount of DM that was not encapsulated, which allowed for assessment of the DM loading properties of the nanoparticles. The mobile phase was a 70:30 mixture (v/v) of water: acetonitrile, and the detection wavelength was set to 238 nm. A calibration curve were constructed by using PeakFit 4.2 software to determine the area under the peak of at least five known concentrations of free drug in the mobile phase ranging from 0.39 mg/L to 100 mg/L. Loading efficiency (LE) and loading capacity (LC) were determined with the following equations:

$$\text{LE} = \frac{m_{MTX\ or\ DM,added} - m_{MTX\ or\ DM,unencapsulated}}{m_{MTX\ or\ DM,added}} \times 100 \quad (6.1)$$

$$\text{LC} = \frac{m_{MTX\ or\ DM,added} - m_{MTX\ or\ DM,unencapsulated}}{m_{Nanoparticles}} \quad (6.2)$$

where $m_{DM,added}$ is the mass of DM added to the PSA solution, $m_{DM,unencapsulated}$ is the mass of DM that has not been encapsulated into the nanoparticles, and $m_{Nanoparticles}$ is the mass of the nanoparticles used for DM loading.

The size and zeta potential of DMARD-loaded PSA-TMC nanoparticles were measured via a Malvern Zetasize NanoZS90 (Malvern Instruments Ltd., Malvern, UK). The size distribution of nanoparticles was reported as the polydispersity index (PDI). Nanoparticles were suspended in deionized water at a concentration 2 mg/ml and transferred into disposable microcuvettes (Malvern Instruments Ltd., Malvern, UK) for size measurements and disposable capillary cells (Malvern Instruments Ltd., Malvern, UK) for zeta potential measurements. For dynamic light scattering, the temperature was set to 25ºC and scattered light was detected at 173º. All measurements were performed triplicate.

6.2.4 In Vitro Cytotoxicity of Nanoparticles

WST-8 assay (Cayman Chemical Company, Ann Arbor, MI) was conducted on the SW-982 cell line, following the manufacturer's instructions, to assess the cytotoxicity of the drug-loaded nanoparticles. Cells were seeded into a 96-well cell culture plate (2×10^4 cells per well) and were cultured with DMEM plus 10% FBS for 24 h at 37 °C, 5% CO_2. Following sterile filtration, drug-loaded nanoparticles were added to yield a series of concentrations from 0.3125 mg/mL to 20 mg/mL, and the cultures were incubated for an additional 24 h. 10 μL of WST-8 solution and 100 μL media were then added to each well. After a 90 min incubation period,

absorbance was measured with a Synergy 2 multimode microplate reader (BioTek Instruments, Winooski, VT) at 450 nm. The cytotoxicities of free TMC, and TMC-PSA nanoparticles without drug were also evaluated. IC_{50} values were determined using the Hill slope model with Kaleidagraph software. Each experiment was repeated independently at least three times.

6.2.5 Cellular Uptake of Nanoparticles In Vitro

SW982 cells were seeded onto lysine coated 35 mm Glass Bottom Culture Dishes (MatTek Corporation, Ashland, MA) at a density of 1 million cells/dish. After a 24 h incubation period in DMEM plus 10% FBS at 37 °C and 5% CO_2, the media was removed, and sterile-filtered, fluorescently labeled (sulforhodamine 101 cadaverine) PSA-TMC nanoparticles in 1X PBS were added. Media from the control cells that did not receive nanoparticles was simultaneously replaced with PBS. Cells were incubated for an additional 60 min at room temperature and washed with PBS three times before imaging with a Nikon Eclipse Ti inverted microscope to observe nanoparticle internalization.

6.2.6 In Vitro Assessment of Bioactivity

SW-982 cells were seeded into a 96-well cell culture plate (5000 cells/well) in the presence of a pro-inflammatory simulant, interleukin-1β (IL-1β) (R&D Systems, Minneapolis, MN), at a concentration of 1 ng/mL. The low concentration of the stimulating agent was able to induce a significant pro-inflammatory response from synovial cells, consistent with previous studies [348-351]. After 24 h of incubation, MTX or DM loaded nanoparticles were added to the IL-1β stimulated cells following sterile filtration. Prior to addition, the MTX- or DM-loaded nanoparticles were suspended in DMEM plus 10% FBS at a concentration of 1.0 mg/ml. Control

groups included stimulated cells without treatment, stimulated cells with addition of free (unloaded) nanoparticles, and stimulated cells with 0.1 mg/mL or 1.0 mg/ml DMARD. After 24 h, culture supernatant was collected and stored in aliquots at -80 °C until pro-inflammatory protein analysis. Supernatant samples were analyzed for pro-inflammatory proteins (IL-6, IL-8, and GM-CSF) using a Bio-Plex Precision Pro human cytokine assay panel (BIO-RAD, Hercules, CA) on a Luminex® 200 system (Austin, TX) following a manufacturer-provided protocol. Each experiment was repeated independently at least three.

6.2.7 Data Analysis

Proteins levels were expressed relative to those obtained from untreated control cells. Data is presented as the mean ± standard deviation ($N \geq 3$). All treatment groups (control, 0.1 mg/mL MTX or DM, 1.0 mg/mL MTX or DM, MTX- or DM- loaded nanoparticles, free nanoparticles) were compared by one-way ANOVA with Fisher's LSD post hoc tests. $p < 0.05$ was considered to be significant.

6.3 Results

6.3.1 Preparation and Characterization of DMARD-Loaded PSA-TMC Nanoparticles

The loading efficiency and loading capacity of PSA-TMC nanoparticles for DM were determined to be 41.3 ± 7% and 0.01 ± 0.02 mg DM/mg nanoparticles, respectively. The values were comparable to those previously obtained in the preparation of MTX-loaded PSA-TMC nanoparticles (LE = 46.3 ± 13%, LC = 0.10 ± 0.03 mg MTX/mg nanoparticles) (Table 6) [347].

Likewise, as provided in Table 7, the size of DM-loaded nanoparticles was slightly greater than that previously observed for free nanoparticles and comparable than that determined for MTX-loaded nanoparticles. All of the nanoparticle formulations yielded a low polydispersityand a zeta potential value greater than 30 mV. The slight increase in size, in conjunction with the lack of an observable effect on zeta potential, suggested that the DMARDs were being entrapped within the nanosized carriers, as expected.

Table 6. Load efficiency and loading capacity of MTX and DM by PSA-TMC nanoparticles (NPs)

	LE	**LC(mg drug/mg nanoparticles)**
MTX-loaded NPs	46.3 ± 13%	0.10 ± 0.03
DM-loaded NPs	41.3 ± 7%	0.10 ± 0.02

Table 7. Size, zeta potential, and polydispersity of NPs and MTX or DM-loaded NPs

	Size (nm)	**Zeta potential (mV)**	**PDI**
NPs	102.2 ± 14.5	33.4 ±1.6	0.12 ± 0.02
MTX-loaded NPs	128.7 ± 5.3	32.7 ± 0.9	0.10 ± 0.02
DM-loaded NPs	120.7 ± 11.1	34.8 ± 2.5	0.12 ± 0.02

6.3.2 In Vitro Cytotoxicity of Drug–Loaded and Plain Nanoparticles

As summarized Table 8 with the calculated IC_{50} values, the free and DMARD-loaded nanoparticles were non-cytotoxic up to high concentrations. Consistent with our prior study using MH7A synovial cells rather than SW-982 cells, the inherent cytotoxicity of quaternized chitosan was significantly reduced upon complexation with PSA to form nanoparticles. Of note,

the IC_{50} value for the PSA-TMC nanoparticles did not change with DMARD loading, providing evidence that MTX and DM did not induce a cellular response by impacting cellular proliferation. This result supported prior research showing that free MTX and DM did not impact cellular proliferation over the range of therapeutic concentrations tested.

Table 8. IC_{50} value of TMC, PSA-TMC NPs, MTX-loaded PSA-TMC NPs, and DM-loaded PSA-TMC NPs. * indicated a significant difference versus TMC (N=3, P<0.05)

	IC_{50} (mg/ml)
TMC	5.16 ± 0.20
PSA-TMC NPs	15.82 ± 1.44 *
MTX-loaded PSA-TMC NPs	14.20 ± 1.20 *
DM-loaded PSA-TMC NPs	16.01 ± 0.42 *

6.3.3 Cellular Uptake of Nanoparticles In Vitro

By modifying PSA with a red fluorescent tag prior to nanoparticle formation, uptake of the PSA-TMC cells by synovial SW982 cells could be observed with the aid of a fluorescent, inverted microscope. As illustrated in Fig. 24, the nanoparticles were associated within the cells following a short incubation period (~60 minutes).

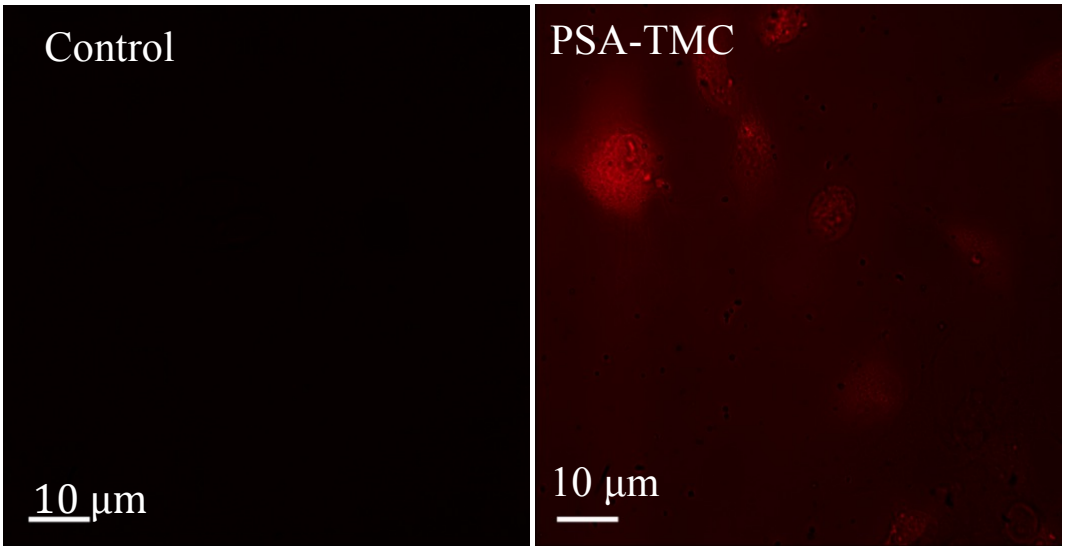

Figure 24. Color composite of fluorescence microscopy images demonstrating nanoparticle uptake at room temperature by human synovial sarcoma SW982 cells. To facilitate fluorescence microscopic evaluation, PSA was conjugated to sulforhodamine 101 cadaverine. Use of identical imaging settings permited direct comparison of fluorescence intensities. Higher intensities indicated more cellular uptake of nanoparticle by cells. Left image: cells not incubated with nanoparticles resulted in negligible signal. Right image: cells incubated with nanoparticles and showed active cellular uptake. Both groups were incubated for 60 min and washed three times with PBS before imaging.

6.3.4 In Vitro Assessment of Bioactivity

MTX-loaded nanoparticles significantly suppressed IL-8 secretion relative to the untreated control group (Fig. 25). The amount of IL-8 suppression was comparable to that achieved with low concentration (0.1 mg MTX/ml) and high concentration (1.0 mg MTX/ml) MTX treatment. Low and high concentration MTX treatment also showed significant inhibition of GM-CSF secretion but not IL-6 secretion. The nanoparticles alone, in contrast, significantly increased GM-CSF secretion, although this effect was eradicated through incorporation of MTX. Low and high concentration free MTX treatment additionally resulted in significant inhibition of IL-6 and GM-CSF secretion relative free nanoparticle treatment. High concentration MTX

treatment also led to a significant decrease in IL-6 levels relative to levels obtained with MTX-loaded nanoparticle treatment. Of note, the raw data showed that the detected concentrations of GM-CSF (<<100 pg/ml) were low and close to the limit of detection.

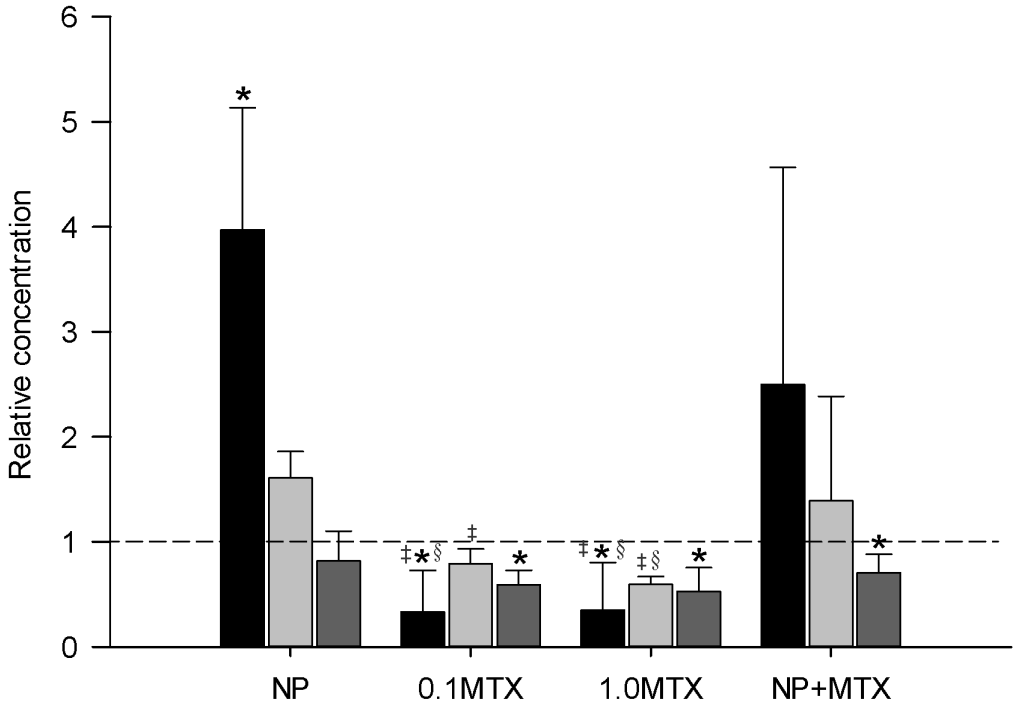

Figure 25. Relative protein secretion (black: GM-CSF; grey: IL-6; dark grey: IL-8) of IL-1β-stimulated SW-982 cells after treatment with free nanoparticles (NP) at a concentration of 1.0 mg/ml, free MTX at a concentration of 0.1 mg/ml (0.1 MTX), free MTX at a concentration of 1.0 mg/ml (1.0 MTX), and MTX-loaded nanoparticles at a concentration of 1.0 mg/ml (NP + MTX). The dashed line at a relative concentration of 1 was intended to serve as a point of reference for unstimulated control cells. * indicated a significant difference versus untreated control cells ($p < 0.05$); ‡ indicated a significant difference versus free nanoparticles ($p < 0.05$); and § indicated a significant difference versus MTX-loaded nanoparticles ($p < 0.05$).

DM-loaded nanoparticles significantly suppressed IL-6 and IL-8 secretion relative to the untreated control group and had comparable efficacy to low concentration (1 mg DM/ml) and high concentration (1.0 mg DM/ml) free DM treatment (Fig. 26). Furthermore, although there

was no significant difference from the control, treatment with DM-loaded nanoparticles, low concentration free DM, and high concentration free DM resulted in significantly lower GMC-SF levels relative to treatment with free nanoparticles.

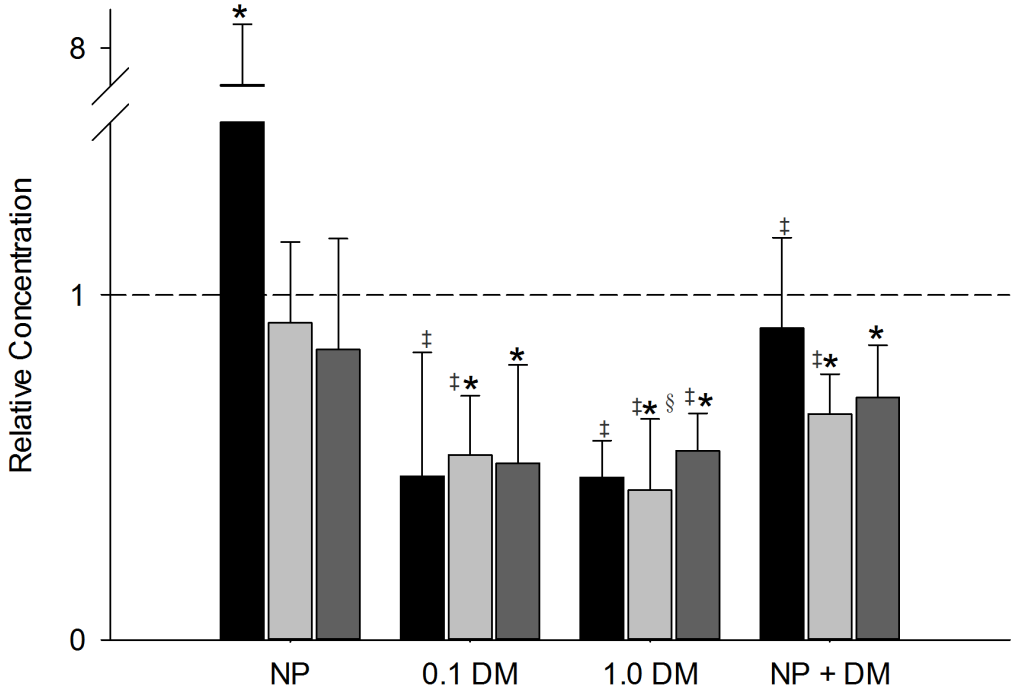

Figure 26. Relative protein secretion (black: GM-CSF; grey: IL-6; dark grey: IL-8) of IL-1β-stimulated SW-982 cells after treatment with free nanoparticles (NP) at a concentration of 1.0 mg/ml, free DM at a concentration of 0.1 mg/ml (0.1 DM), free DM at a concentration of 1.0 mg/ml (1.0 DM), and DM-loaded nanoparticles at a concentration of 1.0 mg/ml (NP + DM). The dashed line at a relative concentration of 1 was intended to serve as a point of reference for unstimulated control cells. * indicated a significant difference versus untreated control cells ($p < 0.05$); ‡ indicated a significant difference versus free nanoparticles ($p < 0.05$); and § indicated a significant difference versus DM-loaded nanoparticles ($p < 0.05$).

6.4 Discussion

MTX is known to be hepatotoxic and patients undergoing treatment must receive periodic liver function tests [352, 353]. Likewise, long-term use of DM is associated with severe side effects, including insulin resistance and osteoporosis [354]. The drawbacks associated with these DMARDs can be attributed to low solubility, unpredictable pharmacokinetics, and non-site specific distribution within the body [352, 353] [354]. As explain in depth our prior study on the development of PSA-TMC nanoparticles, the sizes and zeta potentials obtained for DMARD-loaded nanoparticles were expected to minimize accumulation within healthy tissue, reduce undesireable uptake by the reticuloendothelial system, and facilitate delivery to the inflamed tissue by exploiting the leaky vasculature that characterizes RA. The nanoparticles also facilitated controlled release of DMARD over a 24 hour period [347]. In the current study, an *in vitro* model of RA based upon IL-1β activated synovial fibroblasts, the so-called conductors of joint destruction [355, 356], was used to demonstrate the therapeutic efficacy of the DMARD-loaded carrier systems.

While some toxicity is permissible in carrier systems designed for cancer therapy, the primary goal of inflammation reduction in RA treatment demands minimal toxicity. Consistent with our previous studies using the MH7A synovial fibroblast cell line [347], the PSA-TMC nanoparticles showed negligible cytotoxicity towards the synovial SW982 cell line over a range of concentrations. The SW982 cell line was used in lieu of the MH7A cell line in the current study due to evidence suggesting that the MH7A cell line might not accurately mimic the cytokine profile observed RA [351]. Furthermore, the SW982 cell line was shown accurately mimic expression of the pro-inflammatory mediator associated with rheumatoid arthritis, including IL-6 and IL-8, particularly after stimulation with IL-1β [348-350]. Loading of MTX and DM had a negligible impact on the IC_{50} values, indicating that any change in the secretion of

pro-inflammatory mediators would be due to cellular response rather than apoptosis. A concentration of 1 mg/ml was used for *in vitro* studies to ensure an observable response without impacting cellular viability. As illustrated in Fig.24, the PSA-TMC nanoparticles were internalized by SW-982 cells. The results confirmed the potential for intracellular delivery of therapeutics via PSA-TMC nanoparticles.

Changes in the secretion of IL-6, IL-8, and GM-CSF by the activated SW982 cells were used to demonstrate the therapeutic efficacy of the DMARD-loaded nanoparticles relative to the free drugs (Figs. 25, 26). IL-6, IL-8, GM-CSF were selected as representative cytokines, chemokines, and growth factors, respectively. A literature survey suggested that the three chosen proteins were critical to the pathogenesis of rheumatoid arthritis [346]. IL-6 was involved in in immune regulation, inflammation, and hematopoiesis. More specifically, IL-6 was thought to simulate T and B cells [346, 357], activate osteoclasts [358], and induce expression of vascular endothelial growth factor (VEGF) [357], which subsequently triggered the angiogenesis that, in part, characterized rheumatoid arthritis. IL-8 stimulated the migration of inflammatory cells into the synovium; activated synovial fibroblasts via an autocrine mechanism to induce secretion of additional pro-inflammatory mediators; and promoted angiogenesis [359, 360]. GM-CSF recruited and activated inflammatory cells, particularly T-cells, while also inhibiting differentiation of osteoclasts [346] . DMARDs, including those used in the current study, had been shown to reduce the secretion of the select pro-inflammatory mediators, thereby disrupting the pro-inflammatory network associated with rheumatoid arthritis.

Of note, although MTX was previously used as a model compound to demonstrate the ability of the nanoparticles to encapsulate and release DMARDs [347], DM, in addition to MTX, was used to observe therapeutic efficacy . While the anti-inflammatory impact of DM when used

in vitro has been well demonstrated, *in vitro* administration of MTX has yielded highly variable responses. Although MTX was as a folate antagonist in the treatment of cancer, the mechanism of action for MTX in the treatment of RA was unclear [361-363] and the inconsistencies in *in vitro* response reflect this lack of understanding. Alterations in the cytokine milieu might not be a direct result of MTX administration[364]. In contrast, DM was known to reduce inflammation in the same manner as other glucocorticoids, where by binding to a glucocorticoid receptor (GR) directly impacted the activity of activator protein-1 (AP-1) and nuclear factor kappaB (NF-κB) [365]. The latter transcription factors have been definitively linked to the expression and secretion of most pro-inflammatory cytokines and chemokines, including IL-6, IL-8, and GM-CSF [366-368].

When applied to our *in vitro* model of RA, the DM- and MTX-loaded nanoparticles, as well as the free DMARDs, yielded significant reductions in the secretion of IL-8 relative to the control, while only DM (free or encapsulated within nanoparticle) led to significantly decreased IL-6 levels relative to the control. In contrast, MTX (free and encapsulated) did not affect IL-6 concentrations relative to the control group, although significant differences were observed comparing treatment with free nanoparticles to free DMARDs. The latter results were reflective of the potential differences in the mechanism of action of MTX and DM, as noted above. The variable results obtained for GM-CSF, with only free MTX yielding a significant decrease in GM-CSF levels, could be attributed to the increased uncertainty in measured concentrations near the limit of detection. More important than comparisons to the control and free nanoparticle groups, there were no significant differences in the concentrations of any of the pro-inflammatory mediators when comparing the free DMARDs and DMARD-loaded nanoparticles, administered at concentration of 0.1 mg/ml and 1.0 mg/ml, respectively. Based on the loading

capacity of the DMARD nanoparticles (0.1 mg/mg), the free DMARDs were administrated at equal weight concentration relative to the DMARDs within the nanoparticles. Thus, the results thus suggested that the DMARD-loaded nanoparticles possessed therapeutic efficacies that were nearly equivalent to those of the free DMARDs. When applied *in vivo*, this is expected to translate to greater success based on passive targeting of the nanoparticles to the inflamed tissue.

6.5 Conclusion

PSA-TMC nanoparticles were previously developed for targeted delivery in the treatment of RA to enhance therapeutic efficacy and reduce non-specific cytotoxicity of DMARDs. The physical characteristics and DMARD-loading capacity of the nanoparticles were suggestive of a suitable carrier system. In this study, an RA *in vitro* model was used to validate that two common DMARDs, MTX and DM, elicited a desirable, anti-inflammatory therapeutic response when entrapped in nanoparticles. The present study provided the foundation for future *in vivo* studies aimed towards demonstrating the site-specific nature of the nanoparticles and the enhanced efficacy of nanoparticle entrapped DMARDs.

Chapter 7 Summary

In sum, two PSA-based micelle systems and one PSA-based nanoparticle system were successfully developed based on the needs of RA. These PSA-based nanocarriers were characterized in terms of composition, size, surface charge, morphology, drug loading and release, toxicity, cellular uptake, and anti-inflammatory efficacy. Results showed that the PSA-based nanocarriers possessed proper sizes between 70-120 nm for passive targeting to inflamed tissues and had high stability, as indicated by high zeta potential values (absolute value larger than 30 mV) and low polydispersity index (PDI). These nanocarriers had been demonstrated to carry sufficient amount of model drugs, specifically methotrexate, dexamethasone, and cyclosporine A, via physical interactions and to release the drugs in a controllable manners. PSA-PCL micelles and PSA-TMC nanoparticles were non-cytotoxic, as indicated by high IC_{50} values, while PSA-DA was cytotoxic. Fluorescent microscopy demonstrated that synovial cells effectively internalized PSA-PCL micelles and PSA-TMC nanoparticles within a short incubation time (60 min). More significantly, DM-loaded and MTX-loaded PSA-TMC nanoparticles had significantly suppressed the secretion of pro-inflammatory proteins by inflamed synovial cells.

To conclude, PSA-PCL micelles and PSA-TMC nanoparticles were good carriers for drugs because of their low toxicity, proper size, good drug loading properties, capacity to deliver drugs, and anti-inflammatory efficacy. Therefore, these two systems could serve as anti-inflammatory drug delivery systems. Addition of an active targeting group and/or stimuli-sensitive moieties to PSA-PCL micelles and PSA-TMC nanoparticles might endow them with enhanced anti-inflammatory efficacy and increased specificity to diseased tissues.

Chapter 8 Future work

PSA-PCL micelles and PSA-TMC nanoparticles were successfully developed in this dissertation. As discussed in separate chapters, PSA-PCL micelles and PSA-TMC nanoparticles possessed small size 70-120 nm, which presumably would target inflamed tissues with enhanced permeability of vasculature *in vivo*. In future, animal models with inflammatory arthritis will be established to test the hypothesis.

Hyaluronic acid (HA) is a natural component in the extracellular matrix (ECM) of human joints that has high affinity to CD 44 receptors. Based on the overexpression of the CD 44 receptors by inflamed synovial fibroblasts, we hypothesize that addition of HA to our established PSA-based nanocarriers will enhance the anti-inflammatory efficacy of associated therapeutics. In preliminary studies, we have fabricated stable HA-g-PSA-TMC nanoparticles.

First, HA oligomer was obtained via enzymatic degradation. 100 mg HA was added to 25 ml PBS solution under stirring at pH 6.5. 2.4 mg hyaluronidase was added to solution and solution was stirring for 1 h at 37 °C and then 20 min at 95 °C. This protocol was established based on unpublished data from Gel Permeability Chromatograph (GPC).

Second, PSA was reacted with crosslinker adipic dihydrazide (ADH) (Figure 27). Briefly, 150 mg PSA (0.485 mmol sialic acid), 15 mg EDC (0.097 mmol), and 11 mg NHS (0.097 mmol) were added into 15 ml DI water and pH of solution was adjusted to 4.5. After 30 min, 8.5 mg ADH (0.0485 mmol) was added to solution and reaction was continued for 2 h. pH was adjusted to 7.0 to quench the reaction and after filtration, reaction solution was dialysis against DI water overnight. Finally, purified solution was lyophilized to produce PSA-ADH. ^{1}H NMR was conducted to confirm the structure of product.

At last, HA was grafted onto PSA via cross-linker ADH (Figure 27). 72.8 mg HA (0.02425 mmol HA oligomer), 7.5 mg EDC (0.0485 mmol), and 5.6 mg NHS (0.0485 mmol) were dissolved in 20 ml DI water and pH of the solution was adjusted to 4.5. 150 mg PSA-ADH (0.0485 mmol sialic acid) was added to the solution after 30 min. The reaction was continued for 2 h and was quenched via adjusting pH to 7.0. Reaction solution was then dialyzed for 2 days and lyophilized to obtain the final product: HA-g-PSA. ^{1}H-NMR was conducted to confirm the structure of product (Figure 40).

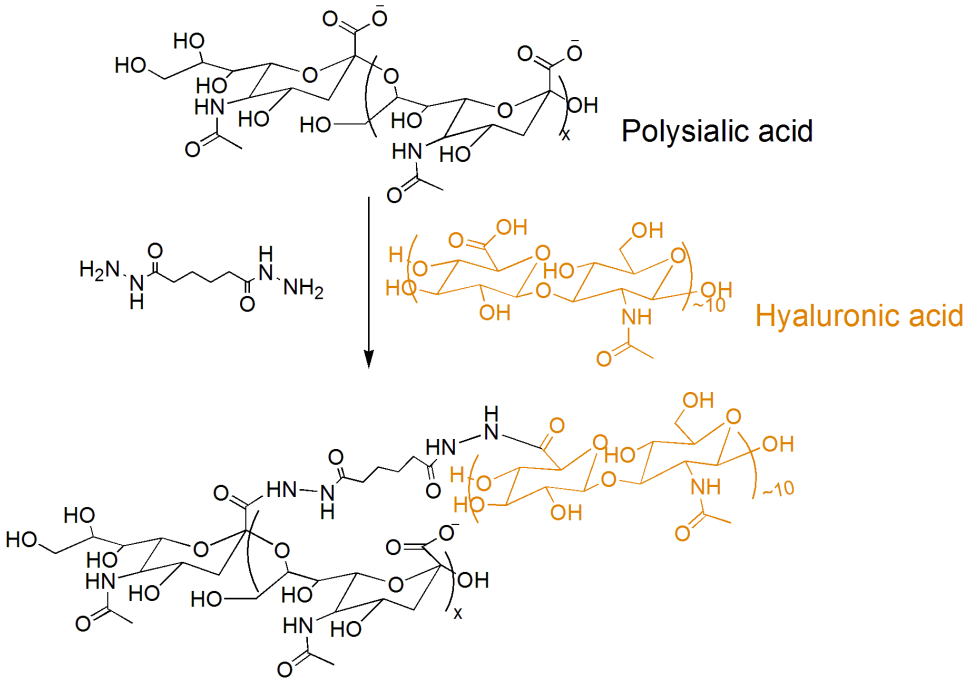

Figure 27. Synthesis of HA-grafted-PSA

Two ratios of TMC: HA-g-PSA and two centrifuge speeds were used to explore an optimal formulation for HA-g-PSA-TMC nanoparticles. Nanoparticles were prepared according to previously published method [1]. Briefly, 6.4 mg TMC was dissolved into 3 ml 0.3% acetic acid solution and 3.2 mg (TMC: HA-g-PSA 1:0.5) or 6.4 mg (TMC: HA-g-PSA 1:1) HA-g-PSA

was mixed into 2 ml DI water with 1 mg TPP. HA-g-PSA solution was added dropwise into TMC solution and the mixed solution was stirred for 20 min. Centrifuge at 2000 rpm or 3000 rpm was performed for 5 min to harvest a white nanoparticle pellet at the bottom. Excess supernatant was removed.

The size and zeta potential of HA-g-PSA-TMC nanoparticles were measured using a Malvern Zetasize NanoZS90 (Malvern Instruments Ltd., Malvern, UK). The particle size distribution of the nanoparticles was reported as a PDI. The nanoparticles were dissolved in DI water at 2 mg/ml and used without filtration. Then, the nanoparticle solutions were transferred to disposable microcuvettes (Malvern Instruments Ltd., Malvern, UK) for size measurements and disposable capillary cells (Malvern Instruments Ltd., Malvern, UK) for zeta potential measurements. For dynamic light scattering measurements, the temperature was set 25 °C, and the scattered light was detected at an angle of 173 °. All measurements were performed in triplicate. Results showed that among different formulations and centrifuge speeds, the most stable nanoparticle was TMC: HA-g-PSA 1:1 centrifuged at 3000 rpm 5 min and the HA-g-PSA-TMC nanoparticles maintained a small size (Figure 28).

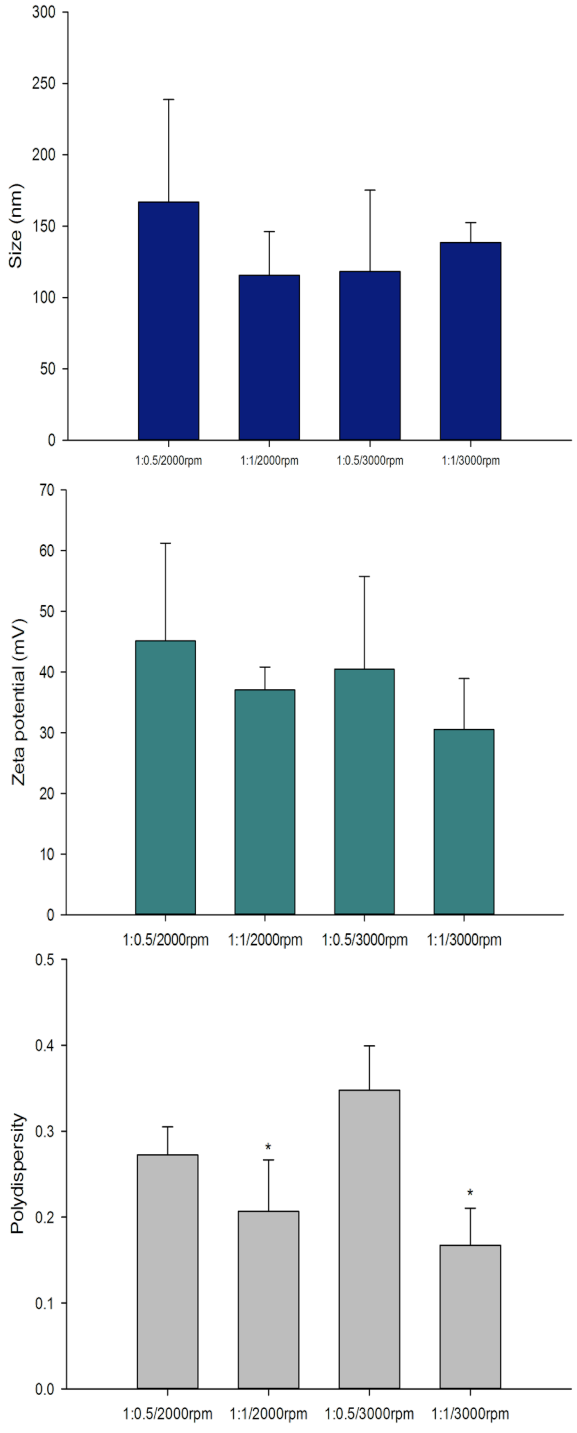

Figure 28. Size (top), zeta potential (middle), and polydispersity (PDI) (bottom) of two formulations, TMC: HA-g-PSA 1: 0.5 and 1:1 after centrifuge at 2000 rpm or 3000 rpm 5 min. * indicated a significant difference versus the formulation, TMC: HA-g-PSA 1: 0.5 (N=3, $P<0.05$)

Uptake of HA-g-PSA-TMC nanoparticles by SW982 cells was verified and compared to PSA-TMC nanoparticles via inverted fluorescence microscopy. The SW982 cells were added to lysine coated Lab-Tek ® Chamber Slides, and fluorescently tagged HA-g-PSA-TMC nanoparticles or PSA-TMC nanoparticles (Sulforhodamine 101 cadaverine) were added 24 h after seeding. After a short incubation period (45 min), nanoparticle solution was removed and cells were washed with PBS for three times. Fluorescence signal was observed with a Nikon Eclipse Ti inverted microscope. The incubation period was selected based on prior optimization experiments and is consistent with other researchers with regards to the short time necessary to observe uptake of chitosan-based nanoparticles.

HA-g-PSA-TMC nanoparticles showed higher cellular internalization by SW982 cells relative to PSA-TMC nanoparticles presumably via interaction with overexpressed CD 44 receptors (Figure 29). In future, more comprehensive experiments will be conducted to explore the mechanism of cellular uptake of HA-g-PSA-TMC nanoparticles by SW982 cell. In addition, drug-loaded HA-g-PSA-TMC nanoparticles will be used to treat inflamed synovial cells and their anti-inflammatory efficacy will be compared to PSA-TMC nanoparticles by analyzing the suppression of pro-inflammatory proteins.

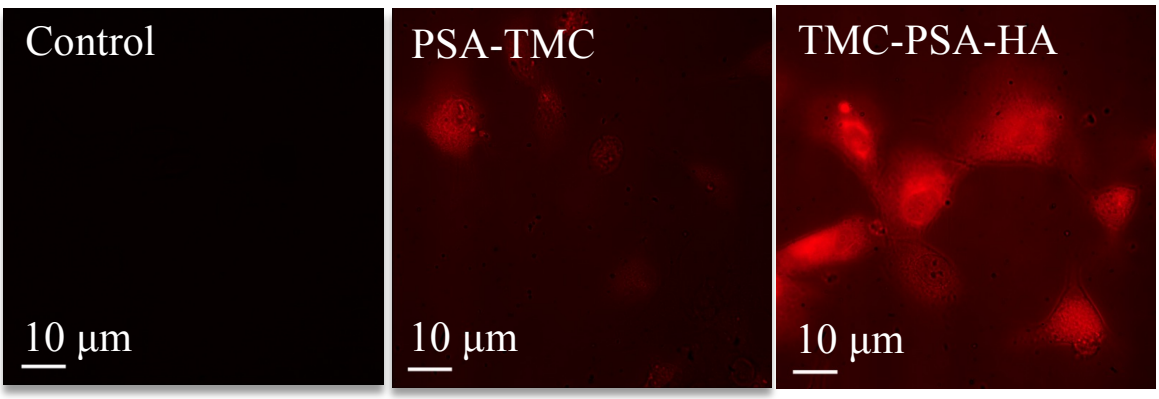

Figure 29. Color composite of fluorescence microscopy images demonstrating nanoparticle uptake at room temperature by human synovial sarcoma SW982 cells. To facilitate fluorescence microscopic evaluation, PSA was conjugated to sulforhodamine 101 cadaverine. Use of identical imaging settings permits direct comparison of fluorescence intensities. Higher intensities indicated more cellular uptake of nanoparticle by cells. Left image: cells not incubated with nanoparticles results in negligible signal. Middle image: cells incubated with nanoparticles and showed active cellular uptake. Right image: cells incubated with HA-coated nanoparticles and demonstrated enhanced cellular uptake. All three groups were incubated for 60 min and washed three times with PBS before imaging.

PSA-PCL micelles have been shown to possess a small size and effectively deliver the immunosuppressive drug-Cyclosporine A (CyA). In preliminary experiments, HA has been grafted onto PSA-PCL micelles for the encapsulation of hydrophobic drugs to achieve enhanced cellular uptake and improved specificity *in vitro* and *in vivo* (Figure 30). Degree of substitution of HA oligomer was low to maintain small size of micelles and prevented potential clearance of HA-g-PSA-PCL micelles by the interaction of HA to HA receptor for endocytosis (HARE) in the liver. HA-g-PSA-PCL micelles have shown a high capacity of simvastatin and lovastatin (Table 9). Fluorescence experiment has been performed to explore and compare cellular uptake of PSA-PCL micelles within/out HA.

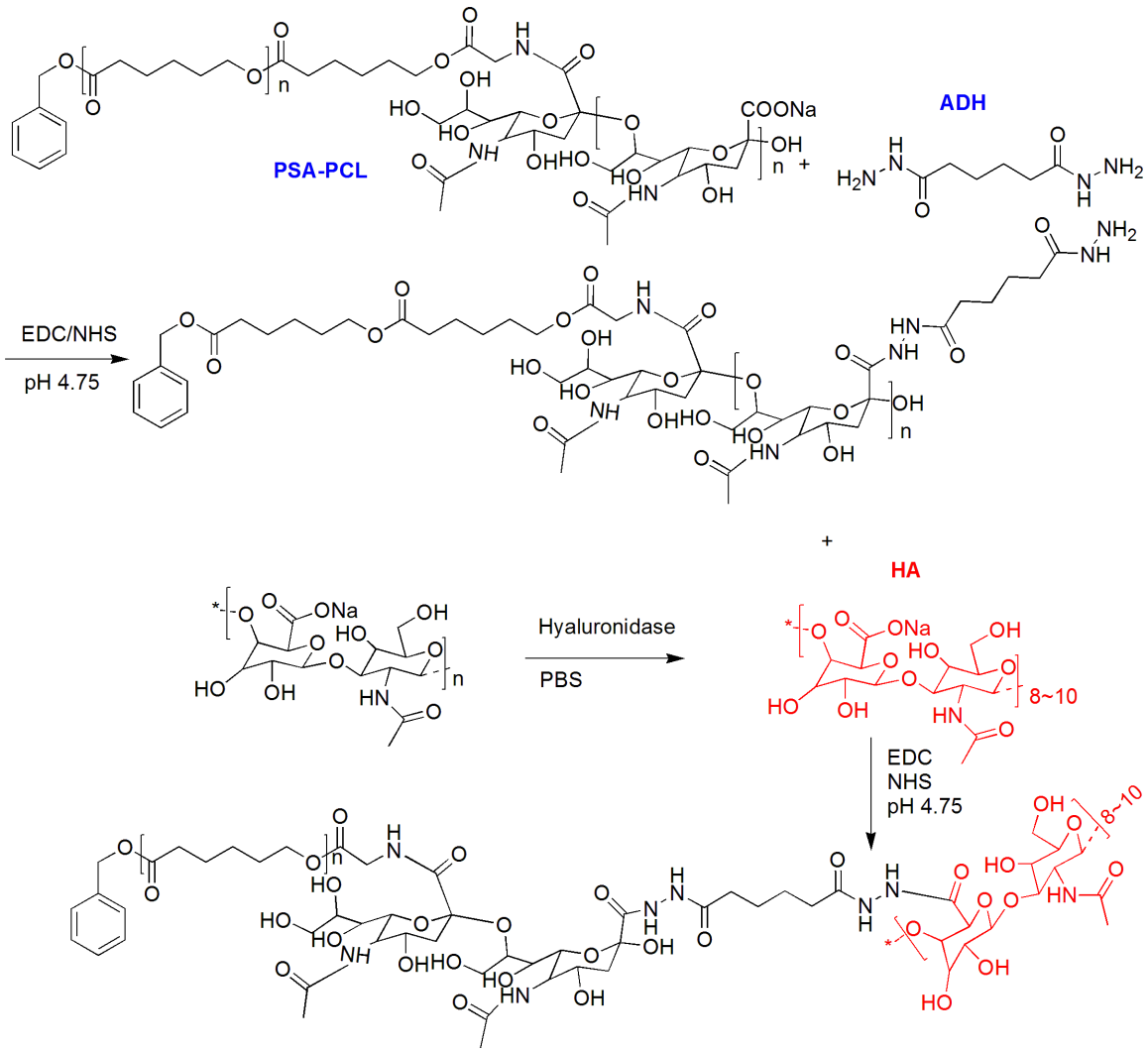

Figure 30. Synthesis of HA-g-PSA-PCL.

Table 9. Loading capacity and loading efficiency of hydrophobic statins with HA-g-PSA-PCL micelles.

	LE (%)	**LC(mg drug/mg micelle)**
Lovastatin	58	0.17
Simvastatin	57	0.14

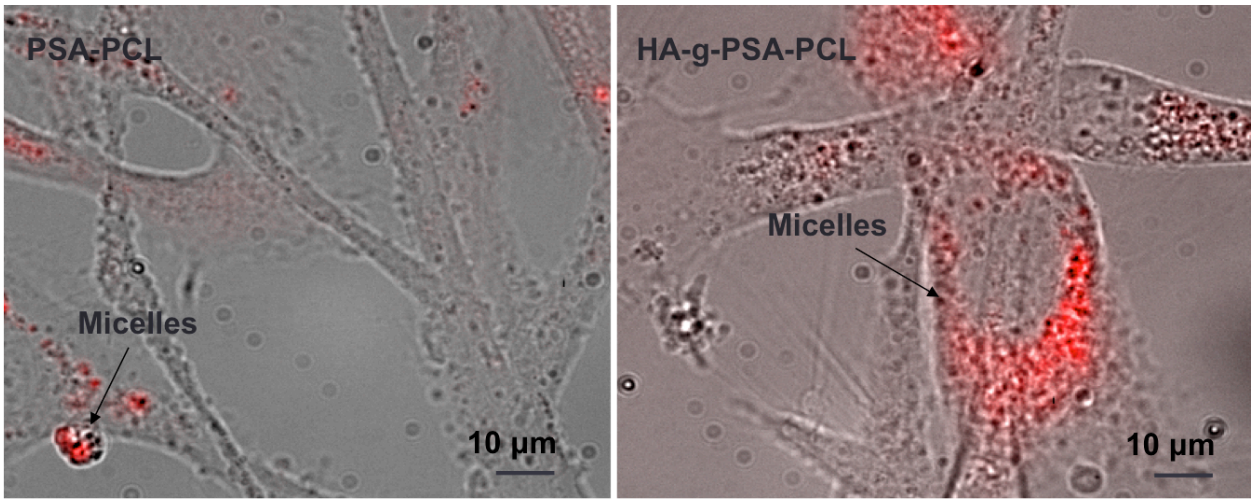

Figure 31. Color composite of fluorescence microscopy images demonstrating micelle uptake at room temperature by primary vascular smooth muscle cells. To facilitate fluorescence microscopic evaluation, PSA was conjugated to sulforhodamine 101 cadaverine. Use of identical imaging settings permits direct comparison of fluorescence intensities. Higher intensities indicated more cellular uptake of nanoparticle by cells. Left image: cells incubated with PSA-PCL micelles results in weak signal. Right image: cells incubated with HA-g-PSA-PCL micelles and demonstrated enhanced cellular uptake. Both groups were incubated for 60 min and washed three times with PBS before imaging.

In future, statin-loaded HA-g-PSA-PCL micelles will be used to evaluate the anti-proliferation and anti-inflammatory efficacy by inflamed vascular smooth muscle cells that are highly involved in cardiovascular diseases.

The next stage of research will be a series of *in vivo* investigation. Inflamed arthritis mice will be injected with nanocarriers, drug-loaded nanocarriers, drug-loaded HA-nanocarriers to study the interaction of these nanocarriers with organs, tissues, and cells in terms of their distribution, circulation, interaction with blood, efficacy of treatment. Outcomes will be compared to free drug treatment and biopsy of joint tissues will be performed at 7 days, 14 days, and 28 days after administration to explore preservations of joints.

Other future directions can be the application of (HA-g)-PSA-PCL micelles and (HA-g)-PSA-TMC nanoparticles for drug delivery to other drugs like genes and proteins and other diseases, such as infection, cardiovascular diseases, and cancer.

APPENDIX A: SPECTRA

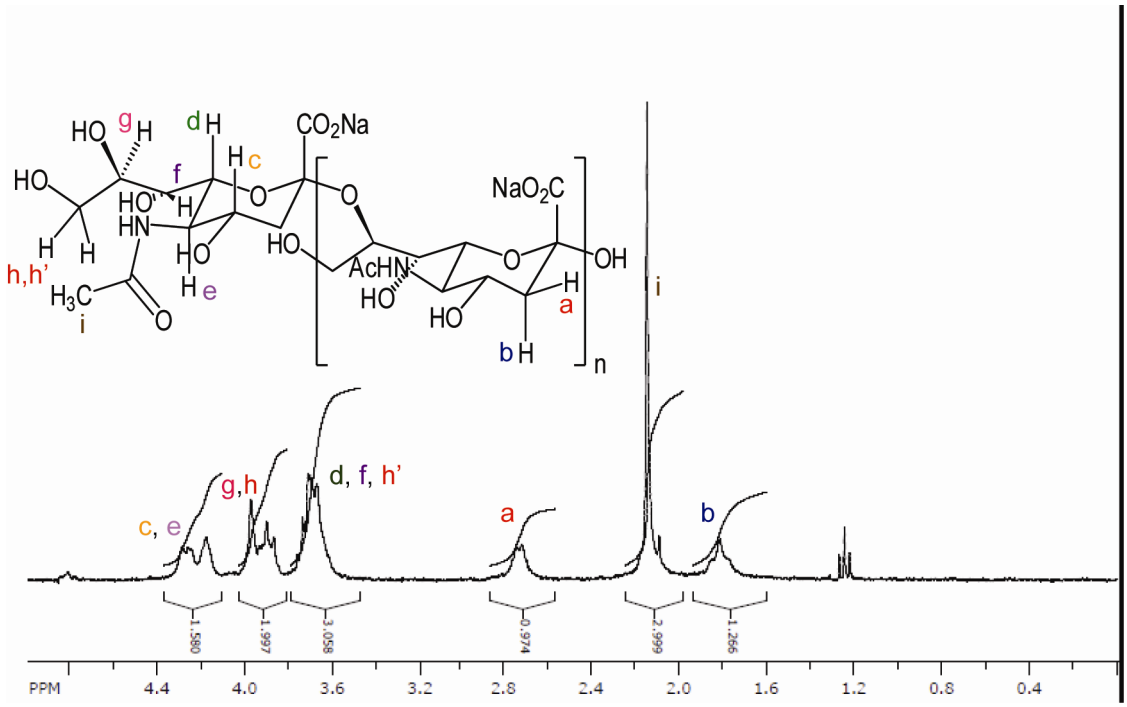

Figure 32. ^{1}H NMR spectrum (D_2O, water suppression) of polysialic acid.

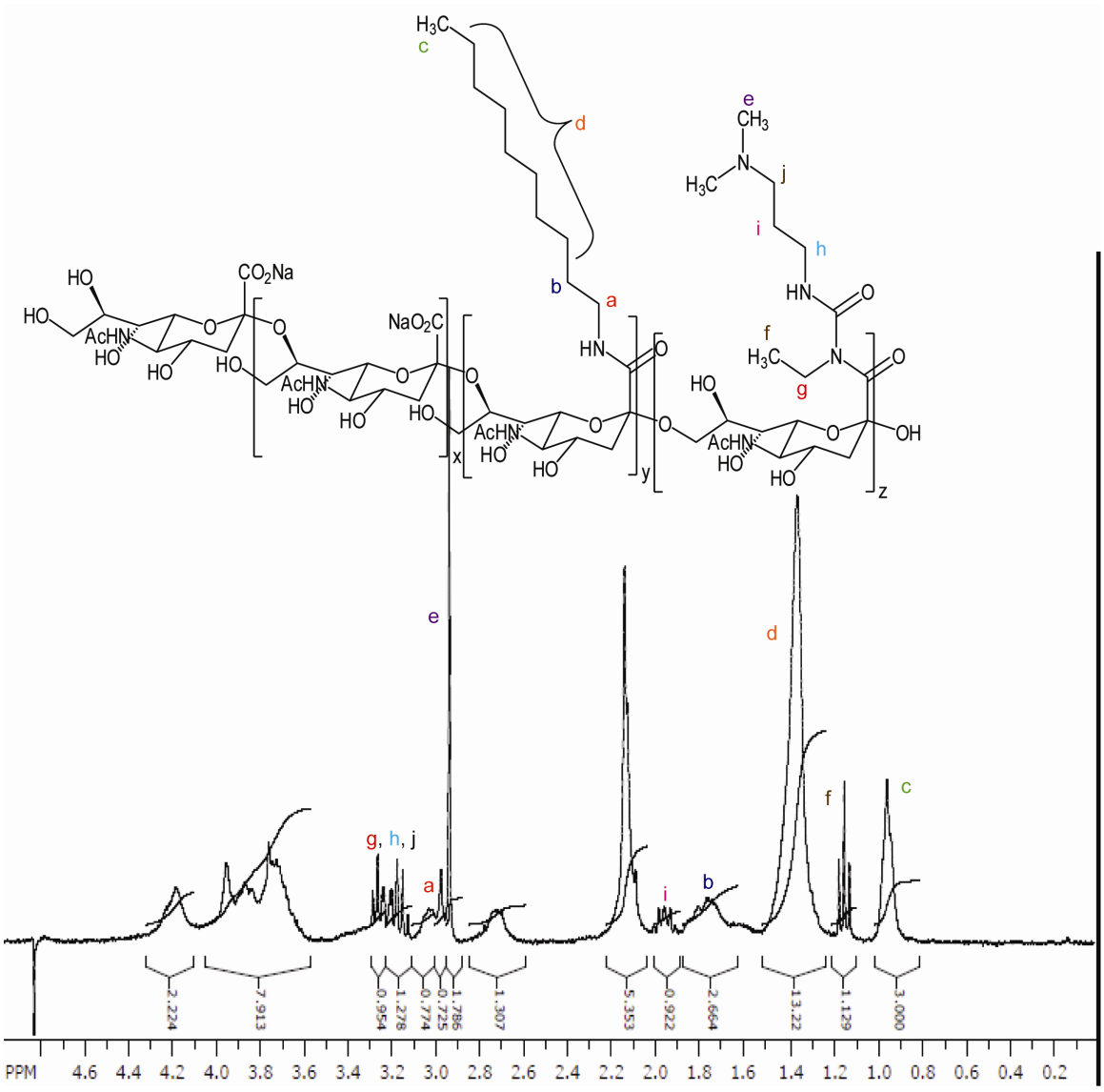

Figure 33. ^{1}H NMR spectrum (D_2O, water suppression) of decylamine modified polysialic acid with a DS of approximately 60%.

Exact Mass of (C64H119N13O13)Na+ = 1300.894252u
Observed Mass = 1300.890393u
Difference = -2.9 ppm

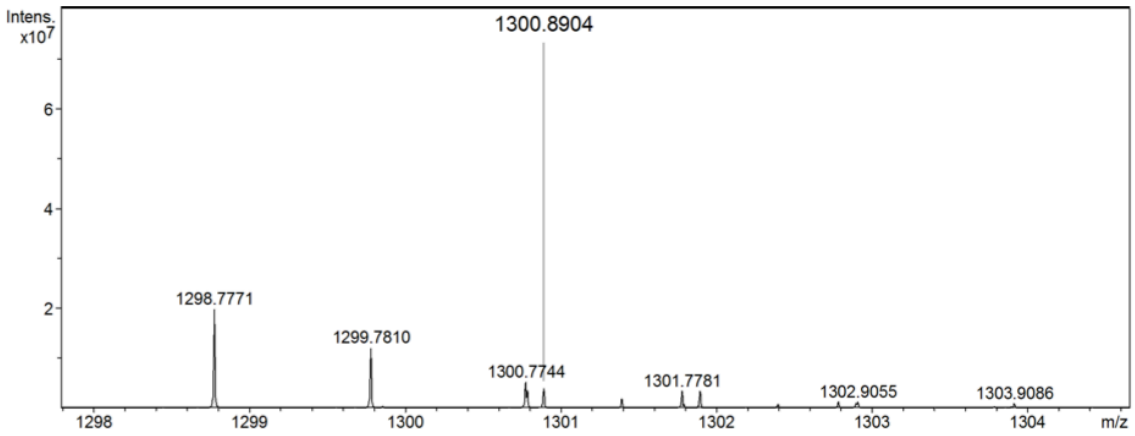

Figure 34. Mass spectra of amine-terminated CyA

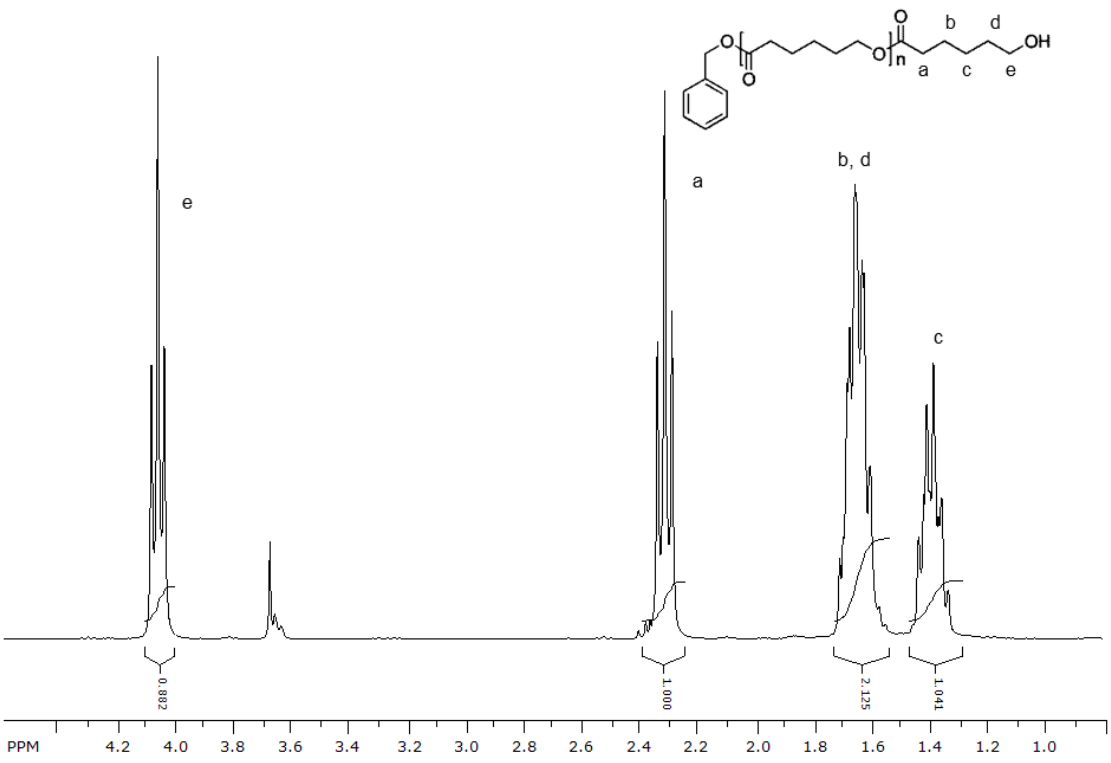

Figure 35. ^{1}H NMR spectrum ($CDCl_3$) of polycaprolactone (PCL).

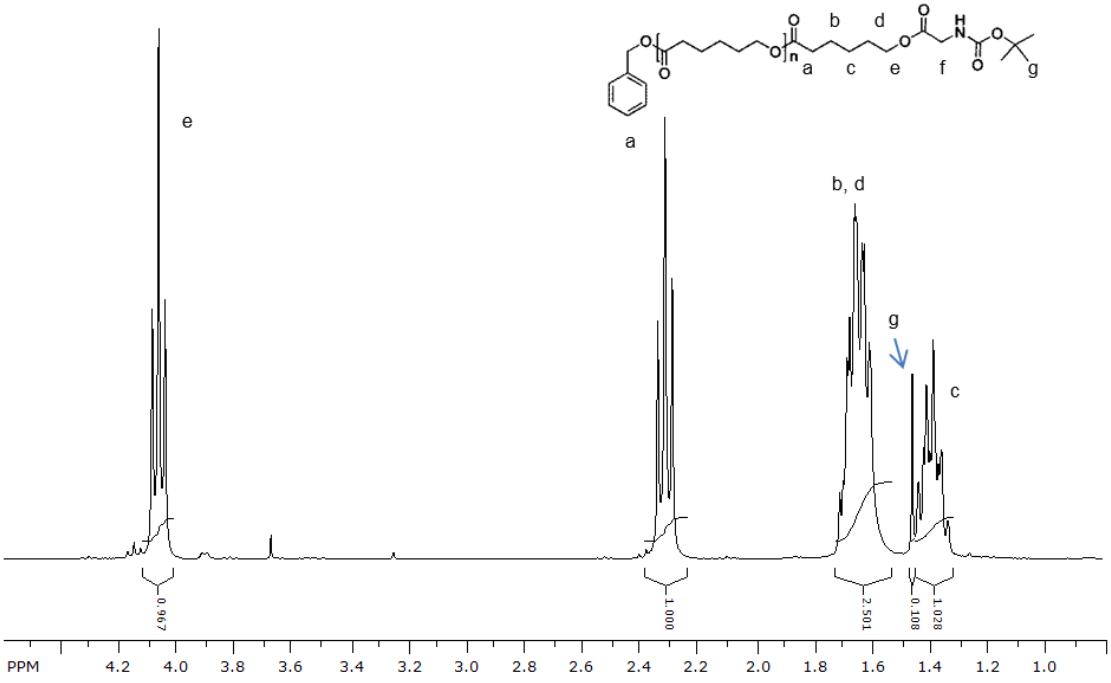

Figure 36. ^{1}H NMR spectrum ($CDCl_3$) of PCL-boc-glycine.

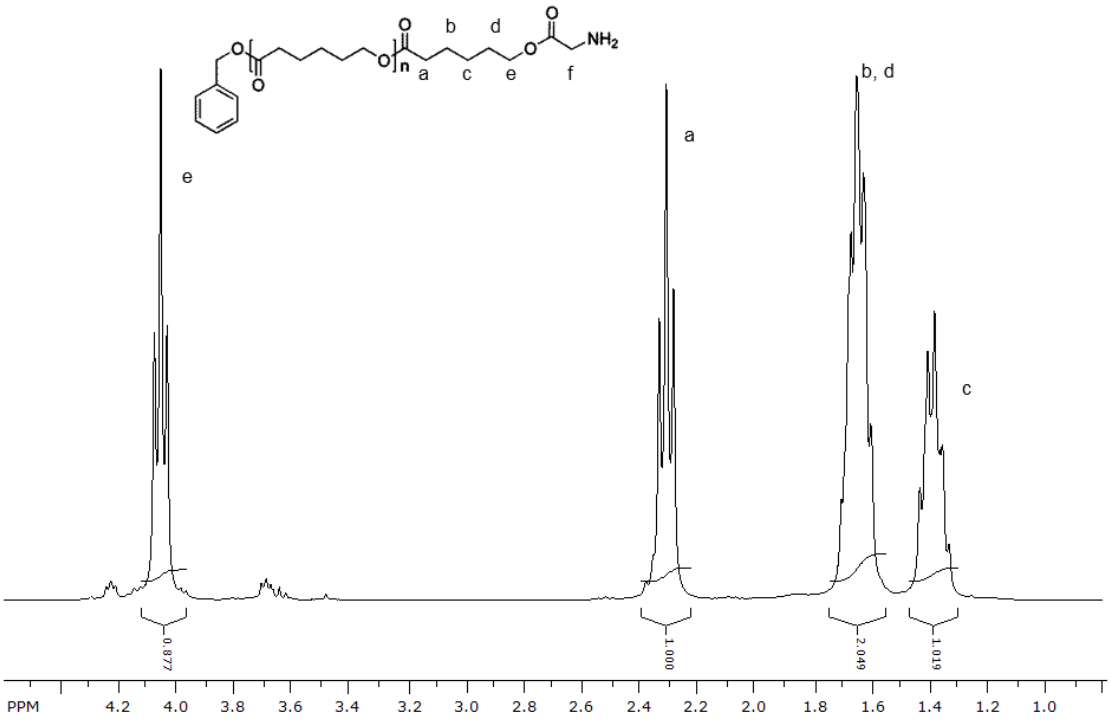

Figure 37. ^{1}H NMR spectrum ($CDCl_3$) of PCL-amine.

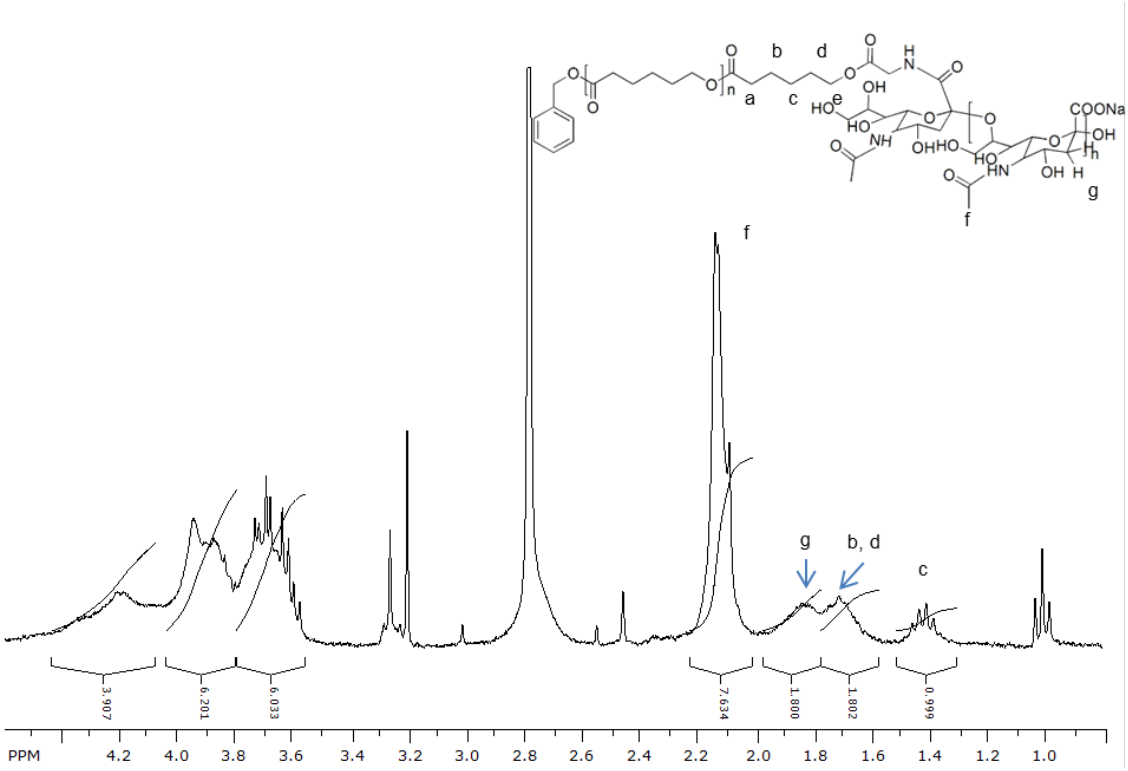

Figure 38. ^{1}H NMR spectrum (D_2O, water suppression) of PSA- PCL.

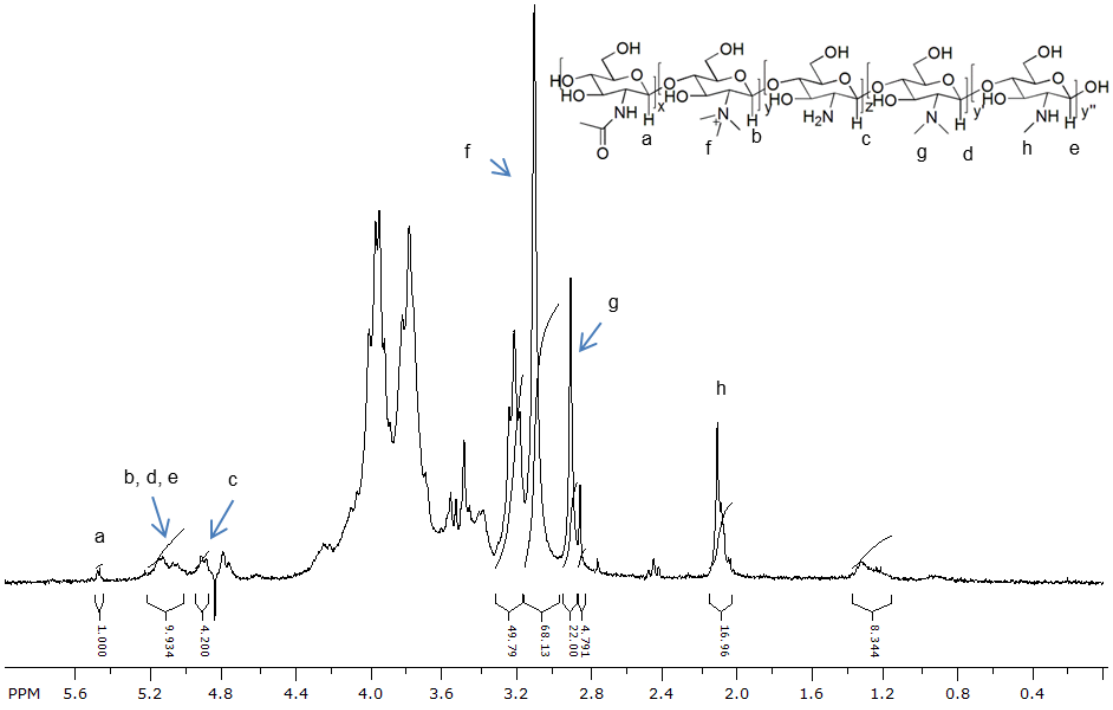

Figure 39. ^{1}H NMR spectrum (D_2O, water suppression) of N, N, N-trimethyl chitosan (TMC) with a DS of approximately 50%.

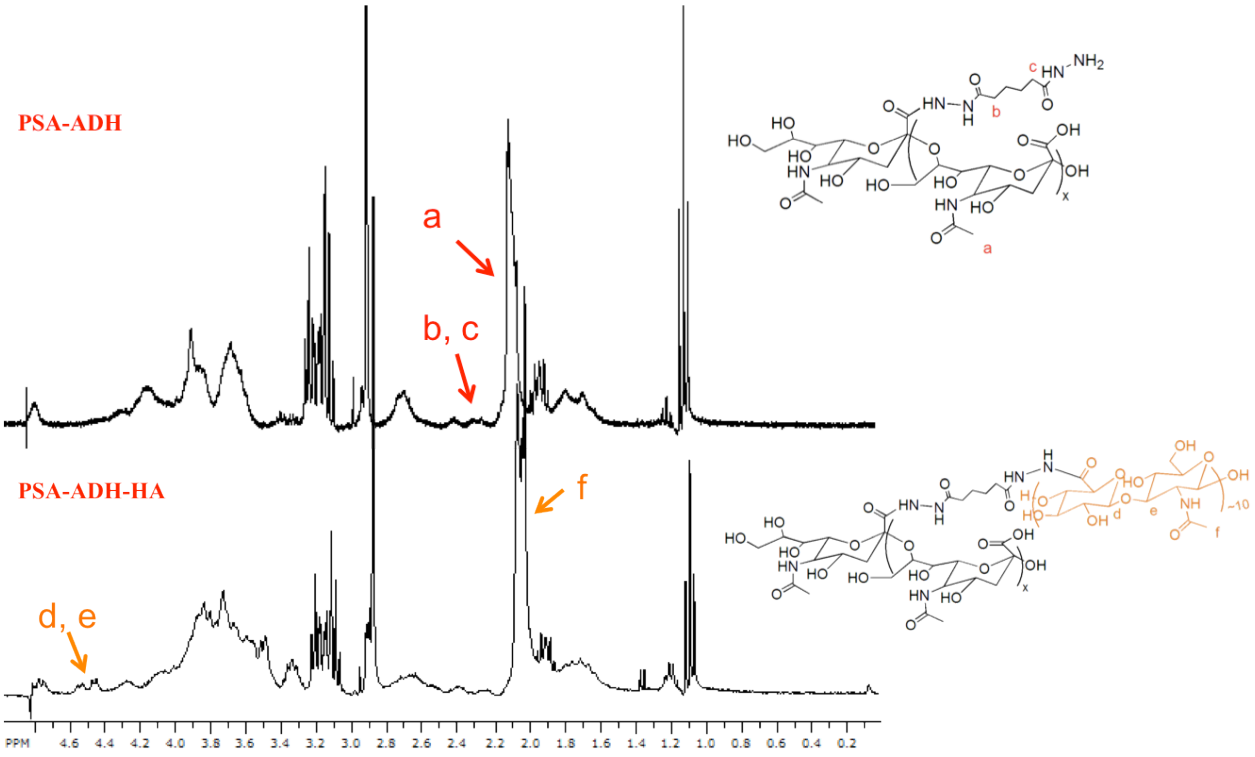

Figure 40. ^{1}H NMR spectrum (D_2O, water suppression) of HA-g-PSA.

APPENDIX B: SUPPLEMENTAL IMAGES OF PSA-PCL MICELLES

Quantitative fluorescence microscopy

Images of cells were taken at identical illumination and exposure settings. The resulting images spanned a very large dynamic range that made it not possible to show images at the same brightness settings. Figure 41 showed the images at settings where the 60 min incubation at room temperature was well visible. At these settings the features in the images at 4°C were barely visible. Conversely, at settings that allowed seeing the features in the images at 4°C, the room temperature images were highly oversaturated (Figure 42). Thus, the images presented in chapter 4 (Figure 15, 16) had different brightness settings for the room temperature and 4°C images, but it was clear from the images here that the amount of drug-loaded micelle uptake was dramatically different at room temperature when compared to incubation at 4°C.

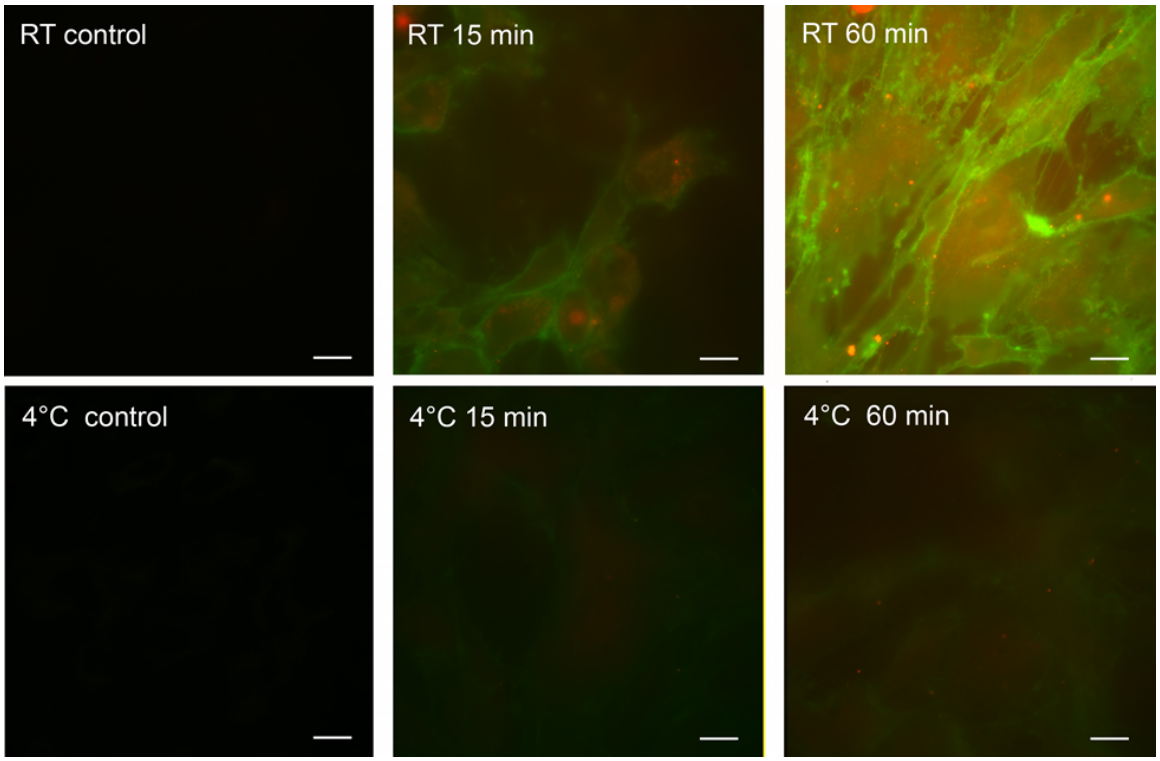

Figure 41. Color composite of fluorescence microscopy images demonstrating nanoparticle uptake and drug release at room temperature. Use of identical imaging settings did not allow for identification of the features in all the images. Here, brightness and contrast were adjusted such that the brightest image (room temperature, 60 min incubation (top right image)) was well visible. The features in the 4°C images (middle and right images in the bottom row) were almost invisible at these parameters. Scale bars were 5 μm.

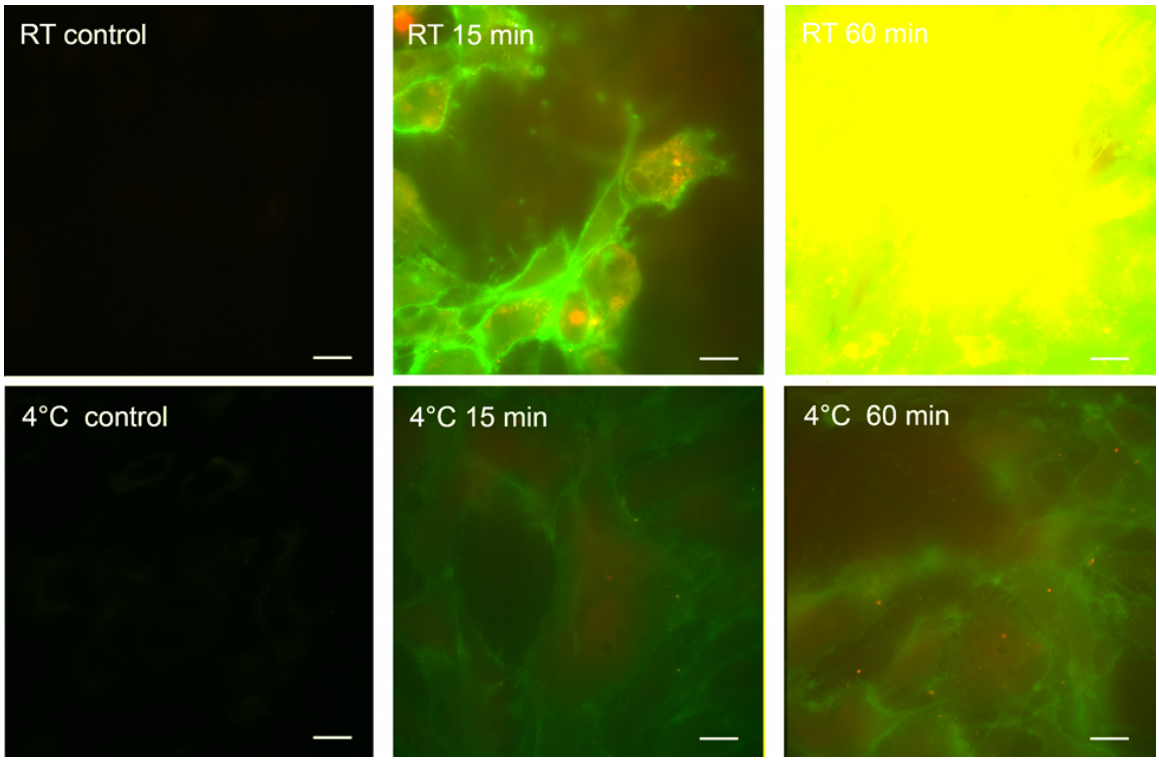

Figure 42. Color composite of fluorescence microscopy images demonstrating nanoparticle uptake and drug release at room temperature. Use of identical imaging settings did not allow for identification of the features in all the images. Here, brightness and contrast were adjusted such that the features in the lower signal images at 4°C were visible (middle and right images in the bottom row). At these settings the room temperature images were so oversaturated that the features completely disappeared (room temperature, 60 min incubation (top right image)). Scale bars were 5 μm.

References

[1] Gregoriadis G, McCormack B, Wang Z, Lifely R. Polysialic acids: potential in drug delivery. FEBS Lett. 1993;315:271-6.
[2] Fernandes AG, G. FC41 catalase-polysialic acid conjugates. European Journal of Pharmaceutical Sciences. 1994;2:111.
[3] Fernandes AI, Gregoriadis G. Synthesis, characterization and properties of sialylated catalase. Biochim Biophys Acta. 1996;1293:90-6.
[4] Fernandes AI, Gregoriadis G. Polysialylated asparaginase: preparation, activity and pharmacokinetics. Biochim Biophys Acta. 1997;1341:26-34.
[5] Fernandes AI, Gregoriadis G. The effect of polysialylation on the immunogenicity and antigenicity of asparaginase: implication in its pharmacokinetics. Int J Pharm. 2001;217:215-24.
[6] Jain S, Hreczuk-Hirst DH, McCormack B, Mital M, Epenetos A, Laing P, et al. Polysialylated insulin: synthesis, characterization and biological activity in vivo. Biochim Biophys Acta. 2003;1622:42-9.
[7] Peppas NA. Historical perspective on advanced drug delivery: How engineering design and mathematical modeling helped the field mature. Advanced Drug Delivery Reviews. 2013;65:5-9.
[8] Maeda H, Seymour LW, Miyamoto Y. CONJUGATES OF ANTICANCER AGENTS AND POLYMERS - ADVANTAGES OF MACROMOLECULAR THERAPEUTICS INVIVO. Bioconjugate Chemistry. 1992;3:351-62.
[9] Gregoriadis G. Engineering liposomes for drug delivery: Progress and problems. Trends in Biotechnology. 1995;13:527-37.
[10] Torchilin VP. Micellar nanocarriers: Pharmaceutical perspectives. Pharmaceutical Research. 2007;24:1-16.
[11] Torchilin VP. Targeted polymeric micelles for delivery of poorly soluble drugs. Cellular and Molecular Life Sciences. 2004;61:2549-59.
[12] Bader H, Ringsdorf H, Schmidt B. Watersoluble Polymers in Medicine. Angewandte Makromolekulare Chemie. 1984;123:457-85.
[13] Torchilin VP. Drug targeting. Eur J Pharm Sci. 2000;11 Suppl 2:S81-91.
[14] Xiong XB, Falamarzian A, Garg SM, Lavasanifar A. Engineering of amphiphilic block copolymers for polymeric micellar drug and gene delivery. J Control Release. 2011;155:248-61.
[15] Jian F, Zhang Y, Wang J, Ba K, Mao RY, Lai WL, et al. Toxicity of Biodegradable Nanoscale Preparations. Current Drug Metabolism. 2012;13:440-6.
[16] Liu ZH, Jiao YP, Wang YF, Zhou CR, Zhang ZY. Polysaccharides-based nanoparticles as drug delivery systems. Advanced Drug Delivery Reviews. 2008;60:1650-62.
[17] Peer D, Karp JM, Hong S, FaroKhzad OC, Margalit R, Langer R. Nanocarriers as an emerging platform for cancer therapy. Nature Nanotechnology. 2007;2:751-60.
[18] Shukla RK, Tiwari A. Carbohydrate polymers: Applications and recent advances in delivering drugs to the colon. Carbohydrate Polymers. 2012;88:399-416.

[19] Saravanakumar G. JDG, Park J.H. Polysaccharide based nanoparticles: A versatile Platform for Drug Delivery and Biomedical Imaging. Current Medicinal Chemistry. 2012;19.
[20] Dang JM, Leong KW. Natural polymers for gene delivery and tissue engineering. Advanced Drug Delivery Reviews. 2006;58:487-99.
[21] Ratner BD, Bryant SJ. Biomaterials: Where we have been and where we are going. Annual Review of Biomedical Engineering. 2004;6:41-75.
[22] Mizrahy S, Peer D. Polysaccharides as building blocks for nanotherapeutics. Chemical Society Reviews. 2012;41:2623-40.
[23] Coviello T, Matricardi P., Marianecci C., Alhaique F. Polysaccharide hydrogels for modified release formulations. Journal of Controlled Release. 2007;119:5-24.
[24] Cadee J. A. BLA, den Otter W., Hennick W. E., van Luyn M. J. A. A comparative biocompatibiltiy study of microspheres based on crosslinked dextran or poly(lactic-co-glycolic)acid after subcutaneous injection in rats. Journal of Biomedical Materials Research. 2001;56:600-9.
[25] Jain A. GY, Jain S.K. Perspectives of Biodegradable Natural Polysaccharides for site specific drug delivery to the colon. JPharm Pharmaceut Sci. 2007;10:86-128.
[26] Rempel BP, Withers SG. Covalent inhibitors of glycosidases and their applications in biochemistry and biology. Glycobiology. 2008;18:570-86.
[27] Mehvar R. Recent trends in the use of polysaccharides for improved delivery of therapeutic agents: Pharmacokinetic and Pharmacodynamic perspectives. Current Pharmaceutical Biotechnology. 2003;4:283-302.
[28] Lim SM, Song DK, Oh SH, Lee-Yoon DS, Bae EH, Lee JH. In vitro and in vivo degradation behavior of acetylated chitosan porous beads. Journal of Biomaterials Science-Polymer Edition. 2008;19:453-66.
[29] Dash M, Chiellini F, Ottenbrite RM, Chiellini E. Chitosan-A versatile semi-synthetic polymer in biomedical applications. Progress in Polymer Science. 2011;36:981-1014.
[30] Morris GA. Polysaccharide drug delivery systems based on pectin and chitosan. Biotechnology and genetic engineering reviews. 2010;27:257-83.
[31] Alonso-Sande M. T-OD, Remunan-Lopez C., Alonso M.J. Glucomannan, a promising polysaccharide for biopharmaceutical purposes. European Journal of Pharmaceutics and Biopharmaceutics. 2009;72:453-62.
[32] Kumar MN, Muzzarelli RA, Muzzarelli C, Sashiwa H, Domb AJ. Chitosan chemistry and pharmaceutical perspectives. Chem Rev. 2004;104:6017-84.
[33] Mourya VK, Inamdar NN. Trimethyl chitosan and its applications in drug delivery. J Mater Sci Mater Med. 2009;20:1057-79.
[34] Thanou M, Verhoef JC, Junginger HE. Chitosan and its derivatives as intestinal absorption enhancers. Adv Drug Deliv Rev. 2001;50 Suppl 1:S91-101.
[35] Thanou M, Verhoef JC, Junginger HE. Oral drug absorption enhancement by chitosan and its derivatives. Adv Drug Deliv Rev. 2001;52:117-26.
[36] Bernkop-Schnurch A, Dunnhaupt S. Chitosan-based drug delivery systems. European Journal of Pharmaceutics and Biopharmaceutics. 2012;81:463-9.
[37] Boddhoi S. KCE, Kipper M. J. Polyelectrolyte multilayer assembly as a function of pH and ionic strength using the polysaccharides chitosan and heparin. Biomacromolecules. 2008;9:2021-8.

[38] Bonferoni MC, Sandri G, Ferrari F, Rossi S, Larghi V, Zambito Y, et al. Comparison of different in vitro and ex vivo methods to evaluate mucoadhesion of glycol-palmitoyl chitosan micelles. Journal of Drug Delivery Science and Technology. 2010;20:419-24.
[39] Reddy K. MGK, Satla S., Gaikwad S. Natural Polysaccharides: Versatile Excipients for controlled drug delivery systems. Journal of Pharmaceutical Sciences. 2011;6:275-86.
[40] Dai T. TM, Huang Y., Hamblin M. Chitosan preparations for wounds and burns: antimicrobial and wound healing effects. Expert review of Anti-infective therapy. 2011;9:857-79.
[41] Young E. The anti-inflammatory effects of heparin and related compounds. Thrombosis Research. 2008;122:743-52.
[42] Olson ST, Shore JD. Binding of high affinity heparin to antithrombin III. Characterization of the protein fluorescence enhancement. J Biol Chem. 1981;256:11065-72.
[43] Olson ST, Srinivasan KR, Bjork I, Shore JD. Binding of high affinity heparin to antithrombin III. Stopped flow kinetic studies of the binding interaction. J Biol Chem. 1981;256:11073-9.
[44] Chen X, Varki A. Advances in the biology and chemistry of sialic acids. ACS Chemical Biology. 2010;5:163-76.
[45] Varki A. Diversity in the Sialic Acids. Glycobiology. 1992;2:25-40.
[46] Varki A, Schauer R. Sialic Acids. 2009.
[47] Varki A, Gagneux P. Multifarious roles of sialic acids in immunity. 2012. p. 16-36.
[48] Gregoriadis G, Jain S, Papaioannou I, Laing P. Improving the therapeutic efficacy of peptides and proteins: A role for polysialic acids. International Journal of Pharmaceutics. 2005;300:125-30.
[49] Ghosh M, Tuesta LM, Puentes R, Patel S, Melendez K, El Maarouf A, et al. Extensive cell migration, axon regeneration, and improved function with polysialic acid-modified Schwann cells after spinal cord injury. Glia. 2012;60:979-92.
[50] Mikkonen M, Soininen H, Kälviäinen R, Tapiola T, Ylinen A, Vapalahti M, et al. Remodeling of neuronal circuitries in human temporal lobe epilepsy: Increased expression of highly polysialylated neural cell adhesion molecule in the hippocampus and the entorhinal cortex. Annals of Neurology. 1998;44:923-34.
[51] Görög P, Kovács IB. Anti-inflammatory effect of sialic acid. Agents Actions. 1978;8:543-5.
[52] Osawa R, Suda I, Numata M, Sugimoto M, Tomita K, Kibushi N. Methods for inhibiting the chemotaxis of neutrophils. 1997.
[53] Liao YH, Jones SA, Forbes B, Martin GP, Brown MB. Hyaluronan: Pharmaceutical characterization and drug delivery. Drug Delivery. 2005;12:327-42.
[54] Cheng KC, Demirci A, Catchmark JM. Pullulan: biosynthesis, production, and applications. Applied Microbiology and Biotechnology. 2011;92:29-44.
[55] Akiyoshi K, Yamaguchi S, Sunamoto J. SELF-AGGREGATES OF HYDROPHOBIC POLYSACCHARIDE DERIVATIVES. Chemistry Letters. 1991:1263-6.
[56] Akiyoshi K, Deguchi S, Moriguchi N, Yamaguchi S, Sunamoto J. SELF-AGGREGATES OF HYDROPHOBIZED POLYSACCHARIDES IN WATER - FORMATION AND CHARACTERISTICS OF NANOPARTICLES. Macromolecules. 1993;26:3062-8.

[57] Akiyoshi K, Kobayashi S, Shichibe S, Mix D, Baudys M, Kim SW, et al. Self-assembled hydrogel nanoparticle of cholesterol-bearing pullulan as a carrier of protein drugs: Complexation and stabilization of insulin. Journal of Controlled Release. 1998;54:313-20.
[58] Akiyoshi K, Nishikawa T, Shichibe S, Sunamoto J. STABILIZATION OF INSULIN UPON SUPRAMOLECULAR COMPLEXATION WITH HYDROPHOBIZED POLYSACCHARIDE NANOPARTICLE. Chemistry Letters. 1995:707-8.
[59] Fujioka-Kobayashi M, Ota MS, Shimoda A, Nakahama K, Akiyoshi K, Miyamoto Y, et al. Cholesteryl group- and acryloyl group-bearing pullulan nanogel to deliver BMP2 and FGF18 for bone tissue engineering. Biomaterials. 2012;33:7613-20.
[60] Miyahara T, Nyan M, Shimoda A, Yamamoto Y, Kuroda S, Shiota M, et al. Exploitation of a novel polysaccharide nanogel cross-linking membrane for guided bone regeneration (GBR). Journal of Tissue Engineering and Regenerative Medicine. 2012;6:666-72.
[61] Kageyama S, Kitano S, Hirayama M, Nagata Y, Imai H, Shiraishi T, et al. Humoral immune responses in patients vaccinated with 1-146 HER2 protein complexed with cholesteryl pullulan nanogel. Cancer Science. 2008;99:601-7.
[62] Satoh K, Chen F, Aoyama A, Date H, Akiyoshi K. Nanoparticle of cholesterol-bearing pullulan as a carrier of anticancer drugs. Ejc Supplements. 2008;6:139-.
[63] Shimizu T, Kishida T, Hasegawa U, Ueda Y, Imanishi J, Yamagishi H, et al. Nanogel DDS enables sustained release of IL-12 for tumor immunotherapy. Biochemical and Biophysical Research Communications. 2008;367:330-5.
[64] Kobayashi H, Katakura O, Morimoto N, Akiyoshi K, Kasugai S. Effects of Cholesterol-Bearing Pullulan (CHP)-Nanogels in Combination with Prostaglandin E1 on Wound Healing. Journal of Biomedical Materials Research Part B-Applied Biomaterials. 2009;91B:55-60.
[65] Jung SW, Jeong YI, Kim SH. Characterization of hydrophobized pullulan with various hydrophobicities. International Journal of Pharmaceutics. 2003;254:109-21.
[66] Jeong YI, Na HS, Oh JS, Choi KC, Song CE, Lee HC. Adriamycin release from self-assembling nanospheres of poly(DL-lactide-co-glycolide)-grafted pullulan. International Journal of Pharmaceutics. 2006;322:154-60.
[67] Seo S, Lee CS, Jung YS, Na K. Thermo-sensitivity and triggered drug release of polysaccharide nanogels derived from pullulan-g-poly(L-lactide) copolymers. Carbohydrate Polymers. 2012;87:1105-11.
[68] Lu DX, Wen XT, Liang J, Gu ZW, Zhang XD, Fan YJ. A pH-Sensitive Nano Drug Delivery System Derived From Pullulan/Doxorubicin Conjugate. Journal of Biomedical Materials Research Part B-Applied Biomaterials. 2009;89B:177-83.
[69] Park KH, Kang D, Na K. Physicochemical characterization and carcinoma cell interaction of self-organized nanogels prepared from polysaccharide/biotin conjugates for development of anticancer drug carrier. Journal of Microbiology and Biotechnology. 2006;16:1369-76.
[70] Akiyoshi K, Sasaki Y, Sunamoto J. Molecular chaperone-like activity of hydrogel nanoparticles of hydrophobized pullulan: thermal stabilization with refolding of carbonic anhydrase B. Bioconjug Chem. 1999;10:321-4.
[71] Wang XH, Tian Q, Wang W, Zhang CN, Wang P, Yuan Z. In vitro evaluation of polymeric micelles based on hydrophobically-modified sulfated chitosan as a carrier of doxorubicin. Journal of Materials Science-Materials in Medicine. 2012;23:1663-74.

[72] Xiong YB, Qi JN, Yao P. Amphiphilic Cholic-Acid-Modified Dextran Sulfate and its Application for the Controlled Delivery of Superoxide Dismutase. Macromolecular Bioscience. 2012;12:515-24.
[73] Nichifor M, Lopes A, Carpov A, Melo E. Aggregation in water of dextran hydrophobically modified with bile acids. Macromolecules. 1999;32:7078-85.
[74] Khatun Z, Nurunnabi M, Cho KJ, Lee YK. Oral delivery of near-infrared quantum dot loaded micelles for noninvasive biomedical imaging. ACS Applied Materials and Interfaces. 2012;4:3880-7.
[75] Nagahama K, Ouchi T, Ohya Y. Biodegradable Nanogels Prepared by Self-Assembly of Poly(L-lactide)-Grafted Dextran: Entrapment and Release of Proteins. Macromolecular Bioscience. 2008;8:1044-52.
[76] Dahmani FZ, Yang H, Zhou JP, Yao J, Zhang T, Zhang Q. Enhanced oral bioavailability of paclitaxel in pluronic/LHR mixed polymeric micelles: Preparation, in vitro and in vivo evaluation. European Journal of Pharmaceutical Sciences. 2012;47:179-89.
[77] Zhang HW, Cai GQ, Tang GP, Wang LQ, Jiang HL. Synthesis, self-assembly, and cytotoxicity of well-defined trimethylated chitosan-O-poly(epsilon-caprolactone): Effect of chitosan molecular weight. Journal of Biomedical Materials Research Part B-Applied Biomaterials. 2011;98B:290-9.
[78] Dionísio M, Cordeiro C, Remuñán-López C, Seijo B, Rosa da Costa AM, Grenha A. Pullulan-based nanoparticles as carriers for transmucosal protein delivery. European Journal of Pharmaceutical Sciences. 2013.
[79] Kamel S, Ali N, Jahangir K, Shah SM, El-Gendy AA. Pharmaceutical significance of cellulose: A review. Express Polymer Letters. 2008;2:758-78.
[80] Francis MF, Piredda M, Winnik FM. Solubilization of poorly water soluble drugs in micelles of hydrophobically modified hydroxypropylcellulose copolymers. Journal of Controlled Release. 2003;93:59-68.
[81] Chayed S, Winnik FM. In vitro evaluation of the mucoadhesive properties of polysaccharide-based nanoparticulate oral drug delivery systems. European Journal of Pharmaceutics and Biopharmaceutics. 2007;65:363-70.
[82] Francis MF, Cristea M, Yang YL, Winnik FM. Engineering polysaccharide-based polymeric micelles to enhance permeability of cyclosporin a across Caco-2 cells. Pharmaceutical Research. 2005;22:209-19.
[83] Shi RW, Burt HM. Synthesis and characterization of amphiphilic hydroxypropylcellulose-graft-poly(epsilon-caprolactone). Journal of Applied Polymer Science. 2003;89:718-27.
[84] Enomoto-Rogers Y, Kamitakahara H, Yoshinaga A, Takano T. Synthesis of diblock copolymers with cellulose derivatives 4. Self-assembled nanoparticles of amphiphilic cellulose derivatives carrying a single pyrene group at the reducing-end. Cellulose. 2011;18:1005-14.
[85] Rahmat D, Muller C, Barthelmes J, Shahnaz G, Martien R, Bernkop-Schnurch A. Thiolated hydroxyethyl cellulose: Design and in vitro evaluation of mucoadhesive and permeation enhancing nanoparticles. European Journal of Pharmaceutics and Biopharmaceutics. 2013;83:149-55.
[86] Clagett GP, Anderson FA, Geerts W, Heit JA, Knudson M, Lieberman JR, et al. Prevention of venous thromboembolism. Chest. 1998;114:531S-60S.

[87] Francis MF, Lavoie L, Winnik FM, Leroux JC. Solubilization of cyclosporin A in dextran-g-polyethyleneglycolalkyl ether polymeric micelles. European Journal of Pharmaceutics and Biopharmaceutics. 2003;56:337-46.
[88] Francis MF, Cristea M, Winnik FM. Exploiting the vitamin B-12 pathway to enhance oral drug delivery via polymeric micelles. Biomacromolecules. 2005;6:2462-7.
[89] Yuan XB, Li H, Zhu XX, Woo HG. Self-aggregated nanoparticles composed of periodate-oxidized dextran and cholic acid: preparation, stabilization and in-vitro drug release. Journal of Chemical Technology and Biotechnology. 2006;81:746-54.
[90] Xu QG, Yuan XB, Chang J. Self-aggregates of cholic acid hydrazide-dextran conjugates as drug carriers. Journal of Applied Polymer Science. 2005;95:487-93.
[91] Liu JY, Zhang LM. Preparation of a polysaccharide-polyester diblock copolymer and its micellar characteristics. Carbohydrate Polymers. 2007;69:196-201.
[92] Houga C, Giermanska J, Lecommandoux S, Borsali R, Taton D, Gnanou Y, et al. Micelles and Polymersomes Obtained by Self-Assembly of Dextran and Polystyrene Based Block Copolymers. Biomacromolecules. 2009;10:32-40.
[93] Daoud-Mahammed S, Couvreur P, Bouchemal K, Cheron M, Lebas G, Amiel C, et al. Cyclodextrin and Polysaccharide-Based Nanogels: Entrapment of Two Hydrophobic Molecules, Benzophenone and Tamoxifen. Biomacromolecules. 2009;10:547-54.
[94] Krasznai DJ, McKenna TFL, Cunningham MF, Champagne P, Smeets NMB. Polysaccharide-stabilized core cross-linked polymer micelle analogues. Polymer Chemistry. 2012;3:992-1001.
[95] Morgen M, Tung D, Boras B, Miller W, Malfait AM, Tortorella M. Nanoparticles for Improved Local Retention after Intra-Articular Injection into the Knee Joint. Pharmaceutical Research. 2013;30:257-68.
[96] Naeye B, Deschout H, Roding M, Rudemo M, Delanghe J, Devreese K, et al. Hemocompatibility of siRNA loaded dextran nanogels. Biomaterials. 2011;32:9120-7.
[97] Xie JQ, Wang HB, Wang YY, Ren FP, Yi W, Zhao K, et al. Induction of Angiogenesis by Controlled Delivery of Vascular Endothelial Growth Factor Using Nanoparticles. Cardiovascular Therapeutics. 2013;31:e12-e8.
[98] Sahu SK, Maiti S, Maiti TK, Ghosh SK, Pramanik P. Hydrophobically modified carboxymethyl chitosan nanoparticles targeted delivery of paclitaxel. Journal of Drug Targeting. 2011;19:104-13.
[99] Huang X, Jiang XH, Hu FQ, Du YZ, Zhu QF, Jin CS. In vitro antitumour activity of stearic acid-g-chitosan oligosaccharide polymeric micelles loading podophyllotoxin. Journal of Microencapsulation. 2012;29:1-8.
[100] Huang ST, Du YZ, Yuan H, Zhang XG, Miao J, Cui FD, et al. Synthesis and anti-hepatitis B virus activity of acyclovir conjugated stearic acid-g-chitosan oligosaccharide micelle. Carbohydrate Polymers. 2011;83:1715-22.
[101] Yuan H, Lu LJ, Du YZ, Hu FQ. Stearic Acid-g-chitosan Polymeric Micelle for Oral Drug Delivery: In Vitro Transport and in Vivo Absorption. Molecular Pharmaceutics. 2011;8:225-38.
[102] Du YZ, Cai LL, Liu P, You J, Yuan H, Hu FQ. Tumor cells-specific targeting delivery achieved by A54 peptide functionalized polymeric micelles. Biomaterials. 2012;33:8858-67.

[103] Wang FH, Zhang DR, Duan CX, Jia LJ, Feng FF, Liu Y, et al. Preparation and characterizations of a novel deoxycholic acid-O-carboxymethylated chitosan-folic acid conjugates and self-aggregates. Carbohydrate Polymers. 2011;84:1192-200.
[104] Huo MR, Zou AF, Yao CL, Zhang Y, Zhou JP, Wang J, et al. Somatostatin receptor-mediated tumor-targeting drug delivery using octreotide-PEG-deoxycholic acid conjugate-modified N-deoxycholic acid-O, N-hydroxyethylation chitosan micelles. Biomaterials. 2012;33:6393-407.
[105] Jin YH, Hu HY, Qiao MX, Zhu J, Qi JW, Hu CJ, et al. pH-sensitive chitosan-derived nanoparticles as doxorubicin carriers for effective anti-tumor activity: preparation and in vitro evaluation. Colloids and Surfaces B-Biointerfaces. 2012;94:184-91.
[106] Tian Q, Wang XH, Wang W, Zhang CN, Wang P, Yuan Z. Self-assembly and liver targeting of sulfated chitosan nanoparticles functionalized with glycyrrhetinic acid. Nanomedicine-Nanotechnology Biology and Medicine. 2012;8:870-9.
[107] Chen C, Cai GQ, Zhang HW, Jiang HL, Wang LQ. Chitosan-poly(epsilon-caprolactone)-poly(ethylene glycol) graft copolymers: Synthesis, self-assembly, and drug release behavior. Journal of Biomedical Materials Research Part A. 2011;96A:116-24.
[108] Mo R, Jin X, Li N, Ju CY, Sun MJ, Zhang C, et al. The mechanism of enhancement on oral absorption of paclitaxel by N-octyl-O-sulfate chitosan micelles. Biomaterials. 2011;32:4609-20.
[109] Lian H, Sun J, Yu YP, Liu YH, Cao W, Wang YJ, et al. Supramolecular micellar nanoaggregates based on a novel chitosan/vitamin E succinate copolymer for paclitaxel selective delivery. International Journal of Nanomedicine. 2011;6:3323-34.
[110] Du YZ, Wang L, Yuan H, Hu FQ. Linoleic acid-grafted chitosan oligosaccharide micelles for intracellular drug delivery and reverse drug resistance of tumor cells. International Journal of Biological Macromolecules. 2011;48:215-22.
[111] Srinophakun T, Boonmee J. Preliminary Study of Conformation and Drug Release Mechanism of Doxorubicin-Conjugated Glycol Chitosan, via cis-Aconityl Linkage, by Molecular Modeling. International Journal of Molecular Sciences. 2011;12:1672-83.
[112] Manaspon C, Viravaidya-Pasuwat K, Pimpha N. Preparation of Folate-Conjugated Pluronic F127/Chitosan Core-Shell Nanoparticles Encapsulating Doxorubicin for Breast Cancer Treatment. Journal of Nanomaterials. 2012.
[113] Li ZG, Li XY, Cao ZX, Xu YZ, Lin HJ, Zhao YL, et al. Camptothecin nanocolloids based on N,N,N-trimethyl chitosan: Efficient suppression of growth of multiple myeloma in a murine model. Oncology Reports. 2012;27:1035-40.
[114] Jiang GB, Lin ZT, Xu XJ, Zhang H, Song K. Stable nanomicelles based on chitosan derivative: In vitro antiplatelet aggregation and adhesion properties. Carbohydrate Polymers. 2012;88:232-8.
[115] Sonaje K, Lin KJ, Tseng MT, Wey SP, Su FY, Chuang EY, et al. Effects of chitosan-nanoparticle-mediated tight junction opening on the oral absorption of endotoxins. Biomaterials. 2011;32:8712-21.
[116] Lin ZT, Song K, Bin JP, Liao YL, Jiang GB. Characterization of polymer micelles with hemocompatibility based on N-succinyl-chitosan grafting with long chain hydrophobic groups and loading aspirin. Journal of Materials Chemistry. 2011;21:19153-65.
[117] Trapani A, Di Gioia S, Ditaranto N, Cioffi N, Goycoolea FM, Carbone A, et al. Systemic heparin delivery by the pulmonary route using chitosan and glycol chitosan nanoparticles. International Journal of Pharmaceutics. 2013;447:115-23.

[118] Calderon L, Harris R, Cordoba-Diaz M, Elorza M, Elorza B, Lenoir J, et al. Nano and rnicroparticulate chitosan-based systems for antiviral topical delivery. European Journal of Pharmaceutical Sciences. 2013;48:216-22.
[119] Chaiyasan W, Srinivas SP, Tiyaboonchai W. Mucoadhesive Chitosan-Dextran Sulfate Nanoparticles for Sustained Drug Delivery to the Ocular Surface. Journal of Ocular Pharmacology and Therapeutics. 2013;29:200-7.
[120] Nogueira DR, Tavano L, Mitjans M, Perez L, Infante MR, Vinardell MP. In vitro antitumor activity of methotrexate via pH-sensitive chitosan nanoparticles. Biomaterials. 2013;34:2758-72.
[121] Wei W, Lv PP, Chen XM, Yue ZG, Fu Q, Liu SY, et al. Codelivery of mTERT siRNA and paclitaxel by chitosan-based nanoparticles promoted synergistic tumor suppression. Biomaterials. 2013;34:3912-23.
[122] Niers TMH, Klerk CPW, DiNisio M, Van Noorden CJF, Buller HR, Reitsma PH, et al. Mechanisms of heparin induced anti-cancer activity in experimental cancer models. Critical Reviews in Oncology Hematology. 2007;61:195-207.
[123] Karti SS, Ovali E, Ozgur O, Yilmaz M, Sonmez M, Ratip S, et al. Induction of apoptosis and inhibition of growth of human hepatoma HepG2 cells by heparin. Hepato-Gastroenterology. 2003;50:1864-6.
[124] Malingre MM, Beijnen JH, Schellens JHM. Oral delivery of taxanes. Investigational New Drugs. 2001;19:155-62.
[125] Chiappetta DA, Sosnik A. Poly(ethylene oxide)-poly(propylene oxide) block copolymer micelles as drug delivery agents: Improved hydrosolubility, stability and bioavailability of drugs. European Journal of Pharmaceutics and Biopharmaceutics. 2007;66:303-17.
[126] Choi JH, Jang JY, Joung YK, Kwon MH, Park KD. Intracellular delivery and anti-cancer effect of self-assembled heparin-Pluronic nanogels with RNase A. Journal of Controlled Release. 2010;147:420-7.
[127] Park K, Kim K, Kwon IC, Kim SK, Lee S, Lee DY, et al. Preparation and characterization of self-assembled nanoparticles of heparin-deoxycholic acid conjugates. Langmuir. 2004;20:11726-31.
[128] Wang Y, Xin DC, Liu KJ, Zhu MQ, Xiang JN. Heparin-Paclitaxel Conjugates as Drug Delivery System: Synthesis, Self-Assembly Property, Drug Release, and Antitumor Activity. Bioconjugate Chemistry. 2009;20:2214-21.
[129] Park IK, Kim YJ, Tran TH, Huh KM, Lee YK. Water-soluble heparin-PTX conjugates for cancer targeting. Polymer. 2010;51:3387-93.
[130] Li L, Moon HT, Park JY, Heo YJ, Choi Y, Tran TH, et al. Heparin-based self-assembled nanoparticles for photodynamic therapy. Macromolecular Research. 2011;19:487-94.
[131] Bader RA, Silvers AL, Zhang N. Polysialic acid-based micelles for encapsulation of hydrophobic drugs. Biomacromolecules. 2011;12:314-20.
[132] Li N, Li XR, Zhou YX, Li WJ, Zhao Y, Ma SJ, et al. The use of polyion complex micelles to enhance the oral delivery of salmon calcitonin and transport mechanism across the intestinal epithelial barrier. Biomaterials. 2012;33:8881-92.
[133] Ha W, Wu H, Wang XL, Peng SL, Ding LS, Zhang S, et al. Self-aggregates of cholesterol-modified carboxymethyl konjac glucomannan conjugate: Preparation, characterization, and preliminary assessment as a carrier of etoposide. Carbohydrate Polymers. 2011;86:513-9.

[134] Ferreira SA, Pereira P, Sampaio P, Coutinho PJG, Gama FM. Supramolecular assembled nanogel made of mannan. Journal of Colloid and Interface Science. 2011;361:97-108.
[135] Ferreira SA, Coutinho PJG, Gama FM. Self-Assembled Nanogel Made of Mannan: Synthesis and Characterization. Langmuir. 2010;26:11413-20.
[136] De Medeiros Modolon S, Otsuka I, Fort S, Minatti E, Borsali R, Halila S. Sweet block copolymer nanoparticles: Preparation and self-assembly of fully oligosaccharide-based amphiphile. Biomacromolecules. 2012;13:1129-35.
[137] Jeong YI, Kim DH, Chung CW, Yoo JJ, Choi KH, Kim CH, et al. Self-assembled nanoparticles of hyaluronic acid/poly(DL-lactide-co-glycolide) block copolymer. Colloids and Surfaces B-Biointerfaces. 2012;90:28-35.
[138] Cho HJ, Yoon IS, Yoon HY, Koo H, Jin YJ, Ko SH, et al. Polyethylene glycol-conjugated hyaluronic acid-ceramide self-assembled nanoparticles for targeted delivery of doxorubicin. Biomaterials. 2012;33:1190-200.
[139] Wu JL, Liu CG, Wang XL, Huang ZH. Preparation and characterization of nanoparticles based on histidine-hyaluronic acid conjugates as doxorubicin carriers. Journal of Materials Science-Materials in Medicine. 2012;23:1921-9.
[140] Jin YJ, Termsarasab U, Ko SH, Shim JS, Chong S, Chung SJ, et al. Hyaluronic Acid Derivative-Based Self-Assembled Nanoparticles for the Treatment of Melanoma. Pharmaceutical Research. 2012;29:3443-54.
[141] Li J, Huo MR, Wang J, Zhou JP, Mohammad JM, Zhang YL, et al. Redox-sensitive micelles self-assembled from amphiphilic hyaluronic acid-deoxycholic acid conjugates for targeted intracellular delivery of paclitaxel. Biomaterials. 2012;33:2310-20.
[142] Liu YH, Sun J, Cao W, Yang JH, Lian H, Li X, et al. Dual targeting folate-conjugated hyaluronic acid polymeric micelles for paclitaxel delivery. International Journal of Pharmaceutics. 2011;421:160-9.
[143] Saravanakumar G, Choi KY, Yoon HY, Kim K, Park JH, Kwon IC, et al. Hydrotropic hyaluronic acid conjugates: Synthesis, characterization, and implications as a carrier of paclitaxel. International Journal of Pharmaceutics. 2010;394:154-61.
[144] Shen Y, Wang BH, Lu Y, Ouahab A, Li Q, Tu JS. A novel tumor-targeted delivery system with hydrophobized hyaluronic acid-spermine conjugates (HHSCs) for efficient receptor-mediated siRNA delivery. International Journal of Pharmaceutics. 2011;414:233-43.
[145] Manju S, Sreenivasan K. Conjugation of curcumin onto hyaluronic acid enhances its aqueous solubility and stability. Journal of Colloid and Interface Science. 2011;359:318-25.
[146] Choi KY, Min KH, Yoon HY, Kim K, Park JH, Kwon IC, et al. PEGylation of hyaluronic acid nanoparticles improves tumor targetability in vivo. Biomaterials. 2011;32:1880-9.
[147] Cafaggi S, Russo E, Stefani R, Parodi B, Caviglioli G, Sillo G, et al. Preparation, characterisation and preliminary antitumour activity evaluation of a novel nanoparticulate system based on a cisplatin-hyaluronate complex and N-trimethyl chitosan. Investigational New Drugs. 2011;29:443-55.
[148] de la Fuente M, Seijo B, Alonso MJ. Bioadhesive hyaluronan-chitosan nanoparticles can transport genes across the ocular mucosa and transfect ocular tissue. Gene Therapy. 2008;15:668-76.
[149] de la Fuente M, Seijo B, Alonso MJ. Novel hyaluronic acid-chitosan nanoparticles for ocular gene therapy. Investigative Ophthalmology & Visual Science. 2008;49:2016-24.

[150] de la Fuente M, Seijo B, Alonso MJ. Novel hyaluronan-based nanocarriers for transmucosal delivery of macromolecules. Macromolecular Bioscience. 2008;8:441-50.
[151] Niu JX, Su ZG, Xiao YY, Huang AW, Li HY, Bao X, et al. Octreotide-modified and pH-triggering polymeric micelles loaded with doxorubicin for tumor targeting delivery. European Journal of Pharmaceutical Sciences. 2012;45:216-26.
[152] Nguyen DH, Joung YK, Choi JH, Moon HT, Park KD. Targeting ligand-functionalized and redox-sensitive heparin-Pluronic nanogels for intracellular protein delivery. Biomedical Materials. 2011;6.
[153] Cai LL, Liu P, Li X, Huang X, Ye YQ, Chen FY, et al. RGD peptide-mediated chitosan-based polymeric micelles targeting delivery for integrin-overexpressing tumor cells. International Journal of Nanomedicine. 2011;6:3499-508.
[154] Tan YL, Liu CG. Preparation and characterization of self-assemblied nanoparticles based on folic acid modified carboxymethyl chitosan. Journal of Materials Science-Materials in Medicine. 2011;22:1213-20.
[155] Zhu HY, Liu F, Guo J, Xue JP, Qian ZY, Gu YQ. Folate-modified chitosan micelles with enhanced tumor targeting evaluated by near infrared imaging system. Carbohydrate Polymers. 2011;86:1118-29.
[156] Nayebsadrian M, Varshosaz J, Hassanzadeh F, Sadeghi H, Banitalebi M, Rostami M. Screening the Most Effective Variables on Physical Properties of Folate-Targeted Dextran/Retinoic Acid Micelles by Taguchi Design. Journal of Nanomaterials. 2012.
[157] Caliceti P, Veronese FM. Pharmacokinetic and biodistribution properties of poly(ethylene glycol)-protein conjugates. Advanced Drug Delivery Reviews. 2003;55:1261-77.
[158] Knop K, Hoogenboom R, Fischer D, Schubert US. Poly(ethylene glycol) in Drug Delivery: Pros and Cons as Well as Potential Alternatives. Angewandte Chemie-International Edition. 2010;49:6288-308.
[159] Hong RL, Huang CJ, Tseng YL, Pang VF, Chen ST, Liu JJ, et al. Direct comparison of liposomal doxorubicin with or without polyethylene glycol coating in C-26 tumor-bearing mice: is surface coating with polyethylene glycol beneficial? Clin Cancer Res. 1999;5:3645-52.
[160] Holland JW, Hui C, Cullis PR, Madden TD. Poly(ethylene glycol)--lipid conjugates regulate the calcium-induced fusion of liposomes composed of phosphatidylethanolamine and phosphatidylserine. Biochemistry. 1996;35:2618-24.
[161] Erbacher P, Bettinger T, Belguise-Valladier P, Zou S, Coll JL, Behr JP, et al. Transfection and physical properties of various saccharide, poly(ethylene glycol), and antibody-derivatized polyethylenimines (PEI). J Gene Med. 1999;1:210-22.
[162] Paillard A, Passirani C, Saulnier P, Kroubi M, Garcion E, Benoit JP, et al. Positively-Charged, Porous, Polysaccharide Nanoparticles Loaded with Anionic Molecules Behave as 'Stealth' Cationic Nanocarriers. Pharmaceutical Research. 2010;27:126-33.
[163] Kim JK, Won YW, Lim KS, Kim YH. Low-Molecular-Weight Methylcellulose-Based Thermo-reversible Gel/Pluronic Micelle Combination System for Local and Sustained Docetaxel Delivery. Pharmaceutical Research. 2012;29:525-34.
[164] Wang X, Chen CJ, Huo D, Qian HQ, Ding Y, Hu Y, et al. Synthesis of beta-cyclodextrin modified chitosan-poly(acrylic acid) nanoparticles and use as drug carriers. Carbohydrate Polymers. 2012;90:361-9.

[165] Na K, Lee KH, Bae YH. pH-sensitivity and pH-dependent interior structural change of self-assembled hydrogel nanoparticles of pullulan acetate/oligo-sulfonamide conjugate. Journal of Controlled Release. 2004;97:513-25.
[166] Lin YH, Chang CH, Wu YS, Hsu YM, Chiou SF, Chen YJ. Development of pH-responsive chitosan/heparin nanoparticles for stomach-specific anti-Helicobacter pylori therapy. Biomaterials. 2009;30:3332-42.
[167] Gong XY, Yin YH, Huang ZJ, Lu B, Xu PH, Zheng H, et al. Preparation, characterization and in vitro release study of a glutathione-dependent polymeric prodrug Cis-3-(9H-purin-6-ylthio)-acrylic acid-graft-carboxymethyl chitosan. International Journal of Pharmaceutics. 2012;436:240-7.
[168] Zheng H, Rao Y, Yin YH, Xiong XO, Xu PH, Lu B. Preparation, characterization, and in vitro drug release behavior of 6-mercaptopurine-carboxymethyl chitosan. Carbohydrate Polymers. 2011;83:1952-8.
[169] Patnaik S, Sharma AK, Garg BS, Gandhi RP, Gupta KC. Photoregulation of drug release in azo-dextran nanogels. International Journal of Pharmaceutics. 2007;342:184-93.
[170] Firestein GS. Evolving concepts of rheumatoid arthritis. Nature. 2003;423:356-61.
[171] Lee DM, Weinblatt ME. Rheumatoid arthritis. Lancet. 2001;358:903-11.
[172] Wolfe F, Mitchell DM, Sibley JT, Fries JF, Bloch DA, Williams CA, et al. The mortality of rheumatoid arthritis. Arthritis Rheum. 1994;37:481-94.
[173] MacGregor AJ, Snieder H, Rigby AS, Koskenvuo M, Kaprio J, Aho K, et al. Characterizing the quantitative genetic contribution to rheumatoid arthritis using data from twins. Arthritis Rheum. 2000;43:30-7.
[174] Wunder A, Müller-Ladner U, Stelzer EH, Funk J, Neumann E, Stehle G, et al. Albumin-based drug delivery as novel therapeutic approach for rheumatoid arthritis. J Immunol. 2003;170:4793-801.
[175] Fiehn C, Müller-Ladner U, Gay S, Krienke S, Freudenberg-Konrad S, Funk J, et al. Albumin-coupled methotrexate (MTX-HSA) is a new anti-arthritic drug which acts synergistically to MTX. Rheumatology (Oxford). 2004;43:1097-105.
[176] Wang D, Miller SC, Liu XM, Anderson B, Wang XS, Goldring SR. Novel dexamethasone-HPMA copolymer conjugate and its potential application in treatment of rheumatoid arthritis. Arthritis Res Ther. 2007;9:R2.
[177] Vanniasinghe AS, Bender V, Manolios N. The potential of liposomal drug delivery for the treatment of inflammatory arthritis. Semin Arthritis Rheum. 2009;39:182-96.
[178] van den Hoven JM, Van Tomme SR, Metselaar JM, Nuijen B, Beijnen JH, Storm G. Liposomal drug formulations in the treatment of rheumatoid arthritis. Mol Pharm. 2011;8:1002-15.
[179] Foong WC, Green KL. Retention and distribution of liposome-entrapped [3H]methotrexate injected into normal or arthritic rabbit joints. J Pharm Pharmacol. 1988;40:464-8.
[180] Foong WC, Green KL. Treatment of antigen-induced arthritis in rabbits with liposome-entrapped methotrexate injected intra-articularly. J Pharm Pharmacol. 1993;45:204-9.
[181] Metselaar JM, van den Berg WB, Holthuysen AE, Wauben MH, Storm G, van Lent PL. Liposomal targeting of glucocorticoids to synovial lining cells strongly increases therapeutic benefit in collagen type II arthritis. Ann Rheum Dis. 2004;63:348-53.

[182] Metselaar JM, Wauben MH, Wagenaar-Hilbers JP, Boerman OC, Storm G. Complete remission of experimental arthritis by joint targeting of glucocorticoids with long-circulating liposomes. Arthritis Rheum. 2003;48:2059-66.
[183] Anderson R, Franch A, Castell M, Perez-Cano FJ, Braeuer R, Pohlers D, et al. Liposomal encapsulation enhances and prolongs the anti-inflammatory effects of water-soluble dexamethasone phosphate in experimental adjuvant arthritis. Arthritis Research & Therapy. 2010;12.
[184] Rauchhaus U, Schwaiger FW, Panzner S. Separating therapeutic efficacy from glucocorticoid side-effects in rodent arthritis using novel, liposomal delivery of dexamethasone phosphate: long-term suppression of arthritis facilitates interval treatment. Arthritis Research & Therapy. 2009;11.
[185] Zhigaltsev IV, Maurer N, Edwards K, Karlsson G, Cullis PR. Formation of drug-arylsulfonate complexes inside liposomes: a novel approach to improve drug retention. J Control Release. 2006;110:378-86.
[186] Higaki M, Ishihara T, Izumo N, Takatsu M, Mizushima Y. Treatment of experimental arthritis with poly(D, L-lactic/glycolic acid) nanoparticles encapsulating betamethasone sodium phosphate. Ann Rheum Dis. 2005;64:1132-6.
[187] Shi Q, Wang H, Tran C, Qiu X, Winnik FM, Zhang X, et al. Hydrodynamic delivery of chitosan-folate-DNA nanoparticles in rats with adjuvant-induced arthritis. J Biomed Biotechnol. 2011;2011:148763.
[188] Schmitt F, Lagopoulos L, Käuper P, Rossi N, Busso N, Barge J, et al. Chitosan-based nanogels for selective delivery of photosensitizers to macrophages and improved retention in and therapy of articular joints. J Control Release. 2010;144:242-50.
[189] Koo OM, Rubinstein I, Onyüksel H. Actively targeted low-dose camptothecin as a safe, long-acting, disease-modifying nanomedicine for rheumatoid arthritis. Pharm Res. 2011;28:776-87.
[190] Greenwald RB. PEG drugs: an overview. J Control Release. 2001;74:159-71.
[191] Greenwald RB. Poly(ethylene glycol) anticancer drug delivery systems. P R Health Sci J. 2002;21:113-21.
[192] Greenwald RB, Choe YH, McGuire J, Conover CD. Effective drug delivery by PEGylated drug conjugates. Adv Drug Deliv Rev. 2003;55:217-50.
[193] Joralemon MJ, McRae S, Emrick T. PEGylated polymers for medicine: from conjugation to self-assembled systems. Chem Commun (Camb). 2010;46:1377-93.
[194] Otsuka H, Nagasaki Y, Kataoka K. PEGylated nanoparticles for biological and pharmaceutical applications. Adv Drug Deliv Rev. 2003;55:403-19.
[195] Rutishauser U. Polysialic acid at the cell surface: biophysics in service of cell interactions and tissue plasticity. J Cell Biochem. 1998;70:304-12.
[196] Dube DH, Bertozzi CR. Glycans in cancer and inflammation--potential for therapeutics and diagnostics. Nat Rev Drug Discov. 2005;4:477-88.
[197] Muhlenhoff M, Eckhardt M, Gerardy-Schahn R. Polysialic acid: three-dimensional structure, biosynthesis and function. Curr Opin Struct Biol. 1998;8:558-64.
[198] Gregoriadis G, Fernandes A, McCormack B, Mital M, Zhang X. Polysialic acids: potential role in therapeutic constructs. Biotechnol Genet Eng Rev. 1999;16:203-15.
[199] Gregoriadis G, Fernandes A, Mital M, McCormack B. Polysialic acids: potential in improving the stability and pharmacokinetics of proteins and other therapeutics. Cell Mol Life Sci. 2000;57:1964-9.

[200] Nishikawa M, Takakura Y, Hashida M. Pharmacokinetic evaluation of polymeric carriers. Advanced Drug Delivery Reviews. 1996;21:135-55.
[201] Constantinou A, Epenetos AA, Hreczuk-Hirst D, Jain S, Deonarain MP. Modulation of antibody pharmacokinetics by chemical polysialylation. Bioconjugate Chemistry. 2008;19:643-50.
[202] Constantinou A, Epenetos AA, Hreczuk-Hirst D, Jain S, Wright M, Chester KA, et al. Site-Specific Polysialylation of an Antitumor Single-Chain Fv Fragment. Bioconjugate Chemistry. 2009;20:924-31.
[203] Constantinou A, Chen C, Deonarain MP. Modulating the pharmacokinetics of therapeutic antibodies. Biotechnology Letters. 2010;32:609-22.
[204] Sadzuka Y, Nakade A, Hirama R, Miyagishima A, Nozawa Y, Hirota S, et al. Effects of mixed polyethyleneglycol modification on fixed aqueous layer thickness and antitumor activity of doxorubicin containing liposome. International Journal of Pharmaceutics. 2002;238:171-80.
[205] Zeisig R, Shimada K, Hirota S, Arndt D. Effect of sterical stabilization on macrophage uptake in vitro and on thickness of the fixed aqueous layer of liposomes made from alkylphosphocholines. Biochim Biophys Acta. 1996;1285:237-45.
[206] Wilhelm M, Zhao CL, Wang YC, Xu RL, Winnik MA, Mura JL, et al. Polymer Micelle Formation .3. Poly(Styrene-Ethylene Oxide) Block Copolymer Micelle Formation in Water - a Fluorescence Probe Study. Macromolecules. 1991;24:1033-40.
[207] Aliabadi HM, Elhasi S, Mahmud A, Gulamhusein R, Mahdipoor P, Lavasanifar A. Encapsulation of hydrophobic drugs in polymeric micelles through co-solvent evaporation: The effect of solvent composition on micellar properties and drug loading. International Journal of Pharmaceutics. 2007;329:158-65.
[208] Aliabadi HM, Mahmud A, Sharifabadi AD, Lavasanifar A. Micelles of methoxy poly(ethylene oxide)-b-poly(epsilon-caprolactone) as vehicles for the solubilization and controlled delivery of Cyclosporine A. Journal of Controlled Release. 2005;104:301-11.
[209] Mocak J, Bond AM, Mitchell S, Scollary G. A statistical overview of standard (IUPAC and ACS) and new procedures for determining the limits of detection and quantification: Application to voltammetric and stripping techniques (technical report). Pure and Applied Chemistry. 1997;69:297-328.
[210] Luo Y, Prestwich GD. Synthesis and selective cytotoxicity of a hyaluronic acid-antitumor bioconjugate. Bioconjugate Chemistry. 1999;10:755-63.
[211] Liang HC, Chang WH, Liang HF, Lee MH, Sung HW. Crosslinking structures of gelatin hydrogels crosslinked with genipin or a water-soluble carbodiimide. Journal of Applied Polymer Science. 2004;91:4017-26.
[212] Dulong V, Le Cerf D, Picton L, Muller G. Carboxymethylpullulan hydrogels with a ionic and/or amphiphilic behavior: Swelling properties and entrapment of cationic and/or hydrophobic molecules. Colloids and Surfaces a-Physicochemical and Engineering Aspects. 2006;274:163-9.
[213] Kuo JW, Swann DA, Prestwich GD. CHEMICAL MODIFICATION OF HYALURONIC-ACID BY CARBODIIMIDES. Bioconjugate Chemistry. 1991;2:232-41.
[214] Darr A, Calabro A. Synthesis and characterization of tyramine-based hyaluronan hydrogels. Journal of Materials Science-Materials in Medicine. 2009;20:33-44.

[215] Liang HC, Chang WH, Lin KJ, Sung HW. Genipin-crosslinked gelatin microspheres as a drug carrier for intramuscular administration: In vitro and in vivo studies. Journal of Biomedical Materials Research Part A. 2003;65A:271-82.
[216] Matsumoto T, Nieuwenhuis EES, Cisneros RL, Ruiz-Perez B, Yamaguchi K, Blumberg RS, et al. Protective effect of ethyl-3-(3-dimethyl aminopropyl)urea dihydrochloride (EDU) against LPS-induced death in mice. Journal of Medical Microbiology. 2004;53:97-102.
[217] Ruiz-Perez B, Cisneros RL, Matsumoto T, Miller RJ, Vasios G, Calias P, et al. Protection against lethal intra-abdominal sepsis by 1-(3-dimethylaminopropyl)-3-ethylurea. Journal of Infectious Diseases. 2003;188:378-87.
[218] Mottram PL. Past, present and future drug treatment for rheumatoid arthritis and systemic lupus erythematosus. Immunology and Cell Biology. 2003;81:350-3.
[219] Schiffelers RM, Banciu M, Metselaar JM, Storm G. Therapeutic application of long-circulating liposomal glucocorticoids in auto-immune diseases and cancer. J Liposome Res. 2006;16:185-94.
[220] Zachariae H. Renal toxicity of long-term ciclosporin. Scandinavian Journal of Rheumatology. 1999;28:65-8.
[221] Lindholm A, Kahan BD. INFLUENCE OF CYCLOSPORINE PHARMACOKINETICS, TROUGH CONCENTRATIONS, AND AUC MONITORING ON OUTCOME AFTER KIDNEY-TRANSPLANTATION. Clinical Pharmacology & Therapeutics. 1993;54:205-18.
[222] Zhang C, Ping QN, Zhang HJ. Self-assembly and characterization of paclitaxel-loaded N-octyl-O-sulfate chitosan micellar system. Colloids and Surfaces B-Biointerfaces. 2004;39:69-75.
[223] Aliabadi HM, Brocks DR, Lavasanifar A. Polymeric micelles for the solubilization and delivery of cyclosporine A: pharmacokinetics and biodistribution. Biomaterials. 2005;26:7251-9.
[224] Lee H, Ahn CH, Park TG. Poly lactic-co-(glycolic acid) -Grafted Hyaluronic Acid Copolymer Micelle Nanoparticles for Target-Specific Delivery of Doxorubicin. Macromolecular Bioscience. 2009;9:336-42.
[225] Esquenet C, Terech P, Boue F, Buhler E. Structural and rheological properties of hydrophobically modified polysaccharide associative networks. Langmuir. 2004;20:3583-92.
[226] Li YY, Chen XG, Liu CS, Cha DS, Park HJ, Lee CM. Effect of the molecular mass and degree of substitution of oleoylchitosan on the structure, rheological properties, and formation of nanoparticles. Journal of Agricultural and Food Chemistry. 2007;55:4842-7.
[227] Du YZ, Wang L, Yuan H, Wei XH, Hu FQ. Preparation and characteristics of linoleic acid-grafted chitosan oligosaccharide micelles as a carrier for doxorubicin. Colloids and Surfaces B-Biointerfaces. 2009;69:257-63.
[228] Esselink FJ, Dormidontova E, Hadziioannou G. Evolution of block copolymer micellar size and structure evidenced with cryo electron microscopy. Macromolecules. 1998;31:2925-32.
[229] Saravanakumar G, Min KH, Min DS, Kim AY, Lee CM, Cho YW, et al. Hydrotropic oligomer-conjugated glycol chitosan as a carrier of paclitaxel: Synthesis, characterization, and in vivo biodistribution. Journal of Controlled Release. 2009;140:210-7.
[230] Gillies ER, Frechet JMJ. Dendrimers and dendritic polymers in drug delivery. Drug Discovery Today. 2005;10:35-43.

[231] Lee CC, Gillies ER, Fox ME, Guillaudeu SJ, Frechet JMJ, Dy EE, et al. A single dose of doxorubicin-functionalized bow-tie dendrimer cures mice bearing C-26 colon carcinomas. Proceedings of the National Academy of Sciences of the United States of America. 2006;103:16649-54.
[232] De Jesus OLP, Ihre HR, Gagne L, Frechet JMJ, Szoka FC. Polyester dendritic systems for drug delivery applications: In vitro and in vivo evaluation. Bioconjugate Chemistry. 2002;13:453-61.
[233] Schwarz C, Mehnert W. Solid lipid nanoparticles (SLN) for controlled drug delivery II. drug incorporation and physicochemical characterization. Journal of Microencapsulation. 1999;16:205-13.
[234] Abdelwahed W, Degobert G, Stainmesse S, Fessi H. Freeze-drying of nanoparticles: formulation, process and storage considerations. Adv Drug Deliv Rev. 2006;58:1688-713.
[235] Tang XL, Pikal MJ. Design of freeze-drying processes for pharmaceuticals: Practical advice. Pharmaceutical Research. 2004;21:191-200.
[236] Di Tommaso C, Como C, Gurny R, Moller M. Investigations on the lyophilisation of MPEG-hexPLA micelle based pharmaceutical formulations. European Journal of Pharmaceutical Sciences. 2010;40:38-47.
[237] Cao ZQ, Yu QM, Xue H, Cheng G, Jiang SY. Nanoparticles for Drug Delivery Prepared from Amphiphilic PLGA Zwitterionic Block Copolymers with Sharp Contrast in Polarity between Two Blocks. Angewandte Chemie-International Edition. 2010;49:3771-6.
[238] Cheng J, Teply BA, Sherifi I, Sung J, Luther G, Gu FX, et al. Formulation of functionalized PLGA-PEG nanoparticles for in vivo targeted drug delivery. Biomaterials. 2007;28:869-76.
[239] Chan JM, Zhang LF, Yuet KP, Liao G, Rhee JW, Langer R, et al. PLGA-lecithin-PEG core-shell nanoparticles for controlled drug delivery. Biomaterials. 2009;30:1627-34.
[240] Yang ZL, Li XR, Yang KW, Liu Y. Amphotericin B-loaded poly(ethylene glycol)-poly(lactide) micelles: Preparation, freeze-drying, and in vitro release. Journal of Biomedical Materials Research Part A. 2008;85A:539-46.
[241] Liu LH, Venkatraman SS, Yang YY, Guo K, Lu J, He BP, et al. Polymeric micelles anchored with TAT for delivery of antibiotics across the blood-brain barrier. Biopolymers. 2008;90:617-23.
[242] Mellor HR, Platt FM, Dwek RA, Butters TD. Membrane disruption and cytotoxicity of hydrophobic N-alkylated imino sugars is independent of the inhibition of protein and lipid glycosylation. Biochemical Journal. 2003;374:307-14.
[243] Strebhardt K, Ullrich A. Paul Ehrlich's magic bullet concept: 100 years of progress. Nat Rev Cancer. 2008;8:473-80.
[244] Parveen S, Sahoo SK. Long circulating chitosan/PEG blended PLGA nanoparticle for tumor drug delivery. Eur J Pharmacol. 2011;670:372-83.
[245] Chaudhari KR, Ukawala M, Manjappa AS, Kumar A, Mundada PK, Mishra AK, et al. Opsonization, biodistribution, cellular uptake and apoptosis study of PEGylated PBCA nanoparticle as potential drug delivery carrier. Pharm Res. 2012;29:53-68.
[246] Cole AJ, David AE, Wang J, Galban CJ, Yang VC. Magnetic brain tumor targeting and biodistribution of long-circulating PEG-modified, cross-linked starch-coated iron oxide nanoparticles. Biomaterials. 2011;32:6291-301.
[247] Hanahan D, Weinberg RA. The hallmarks of cancer. Cell. 2000;100:57-70.

[248] Hanahan D, Weinberg RA. Hallmarks of cancer: the next generation. Cell. 2011;144:646-74.
[249] Elward K, Gasque P. "Eat me" and "don't eat me" signals govern the innate immune response and tissue repair in the CNS: emphasis on the critical role of the complement system. Mol Immunol. 2003;40:85-94.
[250] Morris SK, Moss WJ, Halsey N. Haemophilus influenzae type b conjugate vaccine use and effectiveness. Lancet Infect Dis. 2008;8:435-43.
[251] von Itzstein M, Wu WY, Kok GB, Pegg MS, Dyason JC, Jin B, et al. Rational design of potent sialidase-based inhibitors of influenza virus replication. Nature. 1993;363:418-23.
[252] Duncan R. The dawning era of polymer therapeutics. Nat Rev Drug Discov. 2003;2:347-60.
[253] Bader RA, Silvers AL, Zhang N. Polysialic Acid-Based Micelles for Encapsulation of Hydrophobic Drugs. Biomacromolecules. 2011;12:314-20.
[254] Kumari A, Yadav SK, Yadav SC. Biodegradable polymeric nanoparticles based drug delivery systems. Colloids Surf B Biointerfaces. 2010;75:1-18.
[255] Sadzuka Y, Sugiyama I, Tsuruda T, Sonobe T. Characterization and cytotoxicity of mixed polyethyleneglycol modified liposomes containing doxorubicin. Int J Pharm. 2006;312:83-9.
[256] Fang C, Shi B, Pei YY, Hong MH, Wu J, Chen HZ. In vivo tumor targeting of tumor necrosis factor-alpha-loaded stealth nanoparticles: effect of MePEG molecular weight and particle size. Eur J Pharm Sci. 2006;27:27-36.
[257] Sadzuka Y, Nakade A, Tsuruda T, Sonobe T. Study on the characterization of mixed polyethyleneglycol modified liposomes containing doxorubicin. J Control Release. 2003;91:271-80.
[258] Shimada K, Miyagishima A, Sadzuka Y, Nozawa Y, Mochizuki Y, Ohshima H, et al. Determination of the thickness of the fixed aqueous layer around polyethyleneglycol-coated liposomes. J Drug Target. 1995;3:283-9.
[259] Moore JS, Stupp SI. Room-Temperature Polyesterification. Macromolecules. 1990;23:65-70.
[260] Lohmeijer BGG, Pratt RC, Leibfarth F, Logan JW, Long DA, Dove AP, et al. Guanidine and amidine organocatalysts for ring-opening polymerization of cyclic esters. Macromolecules. 2006;39:8574-83.
[261] Lu FZ, Xiong XY, Li ZC, Du FS, Zhang BY, Li FM. A convenient method for the synthesis of amine-terminated poly(ethylene oxide) and poly(epsilon-caprolactone). Bioconjugate Chemistry. 2002;13:1159-62.
[262] Oudshoorn MHM, Rissmann R, Bouwstra JA, Hennink WE. Synthesis of methacrylated hyaluronic acid with tailored degree of substitution. Polymer. 2007;48:1915-20.
[263] Astafieva I, Zhong XF, Eisenberg A. CRITICAL MICELLIZATION PHENOMENA IN BLOCK POLYELECTROLYTE SOLUTIONS. Macromolecules. 1993;26:7339-52.
[264] Chen CJ, Liu GY, Shi YT, Zhu CS, Pang SP, Liu XS, et al. Biocompatible micelles based on comb-like PEG derivates: formation, characterization, and photo-responsiveness. Macromol Rapid Commun. 2011;32:1077-81.
[265] Lu ZR, Gao SQ, Kopeckova P, Kopecek J. Modification of cyclosporin A and conjugation of its derivative to HPMA copolymers. Bioconjugate Chemistry. 2001;12:129-33.
[266] Du YZ, Weng Q, Yuan H, Hu FQ. Synthesis and antitumor activity of stearate-g-dextran micelles for intracellular doxorubicin delivery. ACS Nano. 2010;4:6894-902.

[267] Yoo JW, Chambers E, Mitragotri S. Factors that control the circulation time of nanoparticles in blood: challenges, solutions and future prospects. Curr Pharm Des. 2010;16:2298-307.
[268] Smolen JS, Steiner G. Therapeutic strategies for rheumatoid arthritis. Nat Rev Drug Discov. 2003;2:473-88.
[269] Walsh DA. Angiogenesis and arthritis. Rheumatology (Oxford). 1999;38:103-12.
[270] Schwarz C, Mehnert W. Solid lipid nanoparticles (SLN) for controlled drug delivery. II. Drug incorporation and physicochemical characterization. J Microencapsul. 1999;16:205-13.
[271] Gou M, Zheng L, Peng X, Men K, Zheng X, Zeng S, et al. Poly(epsilon-caprolactone)-poly(ethylene glycol)-poly(epsilon-caprolactone) (PCL-PEG-PCL) nanoparticles for honokiol delivery in vitro. Int J Pharm. 2009;375:170-6.
[272] Lemarchand C, Gref R, Passirani C, Garcion E, Petri B, Muller R, et al. Influence of polysaccharide coating on the interactions of nanoparticles with biological systems. Biomaterials. 2006;27:108-18.
[273] Zachariae H. Renal toxicity of long-term cyclosporin. Scand J Rheumatol. 1999;28:65-8.
[274] Weinblatt ME, Kremer JM. Methotrexate in rheumatoid arthritis. J Am Acad Dermatol. 1988;19:126-8.
[275] Bentin J. Mechanism of action of cyclosporin in rheumatoid arthritis. Clin Rheumatol. 1995;14 Suppl 2:22-5.
[276] Shevach EM. The effects of cyclosporin A on the immune system. Annu Rev Immunol. 1985;3:397-423.
[277] Cho ML, Cho CS, Min SY, Kim SH, Lee SS, Kim WU, et al. Cyclosporine inhibition of vascular endothelial growth factor production in rheumatoid synovial fibroblasts. Arthritis Rheum. 2002;46:1202-9.
[278] Cho ML, Kim WU, Min SY, Min DJ, Min JK, Lee SH, et al. Cyclosporine differentially regulates interleukin-10, interleukin-15, and tumor necrosis factor a production by rheumatoid synoviocytes. Arthritis Rheum. 2002;46:42-51.
[279] Russell RG, Graveley R, Coxon F, Skjodt H, Del Pozo E, Elford P, et al. Cyclosporin A. Mode of action and effects on bone and joint tissues. Scand J Rheumatol Suppl. 1992;95:9-18.
[280] Szamel M, Berger P, Resch K. Inhibition of T lymphocyte activation by cyclosporin A: interference with the early activation of plasma membrane phospholipid metabolism. J Immunol. 1986;136:264-9.
[281] Niebylski CD, Petty HR. Physical characterization of cyclosporine binding sites in lymphocytes. Biophys J. 1993;64:701-8.
[282] Tang X, Pikal MJ. Design of freeze-drying processes for pharmaceuticals: practical advice. Pharm Res. 2004;21:191-200.
[283] Lee CC, Gillies ER, Fox ME, Guillaudeu SJ, Frechet JM, Dy EE, et al. A single dose of doxorubicin-functionalized bow-tie dendrimer cures mice bearing C-26 colon carcinomas. Proc Natl Acad Sci U S A. 2006;103:16649-54.
[284] MacKay JA, Chen M, McDaniel JR, Liu W, Simnick AJ, Chilkoti A. Self-assembling chimeric polypeptide-doxorubicin conjugate nanoparticles that abolish tumours after a single injection. Nat Mater. 2009;8:993-9.

[285] Hirota S. Physicochemical specification of drug carrying liposomes for the quality control in the industrial production. International Journal of Pharmaceutics. 1998;162:185-94.
[286] Niebylski CD, Petty HR. CYCLOSPORINE-A INDUCES AN EARLY AND TRANSIENT RIGIDIFICATION OF LYMPHOCYTE MEMBRANES. Journal of Leukocyte Biology. 1991;49:407-15.
[287] Lambros MP, Rahman YE. Effects of cyclosporin A on model lipid membranes. Chemistry and Physics of Lipids. 2004;131:63-9.
[288] Kroggel R, Goppeltstrube M, Martin M, Resch K. THE IMMUNOSUPPRESSIVE ACTIVITIES OF DIFFERENT CYCLOSPORINS ARE CORRELATED TO INHIBITION OF THE EARLY MEMBRANE PHOSPHOLIPID-METABOLISM IN ACTIVATED LYMPHOCYTES. Immunobiology. 1987;175:159-71.
[289] Dausend J, Musyanovych A, Dass M, Walther P, Schrezenmeier H, Landfester K, et al. Uptake Mechanism of Oppositely Charged Fluorescent Nanoparticles in HeLa Cells. Macromolecular Bioscience. 2008;8:1135-43.
[290] Arnaiz B, Martinez-Avila O, Falcon-Perez JM, Penades S. Cellular Uptake of Gold Nanoparticles Bearing HIV gp120 Oligomannosides. Bioconjugate Chemistry. 2012;23:814-25.
[291] Panyam J, Zhou WZ, Prabha S, Sahoo SK, Labhasetwar V. Rapid endo-lysosomal escape of poly(DL-lactide-co-glycolide) nanoparticles: implications for drug and gene delivery. Faseb Journal. 2002;16.
[292] Krakauer KA, Zurier RB. PINOCYTOSIS IN HUMAN SYNOVIAL-CELLS INVITRO - EVIDENCE FOR ENHANCED ACTIVITY IN RHEUMATOID-ARTHRITIS. Journal of Clinical Investigation. 1980;66:592-8.
[293] Soppimath KS, Aminabhavi TM, Kulkarni AR, Rudzinski WE. Biodegradable polymeric nanoparticles as drug delivery devices. Journal of Controlled Release. 2001;70:1-20.
[294] Kontermann RE. Strategies for extended serum half-life of protein therapeutics. Current Opinion in Biotechnology. 2011;22:868-76.
[295] Gaberc-Porekar V, Zore I, Podobnik B, Menart V. Obstacles and pitfalls in the PEGylation of therapeutic proteins. Current Opinion in Drug Discovery & Development. 2008;11:242-50.
[296] Bergfeld AK, Claus H, Vogel U, Muhlenhoff M. Biochemical characterization of thepolysialic acid-specific O-acetyltransferase NeuO of Escherichia coli K1. Journal of Biological Chemistry. 2007;282:22217-27.
[297] Rutishauser U. Polysialic acid and the regulation of cell interactions. Current Opinion in Cell Biology. 1996;8:679-84.
[298] Bondioli L, Costantino L, Ballestrazzi A, Lucchesi D, Boraschi D, Pellati F, et al. PLGA nanoparticles surface decorated with the sialic acid, N-acetylneuraminic acid. Biomaterials. 2010;31:3395-403.
[299] Illum L. Chitosan and its use as a pharmaceutical excipient. Pharm Res. 1998;15:1326-31.
[300] Felt O, Buri P, Gurny R. Chitosan: a unique polysaccharide for drug delivery. Drug Dev Ind Pharm. 1998;24:979-93.
[301] Gan Q, Wang T, Cochrane C, McCarron P. Modulation of surface charge, particle size and morphological properties of chitosan-TPP nanoparticles intended for gene delivery. Colloids and Surfaces B-Biointerfaces. 2005;44:65-73.

[302] Park JH, Saravanakumar G, Kim K, Kwon IC. Targeted delivery of low molecular drugs using chitosan and its derivatives. Adv Drug Deliv Rev. 2010;62:28-41.
[303] Jayakumar R, Chennazhi KP, Muzzarellli RAA, Tamura H, Nair SV, Selvamurugan N. Chitosan conjugated DNA nanoparticle in gene therapy. Carbohydr Polym. 2010;79:1-8.
[304] Amidi M, Mastrobattista E, Jiskoot W, Hennink WE. Chitosan-based delivery systems for protein therapeutics and antigens. Adv Drug Deliv Rev. 2010;62:59-82.
[305] Amidi M, Romeijn SG, Borchard G, Junginger HE, Hennink WE, Jiskoot W. Preparation and characterization of protein-loaded N-trimethyl chitosan nanoparticles as nasal delivery system. J Control Release. 2006;111:107-16.
[306] Sadeghi AM, Dorkoosh FA, Avadi MR, Saadat P, Rafiee-Tehrani M, Junginger HE. Preparation, characterization and antibacterial activities of chitosan, N-trimethyl chitosan (TMC) and N-diethylmethyl chitosan (DEMC) nanoparticles loaded with insulin using both the ionotropic gelation and polyelectrolyte complexation methods. Int J Pharm. 2008;355:299-306.
[307] Chen F, Zhang ZR, Yuan F, Qin X, Wang M, Huang Y. In vitro and in vivo study of N-trimethyl chitosan nanoparticles for oral protein delivery. Int J Pharm. 2008;349:226-33.
[308] Wang S, Jiang T, Ma M, Hu Y, Zhang J. Preparation and evaluation of anti-neuroexcitation peptide (ANEP) loaded N-trimethyl chitosan chloride nanoparticles for brain-targeting. International Journal of Pharmaceutics. 2010;386:249-55.
[309] Bal SM, Slutter B, van Riet E, Kruithof AC, Ding Z, Kersten GF, et al. Efficient induction of immune responses through intradermal vaccination with N-trimethyl chitosan containing antigen formulations. J Control Release. 2010;142:374-83.
[310] Chono S, Li SD, Conwell CC, Huang L. An efficient and low immunostimulatory nanoparticle formulation for systemic siRNA delivery to the tumor. J Control Release. 2008;131:64-9.
[311] Vinogradov SV, Bronich TK, Kabanov AV. Nanosized cationic hydrogels for drug delivery: preparation, properties and interactions with cells. Adv Drug Deliv Rev. 2002;54:135-47.
[312] Dash PR, Read ML, Barrett LB, Wolfert MA, Seymour LW. Factors affecting blood clearance and in vivo distribution of polyelectrolyte complexes for gene delivery. Gene Ther. 1999;6:643-50.
[313] M. L. Nucci RS, A. Abuchowski. The therapeuticvalue of poly(ethylene glycol)-modified proteins. Adv Drug Deliv Rev. 1991;6:133-51.
[314] Sieval AB, Thanou M, Kotze AF, verhoef JC, Brussee J, Junginger HE. Preparation and NMR charaterization of highly substituted N-trimethyl chitosan chloride. Carbohydr Polym. 1998;36:157-65.
[315] Thanou M, Kotze AF, Scharringhausen T, Luebetaen HL, De Boer AG, verhoef JC, et al. Effect of degree of quaternisation of N-trimethyl chitosan chloride for enhanced transport of hydrophilic compounds across intestinal Caco-2 cell monolayers. J Control Release. 2000;64:15-25.
[316] Lopez-Leon T, Carvalho E, Seijo B, Ortega-Vinuesa JL, Bastos-Gonzalez D. Physicochemical characterization of chitosan nanoparticles: electrokinetic and stability behavior. J Colloid Interf Sci. 2005;283:344-51.
[317] Calvo P, Remunan-lopez JL, vila-Jato JL, alonso J. Novel hydrophilic chitosan-polyehtylene oxide nanoparticles as protein carriers. J Appl Polym Sci. 1997;63:125-32.

[318] Enriquez-de-Salamanca A, Calonge M. Muscarinic receptors in the ocular surface. Current Opinion in Allergy and Clinical Immunology. 2006;6:379-82.
[319] Huang M, Ma ZS, Khor E, Lim LY. Uptake of FITC-chitosan nanoparticles by a549 cells. Pharmaceutical Research. 2002;19:1488-94.
[320] Huang M, Khor E, Lim LY. Uptake and cytotoxicity of chitosan molecules and nanoparticles: Effects of molecular weight and degree of deacetylation. Pharmaceutical Research. 2004;21:344-53.
[321] Jintapattanakit A, Mao S, Kissel T, Junyaprasert VB. Physicochemical properties and biocompatibility of N-trimethyl chitosan: effect of quaternization and dimethylation. Eur J Pharm Biopharm. 2008;70:563-71.
[322] Chen F, Zhang ZR, Huang Y. Evaluation and modification of N-trimethyl chitosan chloride nanoparticles as protein carriers. Int J Pharm. 2007;336:166-73.
[323] Polakovic M, Gorner T, Gref R, Dellacherie E. Lidocaine loaded biodegradable nanospheres II. Modelling of drug release. Journal of Controlled Release. 1999;60:169-77.
[324] Vila A, Sanchez A, Janes K, Behrens I, Kissel T, Jato JLV, et al. Low molecular weight chitosan nanoparticles as new carriers for nasal vaccine delivery in mice. European Journal of Pharmaceutics and Biopharmaceutics. 2004;57:123-31.
[325] Csaba N, Koping-Hoggard M, Alonso MJ. Ionically crosslinked chitosan/tripolyphosphate nanoparticles for oligonucleotide and plasmid DNA delivery. International Journal of Pharmaceutics. 2009;382:205-14.
[326] Palmeira-de-Oliveira R, Palmeira-de-Oliveira A, Gaspar C, Silvestre S, Martinez-de-Oliveira J, Amaral MH, et al. Sodium Tripolyphosphate: An excipient with intrinsic in vitro anti-Candida activity. International Journal of Pharmaceutics. 2011;421:130-4.
[327] Trapani A, Denora N, Iacobellis G, Sitterberg J, Bakowsky U, Kissel T. Methotrexate-Loaded Chitosan- and Glycolchitosan-Based Nanoparticles: A Promising Strategy for the Administration of the Anticancer Drug to Brain Tumors. Aaps Pharmscitech. 2011;12:1302-11.
[328] Kukowska-Latallo JF, Candido KA, Cao ZY, Nigavekar SS, Majoros IJ, Thomas TP, et al. Nanoparticle targeting of anticancer drug improves therapeutic response in animal model of human epithelial cancer. Cancer Research. 2005;65:5317-24.
[329] Saboktakin MR, Tabatabaie RM, Maharramov A, Ramazanov MA. Synthesis and characterization of pH-dependent glycol chitosan and dextran sulfate nanoparticles for effective brain cancer treatment. International Journal of Biological Macromolecules. 2011;49:747-51.
[330] Taheri A, Dinarvand R, Atyabi F, Nouri F, Ahadi F, Ghahremani MH, et al. Targeted Delivery of Methotrexate to Tumor Cells Using Biotin Functionalized Methotrexate-Human Serum Albumin Conjugated Nanoparticles. Journal of Biomedical Nanotechnology. 2011;7:743-53.
[331] Seo DH, Jeong YI, Kim DG, Jang MJ, Jang MK, Nah JW. Methotrexate-incorporated polymeric nanoparticles of methoxy poly(ethylene glycol)-grafted chitosan. Colloids and Surfaces B-Biointerfaces. 2009;69:157-63.
[332] Thomas TP, Goonewardena SN, Majoros IJ, Kotlyar A, Cao ZY, Leroueil PR, et al. Folate-Targeted Nanoparticles Show Efficacy in the Treatment of Inflammatory Arthritis. Arthritis and Rheumatism. 2011;63:2671-80.

[333] Ji JG, Hao SL, Wu DJ, Huang R, Xu Y. Preparation, characterization and in vitro release of chitosan nanoparticles loaded with gentamicin and salicylic acid. Carbohydrate Polymers. 2011;85:803-8.
[334] Zykova MG, Prozorovskiĭ VN, Ipatova OM, Torkhovskaia TI, Glazatov VV. [Antirheumatoid activity of methotrexate in phospholipid nanoparticles (Phosphogliv)]. Biomed Khim. 2007;53:435-41.
[335] Lindholm A, Kahan BD. Influence of cyclosporine pharmacokinetics, trough concentrations, and AUC monitoring on outcome after kidney transplantation. Clin Pharmacol Ther. 1993;54:205-18.
[336] Liu Z, Jiao Y, Wang Y, Zhou C, Zhang Z. Polysaccharides-based nanoparticles as drug delivery systems. Adv Drug Deliv Rev. 2008;60:1650-62.
[337] Prabaharan M, Mano JF. Chitosan-based particles as controlled drug delivery systems. Drug Deliv. 2005;12:41-57.
[338] Ko JA, Park HJ, Hwang SJ, Park JB, Lee JS. Preparation and characterization of chitosan microparticles intended for controlled drug delivery. Int J Pharm. 2002;249:165-74.
[339] Janes KA, Fresneau MP, Marazuela A, Fabra A, Alonso MJ. Chitosan nanoparticles as delivery systems for doxorubicin. J Control Release. 2001;73:255-67.
[340] Fernandez-Urrusuno R, Calvo P, Remunan-Lopez C, Vila-Jato JL, Alonso MJ. Enhancement of nasal absorption of insulin using chitosan nanoparticles. Pharm Res. 1999;16:1576-81.
[341] Katas H, Alpar HO. Development and characterisation of chitosan nanoparticles for siRNA delivery. J Control Release. 2006;115:216-25.
[342] Zhang N, Bader RA. Synthesis and characterization of polysialic acid-N-trimethyl chitosan nanoparticles for drug delivery. NanoLife. 2012;in press.
[343] Tarner IH, Muller-Ladner U. Drug delivery systems for the treatment of rheumatoid arthritis. Expert Opin Drug Deliv. 2008;5:1027-37.
[344] Boumpas DT, Chrousos GP, Wilder RL, Cupps TR, Balow JE. Glucocorticoid therapy for immune-mediated diseases: basic and clinical correlates. Ann Intern Med. 1993;119:1198-208.
[345] Ritchlin C. Fibroblast biology. Effector signals released by the synovial fibroblast in arthritis. Arthritis Res. 2000;2:356-60.
[346] McInnes IB, Schett G. Cytokines in the pathogenesis of rheumatoid arthritis. Nat Rev Immunol. 2007;7:429-42.
[347] Zhang N, Bader RA. Synthesis and characterization of polysialic acid-N-Trimethyl chitosan nanoparticles for drug delivery. NanoLIFE. 2012;2:1241003.
[348] Yamazaki T, Yokoyama T, Akatsu H, Tukiyama T, Tokiwa T. Phenotypic characterization of a human synovial sarcoma cell line, SW982, and its response to dexamethasone. In Vitro Cellular & Developmental Biology-Animal. 2003;39:337-9.
[349] Choi EM, Lee YS. Luteolin suppresses IL-1 beta-induced cytokines and MMPs production via p38 MAPK, JNK, NF-kappaB and AP-1 activation in human synovial sarcoma cell line, SW982. Food and Chemical Toxicology. 2010;48:2607-11.
[350] Wada Y, Shimada K, Kimura T, Ushiyama S. Novel p38 MAP kinase inhibitor R-130823 suppresses IL-6, IL-8 and MMP-13 production in spheroid culture of human synovial sarcoma cell line SW 982. Immunology Letters. 2005;101:50-9.
[351] Wagoner KL, Bader RA. Evaluation of SV40-transformed synovial fibroblasts in the study of rheumatoid arthritis pathogenesis. Rheumatol Int. 2012;32:1885-91.

[352] Goodman TA, Polisson RP. METHOTREXATE - ADVERSE REACTIONS AND MAJOR TOXICITIES. Rheumatic Disease Clinics of North America. 1994;20:513-28.
[353] Wolverton SE, Remlinger K. Suggested guidelines for patient monitoring: Hepatic and hematologic toxicity attributable to systemic dermatologic drugs. Dermatologic Clinics. 2007;25:195-+.
[354] Baschant U, Lane NE, Tuckermann J. The multiple facets of glucocorticoid action in rheumatoid arthritis. Nature Reviews Rheumatology. 2012;8:645-55.
[355] Huber LC, Distler O, Tarner I, Gay RE, Gay S, Pap T. Synovial fibroblasts: key players in rheumatoid arthritis. Rheumatology (Oxford). 2006;45:669-75.
[356] Pap T, Muller-Ladner U, Gay RE, Gay S. Fibroblast biology. Role of synovial fibroblasts in the pathogenesis of rheumatoid arthritis. Arthritis Res. 2000;2:361-7.
[357] Nakahara H, Song J, Sugimoto M, Hagihara K, Kishimoto T, Yoshizaki K, et al. Anti-interleukin-6 receptor antibody therapy reduces vascular endothelial growth factor production in rheumatoid arthritis. Arthritis Rheum. 2003;48:1521-9.
[358] Kudo O, Sabokbar A, Pocock A, Itonaga I, Fujikawa Y, Athanasou NA. Interleukin-6 and interleukin-11 support human osteoclast formation by a RANKL-independent mechanism. Bone. 2003;32:1-7.
[359] Nanki T, Nagasaka K, Hayashida K, Saita Y, Miyasaka N. Chemokines regulate IL-6 and IL-8 production by fibroblast-like synoviocytes from patients with rheumatoid arthritis. Journal of Immunology. 2001;167:5381-5.
[360] Koch AE. Chemokines and Their Receptors in Rheumatoid Arthritis Future Targets? Arthritis and Rheumatism. 2005;52:710-21.
[361] Chan ESL, Cronstein BN. Methotrexate-how does it really work? Nature Reviews Rheumatology. 2010;6:175-8.
[362] Chan ESL, Cronstein BN. Molecular action of methotrexate in inflammatory diseases. Arthritis Research. 2002;4:266-73.
[363] Cronstein BN. Low-dose methotrexate: A mainstay in the treatment of rheumatoid arthritis. Pharmacological Reviews. 2005;57:163-72.
[364] Swierkot J, Szechinski J. Methotrexate in rheumatoid arthritis. Pharmacol Rep. 2006;58:473-92.
[365] Scheinman RI, Gualberto A, Jewell CM, Cidlowski JA, Baldwin AS. CHARACTERIZATION OF MECHANISMS INVOLVED IN TRANSREPRESSION OF NF-KAPPA-B BY ACTIVATED GLUCOCORTICOID RECEPTORS. Molecular and Cellular Biology. 1995;15:943-53.
[366] Barnes PJ, Adcock IM. How do corticosteroids work in asthma? Annals of Internal Medicine. 2003;139:359-70.
[367] Leung DYM, Bloom JW. Update on glucocorticoid action and resistance. Journal of Allergy and Clinical Immunology. 2003;111:3-23.
[368] Muller-Ladner U, Nishioka K. p53 in rheumatoid arthritis: friend or foe? Arthritis Research. 2000;2:175-8.

VITA

NAME OF AUTHOR: Nan Zhang

PLACE OF BIRTH: Xuchang, HeNan, PR China

DATE OF BIRTH: Dec 22, 1987

UNDERGRADUATE SCHOOLS ATTENDED:

Zhengzhou University, Zhengzhou, HeNan, PR China

DEGREE AWARDED

Bachelor of Science, 2009, Zhengzhou University